

# 國立交通大學

應用化學系

博士論文

新穎含矽氧烷、醯亞胺聚氧代氮代苯并環己烷材料  
製備及其特性之研究



Preparation of Novel Siloxane-Imide-Containing  
Polybenzoxazines and Characterization of Their High  
Performance Thermosets

研究生：陳凱琪

指導教授：孫建文 教授

張豐志 教授

中華民國一百年一月

新穎含矽氧烷、醯亞胺聚氧代氮代苯并環己烷材料  
製備及其特性之研究

Preparation of Novel Siloxane-Imide-Containing  
Polybenzoxazines and Characterization of Their High  
Performance Thermosets

研 究 生：陳凱琪

Student : Kai-Chi Chen

指導教授：孫建文

Advisor : Kein-Wen Sun

指導教授：張豐志

Advisor : Feng-Chih Chang



A Dissertation  
Submitted to Department of Applied Chemistry  
College of Science  
National Chiao Tung University  
in Partial Fulfillment of the Requirements  
for the Degree of  
Doctor of Philosophy  
in  
Applied Chemistry

January 2011  
Hsinchu, Taiwan, Republic of China

中華民國一〇一一年一月

## 誌謝

轉眼間在交大應化系修讀博士學位已經四年半了，曾經我認為自己的學生生涯在台大材料所碩士班畢業後就劃下了句點，不過畢業後進入了工研院材化所就職，工作的內容離不開新技術的研究與發展，唯有不斷的吸取新知、成為不生苔的滾石方能勝任，很慶幸遇到了支持我繼續進修的長官，讓我得以在工作與學業間並行兼顧、繼續進修。

首先，我要感謝指導教授孫建文老師與張豐志老師提供了這良好的研究環境，不僅在專業知識的殿堂上給予我非常多的指導、也教導我在學校做的基礎研究如果能夠在不久的將來找到適合的應用載具更可以賦予研究更高的價值。在回到學校的初期，由於已經在工研院工作幾年了、對於重拾學術研究一開始有些不適應，包括如何將實驗結果精簡扼要的以論文的方式完整的呈現，謝謝老師耐心的指正、讓我能漸入佳境。

感謝口試委員：黃介銘教授、郭紹偉教授、陳建光教授、王志逢教授以及陳俊太教授在學生論文上提供了寶貴的意見與指導，使得學生論文可以更加豐富與完整。

感謝實驗室的學弟英傑、智嘉、didi，因為我在工研院上班，學校的事務常常麻煩各位學弟，真的謝謝有你們的幫忙。謝謝春雄，在實驗合成初期是我重要的左右手，來院內工讀時也常常互相交流討論實驗的方向，這對我幫助頗大喔。謝謝懷廣，我還記得當年一同修課時你請囊相授了考試秘訣，相當受用；謝謝世堅、宜弘、哲豪在實驗及論文上的幫忙。謝謝你們讓我的研究所生涯充滿溫馨的回憶。

要非常感謝的是天哥，你是我就讀博士班的大推手，沒有你給我的信心我可能至今還在原地踏步，我不會忘記當我實驗遇到瓶頸時你比我還用心的協助我解決了一個又一個的難題，不管是實驗上的困難或是心理上的沮喪，你始終支持著陪我走在這條道路上。再來要謝謝工研院材化所小李研究團隊的大家，禎姐、文彬、嘉紋、志浩、語恒，我們有著革命式的情感一同在工研院共事了許久，雖然常常彼此吐槽但是大夥兒都是互相幫忙，在我在學校公司兩頭跑時也常二話不說的伸出援手，有你們這群相挺的好同事、我很幸運。

最後將這論文獻給我最愛的家人，謝謝老爸老媽對於我工作多年之後還要回學校唸書給予無怨無悔的支持，謝謝三位姊姊及姊夫，曾經因工作學業兩頭忙而動念想留職停薪先完成學業時、大姊第一時間的支持、我很是感動，有家人滿滿的愛，最後我終於能兩邊兼顧的完成學業。

謹以這份論文，獻給在我求學路上關心與照顧我的各位。

# Outline of Contents

	<b>Pages</b>
Acknowledgments	
Outline of Contents	I
List of Schemes	IV
List of Tables	IV
List of Figures	V
Abstract (in Chinese)	IX
Abstract (in English)	XI
<b>Chapter 1 Introduction</b>	
1.1 Overview on Benzoxazines and Polybenzoxazines	1
1.2 Chemical Methodologies for Synthesis of Benzoxazine Monomers	6
1.2.1 Mono-functional Benzoxazine Monomers	6
1.2.2 Di-functional and Multifunctional Benzoxazine Monomers	7
1.2.3 Allyl-containing Benzoxazine Monomers	8
1.2.4 Maleimide and Norbornane-containing Benzoxazine Monomers	9
1.3 Polymerization of Benzoxazines and Their Blends and Composites	10
1.3.1 Photoinitiated Polymerization of Benzoxazines	10
1.3.2 Thermal Polymerization of Benzoxazines	11
1.3.3 Properties of Epoxy- Polymbenzoxazine	15
References	17
<b>Chapter 2 Synthesis of Siloxane-Imide-Containing Benzoxazines</b>	
2.1 Synthesis of Siloxane-Imide-Containing Benzoxazine (BZ-A1)	20
2.1.1 Materials and Characterization	20
2.1.2 Synthesis of the siloxane-containing dihydroxyl (A1-OH)	21
2.1.3 Synthesis of the siloxane-imide-containing benzoxazine ,N'-bis(N-phenyl-3,4-dihydro-2H-benzo[1,3]oxazine)-5,5'-bis(1,1',3,3'-tetramethyldisiloxane-1,3-diyl)-bis(norborane-2,3-dicarboximide) (BZ-A1)	22
2.2 Synthesis of Siloxane-Imide-Containing Benzoxazine (BZ-A6)	26
2.2.1 Materials	26
2.2.2 Synthesis of dinoborane anhydride terminated polydimethylsiloxane (A6)	26
2.2.3 Imidization of siloxane-imide-containing dianhydride (A6-OH)	27

2.2.4 Synthesis of siloxane-imide-containing benzoxazine (BZ-A6)	27
References	31
<b>Chapter 3 Curing Behavior of Siloxane-Imide-Containing Benzoxazines</b>	
3.1 Curing behavior of the siloxane-imide-containing benzoxazine BZ-A1	32
3.2 Curing behavior of the siloxane-imide-containing benzoxazine BZ-A6	34
References	36
<b>Chapter 4 Thermal/ Mechanical Properties of Siloxane-Imide-Containing Polybenzoxazines</b>	
4.1 Thermal stability of the poly-siloxane-imide-containing benzoxazine PBZ-A137	
4.1.1 Materials and Characterization	37
4.1.2 TGA of the poly-siloxane-imide-containing benzoxazine PBZ-A1	38
4.2 Thermal stability of the poly-siloxane-imide-containing benzoxazine PBZ-A643	
4.2.1 Materials and Characterization	43
4.2.2 TGA of the poly-siloxane-imide-containing benzoxazine PBZ-A6	44
4.2.3 DMA of the poly-siloxane-imide-containing benzoxazine PBZ-A6	48
References	51
<b>Chapter 5 Extremely Low Surface Free Energy and UV Stability of Siloxane-Imide-Containing Polybenzoxazines</b>	
5.1 Introduction of Surface Free Energy	52
5.1.1 Interfacial Thermodynamics	52
5.1.2 Contact Angle Equilibrium: Young Equation	54
5.1.3 Determination of Surface Free Energy	57
5.1.4 Surface Free Energy of Polymer	63
5.2 Superhydrophobic Surfaces	69
5.2.1 Natural Examples	70
5.2.2 Synthetic Substrates	73
5.3 Surface behavior of siloxane-imide-containing polybenzoxazines	76
5.3.1 Surface behavior of PBZ-A1 and PBa	76
5.3.2 Surface behavior and thermal resistant of PBZ-A6, PBZ-A1 and PBa	80
5.3.3 Surface behavior and ultraviolet resistant of PBZ-A6, PBZ-A1 and PBa	83
References	85
<b>Chapter 6 New Thermosetting Resin from Siloxane-Containing Benzoxazine and Epoxy Resin</b>	

Abstract	89
6.1 Introduction	90
6.2 Experiment	92
6.2.1 Materials	92
6.2.2 Synthesis of siloxane-imide-containing benzoxazine (BZ-A6)	93
6.2.3 Curing conditions of neat resin	93
6.2.4 Preparation of polybenzoxazine film	93
6.2.5 Characterization	94
6.3 Results and discussion	95
6.3.1 Curing behavior of benzoxazine with epoxy resin	95
6.3.2 FT-IR Characterization of copolymerization	97
6.3.3 Scanning DSC studies	99
6.3.4 Thermogravimetric analysis	104
6.3.5 UV stability properties	105
6.4 Conclusions	107
References	108
<b>Chapter 7 Conclusions</b>	110
<b>List of Publications</b>	112
<b>Introduction to the Author</b>	113



## List of Schemes

	<b>Pages</b>
Scheme 1-1. The syntheses and thermal curing of (A) monofunctional benzoxazines and (B) difunctional benzoxazines	3
Scheme 1-2. Synthesis of 3,4-dihydro-2 <i>H</i> -1,3-benzoxazines	6
Scheme 1-3. Ring opening of benzoxazine in acidic medium	7
Scheme 1-4. Synthesis of allyl containing benzoxazine monomers	9
Scheme 1-5. Photoinitiated polymerization of <i>N</i> -phenyl-3,4-dihydro-2 <i>H</i> -1,3-benzoxazine	11
Scheme 2-1. Preparation of the siloxane-imide-containing dianhydride (A1) and dihydroxyl compound (A1-OH)	22
Scheme 2-2. Preparation of the siloxane-imide-containing benzoxazine monomer BZ-A1 from A1 and A1-OH	23
Scheme 2-3. Syntheses of compounds A6 and A6-OH	30
Scheme 2-4. Preparation of compound BZ-A6	30



## List of Tables

	<b>Pages</b>
Table 1-1. Comparative polybenzoxazine properties of various high performance polymers	5
Table 1-2. Di-functional benzoxazine monomers	8
Table 1-3. Maleimidyl and Norbornyl Functional Benzoxazines	10
Table 1-4. Thermal properties of polybenzoxazines	13
Table 3-1. Curing conditions for PBZs	33
Table 3-2. Curing conditions for PBZs	35
Table 4-1. Thermostabilities of the cured PBZs PBa and PBZ-A1 (in air)	41
Table 4-2. Thermostabilities of the cured PBZs PBa and PBZ-A1 (under N <sub>2</sub> )	43
Table 4-3. Thermostability of cured polybenzoxazine PBa, PBZ-A1 and PBZ-A6 (in air)	45
Table 4-4. Thermostability of cured PBZ PBa, PBZ-A1, and PBZ-A6 (in N <sub>2</sub> )	47
Table 4-5. Thermal mechanical analysis data for PBZ-A6	49
Table 5-1. Numerical constant for molecular weight dependence of surface free energy	64

Table 5-2. Macleod's exponent for some polymers	66
Table 5-3. Surface free energies of the cured and annealed PBa and PBZ-A1	78
Table 5-4. Advancing contact angles and corresponding surface free energies for PBZ films prepared from Ba, BZ-A1, and BZ-A6	81
Table 6-1. The kinetic parameters evaluated for the curing of benzoxazine/ epoxy copolymers	101
Table 6-2. Thermostability of cured resins from Ba/ DGEBA and BZ-A6/ GT-1000	105
Table 6-3. Contact angles of cured resins from Ba/ DGEBA and BZ-A6/ GT-1000 after UV exposure for various periods of time	106

## List of Figures

	Pages
Figure 2-1. Structure of the bifunctional bisphenol A-type benzoxazine Ba	21
Figure 2-2. IR spectrum of the siloxane-imide-containing benzoxazine BZ-A1	24
Figure 2-3. <sup>1</sup> H NMR spectrum of the siloxane-imide-containing benzoxazine BZ-A1	24
Figure 2-4. LC/Mass spectrum of the siloxane-imide-containing benzoxazine BZ-A1	25
Figure 2-5. <sup>1</sup> H-NMR spectrum of the siloxane-imide-containing benzoxazine BZ-A6	28
Figure 2-6. FT-IR spectrum of the siloxane-imide-containing benzoxazine BZ-A6	29
Figure 3-1. DSC thermograms of Ba and BZ-A1	33
Figure 3-2. Glass transition temperature ( $T_g$ ) of PBZ-A1, determined from the DSC trace	34
Figure 3-3. DSC thermograms of BZ-A6 monomer and polymerized BZ-A6 (after curing)	35
Figure 4-1. Structure of the bifunctional bisphenol A-type benzoxazine Ba	38
Figure 4-2. Structure of the BZ-A1	38
Figure 4-3. Glass transition temperature ( $T_g$ ) of PBZ-A1, determined from the DSC trace	40
Figure 4-4. TGA thermograms of PBa and PBZ-A1 (in air)	41
Figure 4-5. Residue and EDS analysis of PBZ-A1 after TGA testing	42
Figure 4-6. TGA thermograms of Ba and BZ-A1 (under N <sub>2</sub> )	42



Figure 4-7. Structure of the BZ-A6	43
Figure 4-8. TGA thermograms of PBa, PBZ-A1 and PBZ-A6 (in air)	45
Figure 4-9. TGA thermograms of PBa, PBZ-A1 and PBZ-A6 (in N <sub>2</sub> )	47
Figure 4-10. DMA thermograms of PBZ-A6: (1) storage modulus (2) tan $\delta$	49
Figure 4-11. Photograph of a thin film of PBZ-A6, a siloxane-imide-containing PBZ	50
Figure 5-1. Work of adhesion	53
Figure 5-2. Work of cohesion	53
Figure 5-3. Contact angle equilibrium on a smooth, homogeneous, planar, and rigid surface	54
Figure 5-4. Advancing contact angle	55
Figure 5-5. Receding contact angle	56
Figure 5-6. Comparison of surface energy and molecular weight between polymers with and without hydrogen bonds	65
Figure 5-7. Linear additivity of surface tension of random copolymers of ethylene oxide and propylene oxide, and surface-active behavior of blends of poly(ethylene oxide) (PEG 300) and poly(propylene oxide) (PPG 425)	67
Figure 5-8. Surface tension versus composition for ABA block copolymers of ethylene oxide (A block) and propylene oxide (B block). Degree of polymerization are (1) DP = 16, (2) DP = 30, (3) DP = 56	68
Figure 5-9. Surface tension of blends of compatible homopolymers. (1) poly(ethylene oxide) (PEG 300) + poly(propylene oxide) (PPG 425), (2) PPG 2025 + polyepichlorohydrin (PECH 1500), (3) PPG 400 + PECH 2000	69
Figure 5-10. (Left) Surfaces without self-cleaning. (Right) Surfaces with self-cleaning	70
Figure 5-11. Water droplets on lotus	71
Figure 5-12. The non-wetting leg of a water strider. (a) Typical side view of a maximal-depth dimple (4.38 mm) just before the leg pierces the water surface. Inset, water droplet on a leg; this makes a contact angle of 167.6°. (b), (c), Scanning electron microscope images of a leg showing numerous oriented spindly microsetae (b) and the fine nanoscale grooved structures on a seta (c). Scale bars: b, 20 $\mu$ m; c, 200 nm	72
Figure 5-13. FE-SEM micrograph of the wing surface of Cicada orni with regularly	

aligned nanoposts	73
Figure 5-14. SEM images of the fractal alkylketene dimmer (AKD) surface: (a,) top view, (b) cross section. Water droplet on AKD surfaces: (c) fractal AKD surface; (d) flat AKD surface	74
Figure 5-15. The profile of a water drop on (a) a smooth i-PP surface (CA = 104°), (b) a superhydrophobic i-PP coating on a glass slide (CA = 160°). (c) SEM picture of a superhydrophobic i-PP film	75
Figure 5-16. (a) Illustration of the solvent effect on the morphologies of PP-PMMA copolymer surface. (b) The profile of a water drop on superhydrophobic polymer surface. (c) SEM images of superhydrophobic polymer. (d) Enlarged view of (c)	75
Figure 5-17. Contact angles of polybenzoxazines during different curing time	78
Figure 5-18. Surface free energies of PBZs after various curing and annealing hours at 230	79
Figure 5-19. Surface free energies of PBZs after curing and annealing at 230 °C	82
Figure 5-20. Water contact angles of PBZ films after UV-A exposure for various periods of time	84
Figure 5-21. UV resistant behavior of PBZ-A6 film	84
Figure 6-1. Structure of bi-functional bisphenol A type benzoxazine (Ba), siloxane-imide-containing benzoxazine (BZ-A6) and siloxane-containing epoxy (GT-1000)	92
Figure 6-2. DSC thermogram of (a) Ba/ DGEBA copolymer and (b) copolymerized Ba/ DGEBA	95
Figure 6-3. DSC thermogram of (a) BZ-A6/ GT-1000 copolymer and (b) copolymerized BZ-A6/ GT-1000	96
Figure 6-4. Ring-opening reaction of benzoxazine with epoxy	97
Figure 6-5. FT-IR spectrum of Ba/ DGEBA copolymer (a) before reaction (b) 200 / 1h (c) 200 / 2h (d) 200 / 2h + 230 / 1h (e) 200 / 2h + 230 / 2h	98
Figure 6-6. FT-IR spectrum of BZ-A6/ GT-1000 copolymer (a) before reaction (b) 150 / 1h (c) 150 / 2h (d) 150 / 2h + 180 / 1h (e) 150 / 2h + 180 / 2h	99
Figure 6-7. Dynamic DSC exothermic curves of Ba/ DGEBA resin at different scan	

rates: 5 / min., 10 / min., 15 / min. and 20 / min.	101
Figure 6-8. Plots for determination of the activation energy of Ba/ DGEBA copolymer by the Kissinger method	102
Figure 6-9. Dynamic DSC exothermic curves of BZ-A6/ GT-1000 resin at different scan rates: 5 / min., 10 / min., 15 / min. and 20 / min.	102
Figure 6-10. Plots for determination of the activation energy of BZ-A6/ GT-1000 copolymer by the Kissinger method.	103
Figure 6-11. TGA thermograms of cured resin from (a) Ba/ DGEBA (in air) (b) BZ-A6/ GT-1000 (in air) (c) Ba/ DGEBA (in N <sub>2</sub> ) (d) BZ-A6/ GT-1000 (in N <sub>2</sub> )	104



## 摘要

在 高 分 子 研 究 領 域 中，化 學 性 質 與 物 理 性 質 皆 具 有 相 當 的 重 要 性，且 兩 者 是 相 輔 相 成 的，我 們 可 藉 由 材 料 分 子 結 構 設 計、化 學 改 質 / 合 成 的 方 法 來 滿 足 某 些 物 理 性 質 的 需 求、或 以 物 理 性 質 研 究 來 延 續 合 成 產 物 的 應 用 性 與 實 用 性。本 論 文 以 含 矽 氧 烷、醯 亞 胺 聚 氧 代 氮 代 苯 并 環 己 烷 (siloxane-imide-containing polybenzoxazine) 為 研 究 主 體，內 容 分 列 為 三 大 主 題：

### 1. 新穎 Siloxane-imide-containing benzoxazine (BZ-A1 與 BZ-A6) 單體合成

在 以 往 的 文 獻 中，polybenzoxazine 聚 合 物 有 許 多 優 點：優 異 的 熱 性 質 (高  $T_g$ 、高 裂 解 溫 度)、無 須 催 化 劑 即 可 進 行 聚 合 反 應，在 我 們 實 驗 室 的 先 前 研 究 中 也 發 現 此 聚 合 物 具 有 較 鐵 氟 龍 更 低 的 表 面 能，是 一 個 新 穎 的 疏 水 低 表 面 能 材 料。此 外，polybenzoxazine 較 一 般 常 見 的 含 氟 低 表 面 能 材 料 具 有 價 格 便 宜 與 易 於 製 程 的 優 點。此 研 究 中，我 們 於 benzoxazine 主 體 上 導 入 siloxane-imide 結 構，選 擇 不 同 矽 氧 烷 鏈 長 的 起 始 物 合 成 出 不 同 矽 氧 烷 鏈 長 (分 子 量) 的 氧 代 氮 代 苯 并 環 己 烷 單 體 (BZ-A1, BZ-A6)。藉 由 siloxane-containing 增 加 材 料 的 柔 軟 特 性 (flexibility) 與 耐 候 特 性、藉 由 imide-containing 維 持 材 料 的 熱 性 質、使  $T_g$  不 因 siloxane 導 入 而 下 降。

### 2. Siloxane-imide-containing benzoxazine 硬化行為與聚合物特性探討

此 部 分 針 對 siloxane-imide-containing benzoxazine 硬 化 行 為 進 行 探 討，BZ-A1 與 BZ-A6 不 但 具 有 一 般 benzoxazine 自 開 環 反 應 的 優 點，形 成 polybenzoxazines (PBZ-A1 與 PBZ-A6) 後 聚 合 物 的 彈 性 模 數 (storage modulus) 在 MPa 範 圍 間，較

bisphenol A 型態的 polybenzoxazine 的 GPa 範圍降低了許多，而且當 siloxane 含量較多時(PBZ-A6)可以得到一單獨的薄膜(a free-standing film)，足見解決了現有 polybenzoxazine 過脆的缺點。而在此 benzoxazine 主鏈上亦導入 imide 基團，因此聚合物的  $T_g$  可以大於 180 ，不因 siloxane 軟鏈段的添加而降低  $T_g$ 。Siloxane-imide-containing polybenzoxazines 也是一疏水材料，PBZ-A6 具有極低的表面能( $\sim 12.4 \text{ mJ/m}^2$ )，PBZ-A1 與 PBZ-A6 同時也展現了極佳的耐熱與耐紫外光特性，有機會應用於自清潔與耐候材料上。

### 3. Siloxane-imide-containing polybenzoxazine/ epoxy 共聚合物(copolymer) 系統探討

除了 Siloxane-imide-containing benzoxazines 本身聚合反應與特性探討外，此部分我們選擇 siloxane-containing epoxy 與之進行共聚物反應(copolymerization)，除了發現共聚物中三級胺鹽含量可催化反應、降低反應溫度外，此共聚物仍具有良好熱性質、耐熱與耐紫外等優異特性，本研究我們利用 Kissinger method 針對 siloxane-containing 共聚合物進行反應動力學探討。

## Abstract

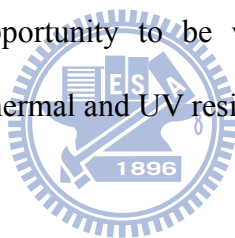
The physical and chemical properties are both important in the polymer researches. We can enhance many properties of polymers by chemical methods (i.e. variation of the functional groups, structure design and synthesis of polymers). By doing detailed studies of physical properties of polymers, we can discover numerous applications of them. In this study, we focus on three major subjects which based on the siloxane-imide-containing polybenzoxazines:

### 1. Synthesis of novel siloxane-imide-containing benzoxazines (BZ-A1 and BZ-A6)

Polybenzoxazines are reported to possess many advantages, good thermal properties (high T<sub>g</sub>, high decomposed temperature), cured without catalyst, etc. In our previous study, surface free energies of polybenzoxazines are even lower than that of pure poly(tetrafluoroethylene) (Teflon). In this study, siloxane-imide containing structure was introduced into the main chain of benzoxazine. Novel siloxane-imide-containing benzoxazines, BZ-A1 and BZ-A6 were synthesized from various siloxane-containing starting material, siloxane-imide-containing di-anhydride. The novel polybenzoxazines have flexibility properties and good weather resistance due to siloxane-containing in the structure. The siloxane-imide-containing polybenzoxazines remain its high T<sub>g</sub> since the imide-containing group. These polybenzoxazines comprise a new class of low-surface-free-energy and weather resistant materials, they are cheaper to prepare and easier to process than are conventional fluoropolymers and silicones.

## **2. Curing behavior of siloxane-imide-containing benzoxazines and properties of polybenzoxazines**

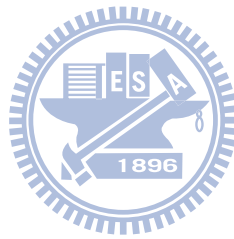
Curing behavior of siloxane-imide-containing benzoxazines and properties of polybenzoxazines were discussed in this study. BZ-A1 and BZ-A6 were crosslinked without any catalyst. Polybenzoxazines from BZ-A6 has lower storage modulus in mega-pascal scale, much lower than the typical bisphenol A type polybenzoxazine which storage modulus is in giga-pascal scale. A flexible, free-standing film could be obtained of PBZ-A6 which has more siloxane-containing segment in benzoxazine. Tg of novel polybenzoxazine is higher than 180 °C since imide group was introduced into the main chain of benzoxazine. Siloxane-imide-containing polybenzoxazines also have hydrophobic properties. PBZ-A6 has extremely low surface free energy as 12.4 mJ/m<sup>2</sup>. PBZ-A1 and PBZ-A6 have opportunity to be weather resistant or self-cleaning materials because of their good thermal and UV resistant properties.



## **3. Copolymerization of siloxane-imide-containing polybenzoxazine and epoxy resin**

Siloxane-imide-containing benzoxazine, BZ-A6, was copolymerized with siloxane-epoxy, GT-1000. The curing behavior of the copolymers was studied using DSC and FT-IR, which indicated a lower curing temperature of 150 °C. The activation energy (E<sub>a</sub>) of BZ-A6/ GT-1000 copolymer is 59.4 KJ/mol. from Kissinger method. The siloxane benzoxazine-epoxy mixture exhibited higher thermal stability, exhibited higher char yield as 44.6% and higher decomposed temperature at 364.9 °C. Moreover, the water contact angle of the BZ-A6/ GT-1000 copolymer is more stable than the conventional bisphenol A type benzoxazine-epoxy, Ba/ DGEBA, during the UV exposure process, indicating that the benzoxazine-epoxy mixture is more suitable to

apply as a hydrophobic material with UV resistant requirement. There are wide applications of siloxane benzoxazine-epoxy mixture since its lower curing temperature and good temperature- and UV- resistant properties.





# Chapter 1

## Introduction

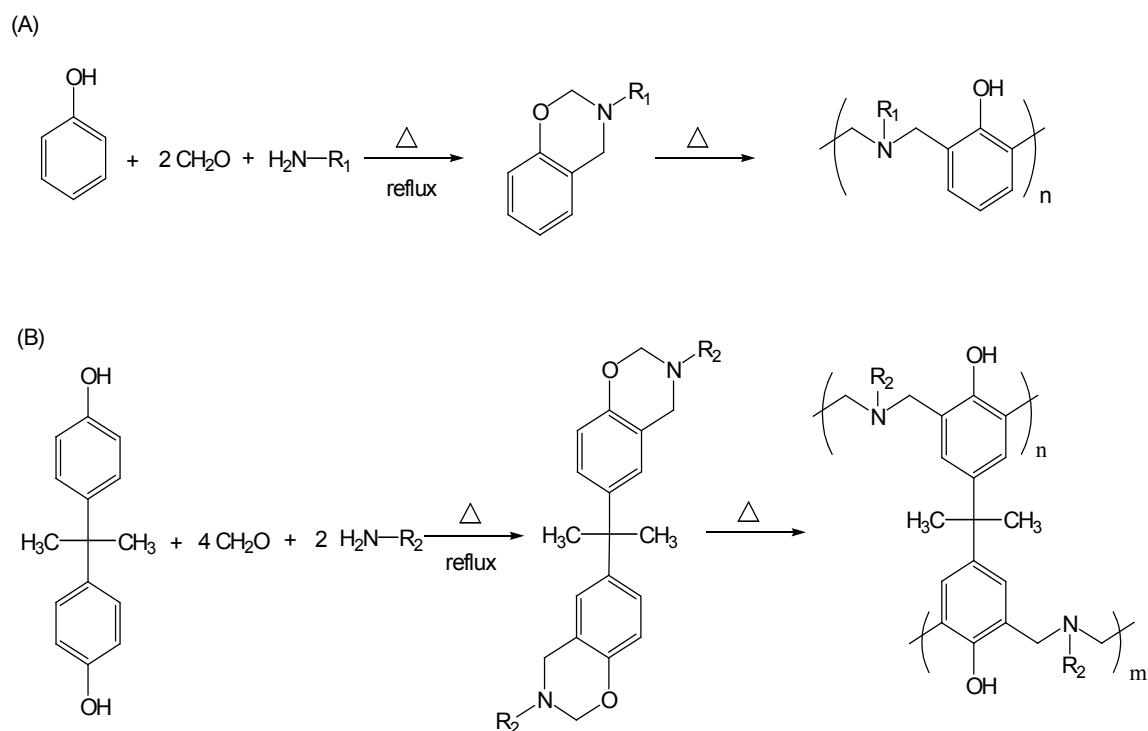
### 1.1 Overview on Benzoxazines and Polybenzoxazines

A interesting addition-cure phenolic system is based on oxazine-modified phenolic resin that encounters a ring-opening polymerization to give polybenzoxazine, which is mainly a poly(amino-phenol). The benzoxazine monomers are formed from amines and phenol in the presence of formaldehyde, which were first synthesized by Holly and Cope [1]. These structures were not recognized as phenolic resin precursors until Schreiber [2] reported in 1973 that a hard and brittle phenolic material was formed from benzoxazine precursors, but no further details about structures and properties were included. In 1986, Riess et al. reported the synthesis and reactions of monofunctional benzoxazine compound. [3] The compounds that they obtained were oligomer phenolic structures because the thermo-dissociation of the monomer was always competing with the chain propagation. The bifunctional benzoxazine precursor synthesized by Ning and Ishida [4] overcame the low degree of crosslinking of above compounds. Furthermore, these samples possess high mechanical integrity and can be easily prepared from inexpensive raw materials. [5-7]

Benzoxazine monomers are typically synthesized using phenol, formaldehyde and amine (aliphatic or aromatic) as starting materials either by employing solution or solventless methods. Various types of benzoxazine monomer can be synthesized using various phenols and amines with different substitution groups attached. These substituting groups can provide additional polymerizable sites and also affect the curing process. Consequently, polymeric materials with desired properties may be obtained by tailoring the benzoxazine monomer. [8]

In phenolic chemistry, both the ortho- and para- position on the benzene ring are reactive toward electrophilic substitution reactions due to the directing effect of the hydroxyl group. Benzoxazines also show multiple reactivities of the benzene ring due to directing effect of both the alkoxy and alkyl groups connected to the benzene ring as shown in Scheme 1-1. Benzoxazines can be polymerized without by using strong acid or basic catalyst, and produce no byproducts through the heterocyclic ring opening reaction. The free ortho- position on a benzene ring in the benzoxazine system has high reactivity toward thermal and phenol-initiated ring-opening polymerizations and forms a phenolic Mannich base (-CH<sub>2</sub>-NR-CH<sub>2</sub>-) polymer structure. In addition, the free para- position also shows reactivity toward a similar type of polymerization [3,9].

The ring-opening polymerization can also be catalyzed by acidic catalysts that permit a wide curing temperature. In the presence of acidic catalysts [10], the curing temperature can be reduced from 160-220 °C to about 130-170 °C and increase the application range. In recent years, thermosetting polybenzoxazines have attracted an intense amount of interest from both academia and industry because of their fascinating characteristics, such as high performance, low cost, and ease of processing. [11-14]



Scheme 1-1. The synthesis and thermal curing of (A) monofunctional benzoxazines and (B) difunctional benzoxazines

In addition to these advantageous features, which they share with traditional phenolic resins, the polybenzoxazines also possess unique properties, such as low degrees of water absorption [15,16] (despite the large number of hydroxyl groups present in their backbone structure), high moduli, [17] excellent resistance to chemicals [18] and UV light, [19] near-zero volumetric shrinkage/expansion upon polymerization, [20] and high glass transition temperatures, even at a relatively low cross-linking density. [21] The polybenzoxazines overcome several defects of traditional novolac and resole-type phenolic resins, while retaining their advantages. Polybenzoxazine resins are supposed to replace traditional phenolics, polyesters, vinyl esters, epoxies, cyanate esters and polyimides in many respects. [22] The molecular structure of polybenzoxazine offers excellent design flexibility that allows properties

of the cured material to be controlled for specific requirements of a wide variety of individual requirements. The resin allows development of new applications by utilizing some of their unique features such as [20, 21, 23]:

- Near zero volumetric change upon polymerization
- No release of volatiles during curing
- Low melting viscosity (for benzoxazine)
- High glass transition temperature ( $T_g$ )
- High thermal stability ( $T_d$ )
- Low CTE
- Low water absorption
- Good mechanical properties
- Excellent electrical properties

Table 1-1 compares the properties of polybenzoxazine with those of the state-of-the-art matrices. The relative benefits of polybenzoxazines are obvious.

Table 1-1 Comparative polybenzoxazine properties of various high performance polymers

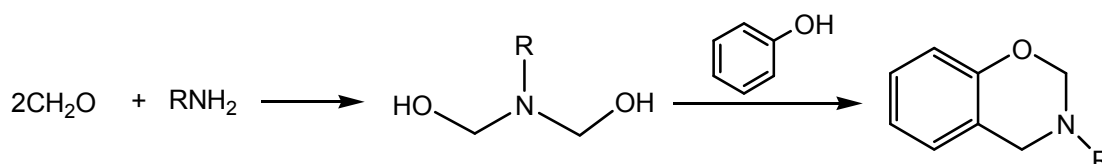
Property	Epoxy	Phenolics	Toughened BMI	Bisox-phen (40:60)	Cyanate ester	P-T resin	
	Polybenzoxazine						
Density (g/cc)	1.2-1.25	1.24-1.32	1.2-1.3	1.3	1.1-1.35	1.25	1.19
Max use temperature ( )	180	200	~200	250	150-200	300-350	130-280
Tensile strength (MPa)	90-120	24-45	50-90	91	70-130	42	100-125
Tensile modulus (GPa)	3.1-3.8	03/05	3.5-4.5	4.6-5.1	3.1-3.4	4.1	3.8-4.5
Elongation (%)	3-4.3	0.3	3	1.8	02/04	2	2.3-2.9
Dielectric constant (1 MHz)	3.8-4.5	04/10	3.4-3.7	-	2.7-3.0	3.1	3-3.5
Cure temperature ( )	RT-180	150-190	220-300	175-225	180-250	177-316	160-220
Cure shrinkage (%)	>3	0.002	0.007	<1	~3	~3	~0
TGA onset (8C)	260-340	300-360	360-400	370-390	400-420	410-450	380-400
Tg ( )	150-220	170	230-380	160-295	250-270	300-400	170-340
G <sub>IC</sub> (J/m <sup>2</sup> )	54-100	-	160-250	157-223	-	-	168
K <sub>IC</sub> (MPa m <sup>1/2</sup> )	0.6	-	0.85	-	-	-	0

## 1.2 Chemical Methodologies for Synthesis of Benzoxazine Monomers

Benzoxazine monomers are typically synthesized using phenol, formaldehyde and amine (aliphatic or aromatic) as starting materials. Various types of benzoxazine monomer can be synthesized using various phenols and amines with different substitution group attached. These substituting groups can provide additional polymerizable sites and also affect the curing process. Consequently, polymeric materials with desired properties may be obtained by tailoring the benzoxazine monomer. [8]

### 1.2.1 Mono-functional Benzoxazine Monomers

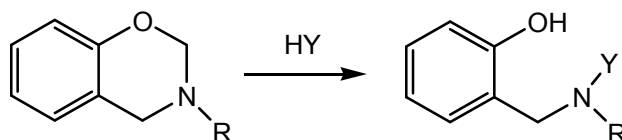
Holly and Cope [1] first reported the condensation reaction of primary amines with formaldehyde and substituted phenols for the synthesis of well defined benzoxazine monomers. According to the report procedure, this reaction was performed in a solvent in two-steps. Later, Burke found that benzoxazine ring reacts preferentially with the free *ortho* positions of a phenolic compound and forms a Mannich bridge. [24] The synthetic procedure of the Mannich condensation for benzoxazine synthesis in a solvent proceeds by first addition of amine to formaldehyde at lower temperatures to form an N,N-dihydroxymethylamine derivative, then reacts with the liable hydrogen of the phenol at the elevated temperature to form oxazine ring [25] (Scheme 1-2).



Scheme 1-2. Synthesis of 3,4-dihydro-2H-1,3-benzoxazines

It has been that the ring opening of some benzoxazines occurs in the presence of

compounds with active hydrogen (HY), such as naphthol, idoles, carbazole, imides and aliphatic nitro compounds, even phenol. Formation of the Mannich bridge structure due to the ring opening of benzoxazine in acidic medium (HY) [26] is shown in Scheme 1-3.

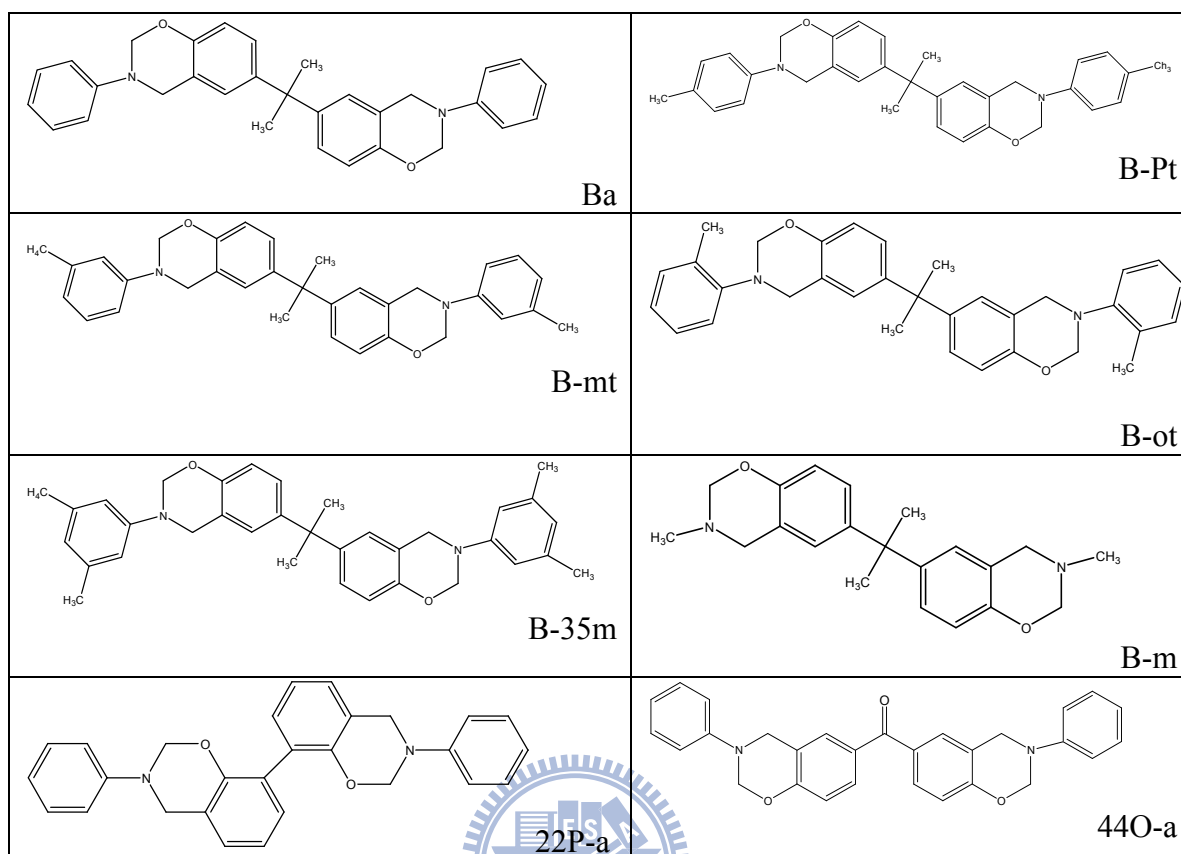


Scheme 1-3. Ring opening of benzoxazine in acidic medium.

### 1.2.2 Di-functional and Multifunctional Benzoxazine Monomers

Ishida and coworkers [11,27] have developed a new class of difunctional or multifunctional benzoxazine monomers, and their curing into phenolic materials with the ring opening reactions being initiated by dimers and higher oligomers in the resin composition. The precursor was synthesized using bisphenol-A, formaldehyde and methyl amine in different solvents and referred to Scheme 1-1. The synthetic method consists of a few simple steps and can easily provide different phenolic structures with wide design flexibility. Solventless method was successfully employed for synthesis of a series of difunctional monomer list in Table 1-2. [8]

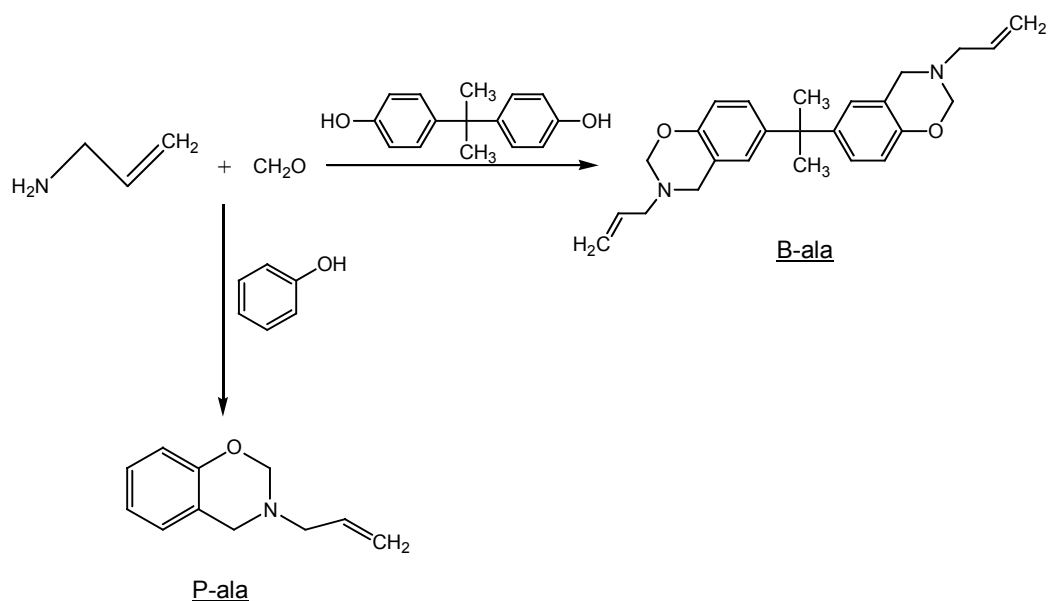
Table 1-2. Di-functional benzoxazine monomers. [8]



### 1.2.3 Allyl-containing Benzoxazine Monomers

The main advantage of the allyl group [27,28] is not only that it provides additional crosslinkable sites, but that it can easily be cured at a temperature lower than that needed for acetylene groups. Allyl-containing monomers have attracted much attention because they are used as reactive diluents of bismaleimides to improve the toughness of the cured resin [29,30]. The synthetic approaches adopted by Agag and Takeichi [31] for the preparation of two novel benzoxazine monomers modified with allyl groups which are shown in Scheme 1-4. It was reported that benzoxazines containing allyl group can polymerize at temperature below 150 °C. However, the polymerization occurring at low temperature is from the allyl group, and a high temperature above 250 °C was needed to complete the polymerization of benzoxazine rings.



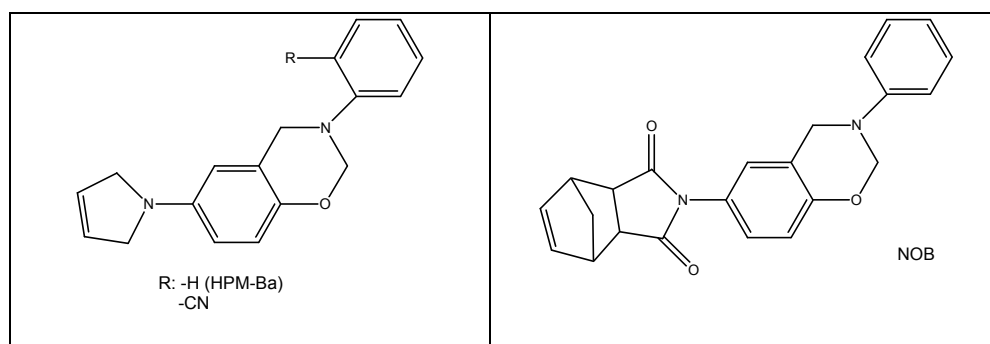


Scheme 1-4. Synthesis of allyl containing benzoxazine monomers.

#### 1.2.4 Maleimide and Norbornane-containing Benzoxazine Monomers

A benzoxazine compound with a maleimide pendant (HPM-Ba) was prepared to achieve attractive processing and thermal properties. It was prepared from N-(4-hydroxyphenyl) maleimide (HPM), formaldehyde and aniline in dioxane medium at 30% yield. Another reported method uses 1,3,5-triphenylhexahydro- 1,3,5-triazine (TPHT). The reaction was performed through a solventless synthesis route where TPHT, aniline, and paraformaldehyde was mixed together and heated at 150 °C for 1.5 hrs. The yield of the final product, HPM-Ba, after washing and precipitation was 70%. Also, a nitrile group containing maleimide benzoxazine was synthesized to further improve thermal properties of polybenzoxazine resin. [32] The structures of benzoxazine monomers having maleimide and norborane functionality are shown in Table 1-3.

Table 1-3. Maleimidyl and Norbornyl Functional Benzoxazines.



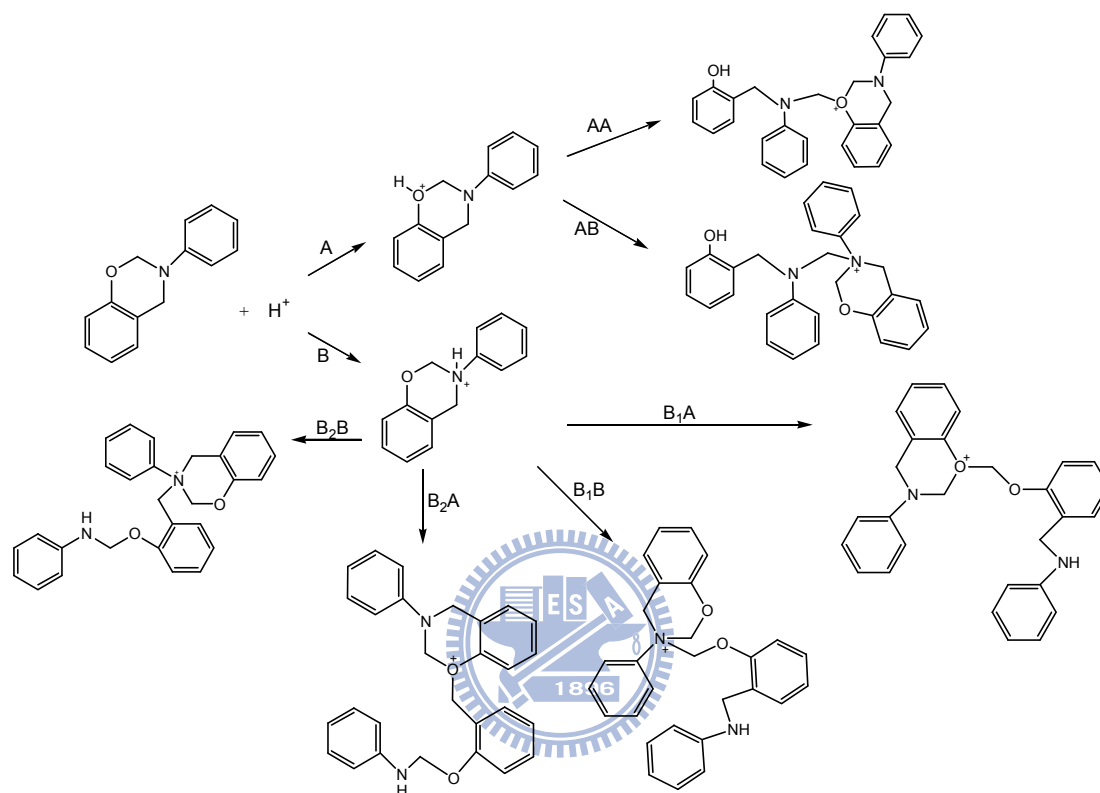
### 1.3 Polymerization of Benzoxazines and Their Blends and Composites

The ring opening reaction of the benzoxazine was first reported by Burke et al. [26] In the reaction of 1,3-dihydrobenzoxazine with a phenol, having both *ortho* and *para* positions free, it was found that aminoalkylation occurred preferentially at the free *ortho* position to form a Mannich base bridge structure, along with small amount reaction at *para* position. To explain this *ortho* preference the formation of an intermolecular hydrogen-bonded intermediate species was proposed. The typical method of polymerization of benzoxazine monomers is thermal curing without any catalyst.

#### 1.3.1 Photoinitiated Polymerization of Benzoxazines

The photoinitiated ring-opening cationic polymerization of a mono-functional benzoxazine, 3-phenyl-3,4-dihydro-2H-1,3-benzoxazine (Pa), with onium salts such as diphenyliodonium hexafluorophosphate and triphenylsulfonium hexafluoro-phosphate as initiators was investigated by Kasapoglu et al. [33] The phenolic mechanism also contributed, but its influence decreased with decreasing monomer concentration. Free radical promoted cationic polymerization of benzoxazine was also examined. The polymerization can be performed at much higher wavelengths and carbon-centered radicals formed from the photolysis of 2,2-dimethoxy-2-phenylacetophenone (DMPA),

were oxidized to produce carbocations. These carbocations are capable to initiate benzoxazine polymerizations. Scheme 1-5 describes that after addition of a proton (or carbocation) to the either heteroatom (oxygen or nitrogen) yields oxonium or ammonium cations, respectively.



Scheme 1-5. Photoinitiated polymerization of *N*-phenyl-3,4-dihydro-2*H*-1,3-benzoxazine.

### 1.3.2 Thermal Polymerization of Benzoxazines

A cross-linked network structured polybenzoxazines, with higher  $T_g$  and degradation temperature, can be obtained when di-functional or multi-functional benzoxazines undergo polymerization. The polymeric structures form due to curing of mono-functional and di-functional benzoxazines are shown in Scheme 1-1. Di-functional benzoxazines derived from diamines are expected to undergo similar cross-linking. [34,35] It has been observed that during synthesis of a difunctional

benzoxazine (from bisphenol A, formaldehyde and methyl amine) not only bisphenol-A based benzoxazine (B-m) monomer forms as major product, but also dimers and small oligomers form by the subsequent reactions between the rings and *ortho* position of bisphenol A hydroxyl groups. These free phenolic hydroxyl structure containing dimers and oligomers trigger the monomer to be self-initiated towards polymerization and cross-linking reactions. [36]

Curing reactions at two different temperatures below and above T<sub>g</sub> temperature, demonstrate that the kinetics are significantly different for the two cure temperatures. Vitrification occurs sooner at higher cure temperature than the lower cure temperature, especially below the T<sub>g</sub>. As vitrification causes a large increase in the viscosity of the system, at the reaction becomes largely diffusion controlled, and greatly affect the curing kinetics. [37]

The thermal properties of polybenzoxazines prepared from different benzoxazine monomers are list in Table 1-4. [8]



Table 1-4. Thermal properties of polybenzoxazines.

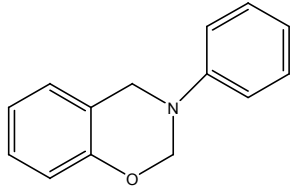
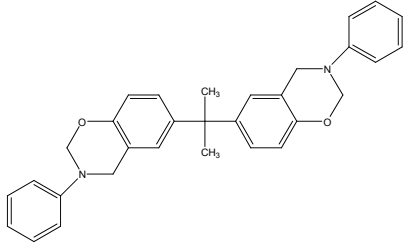
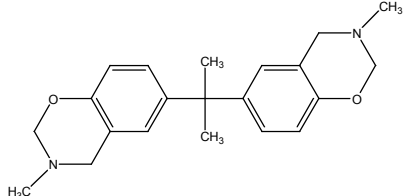
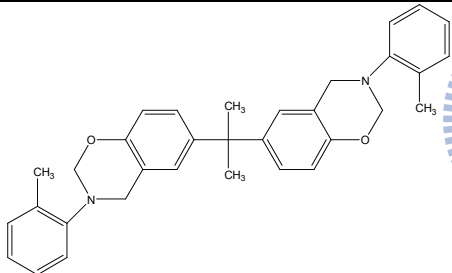
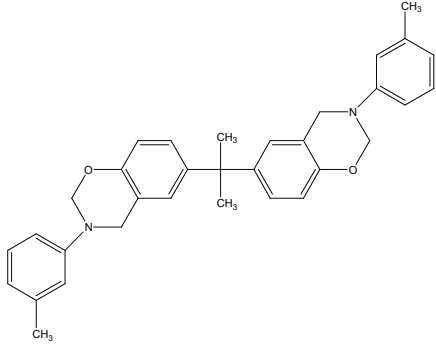
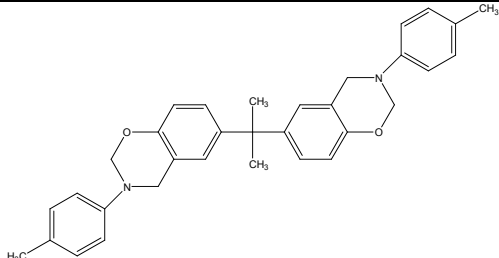
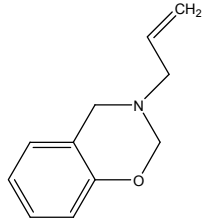
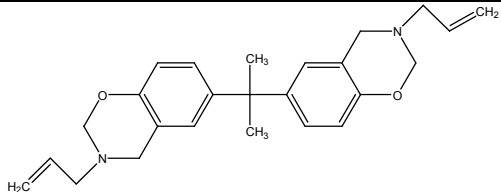
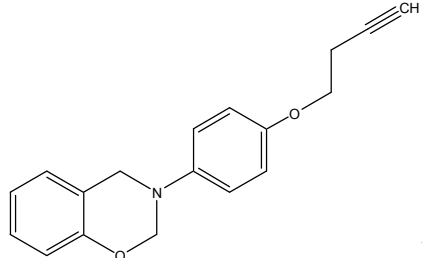
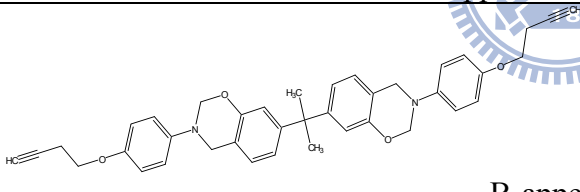
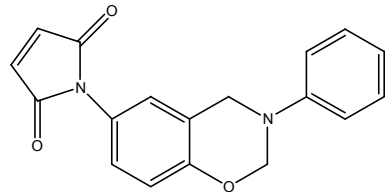
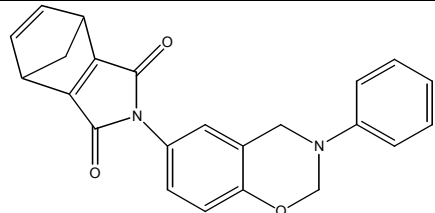
Monomers	T <sub>g</sub> ( )	T <sub>5%</sub> ( )	T <sub>10%</sub> ( )	Chard yield (%)
 <p><b>Pa</b></p>	146	342	369	44
 <p><b>Ba</b></p>	150	310	327	32
 <p><b>Bm</b></p>	170	-	-	-
 <p><b>B-ot</b></p>	228	-	-	32
 <p><b>B-mt</b></p>	209	350	-	31
 <p><b>B-pt</b></p>	158	305	-	32

Table 1-4 (continued)

Monomers	T <sub>g</sub> ( )	T <sub>5%</sub> ( )	T <sub>10%</sub> ( )	Chard yield (%)
Allyl functionalized monomer  <b>P-ala</b>	285	348	374	44
 <b>B-ala</b>	298	343	367	28
Phenyl propargyl functionalized monomers  <b>P-appe</b>	249	362	400	66
 <b>B-appe</b>	295	352	388	66
Maleimide functionalized monomers  <b>MIB</b>	252	375	392	56
 <b>NOB</b>	Above 250	365	383	58

### 1.3.3 Properties of Epoxy- Polymbenzoxazine

For the improvement of the mechanical and water resistance properties of the cured resins from benzoxazine compounds and epoxy resins, terpendiphenol-based benzoxazines were synthesized and their curing with epoxy resins was investigated. [38] It has been observed that the curing reaction did not proceed below 150 °C, but it proceeded quantitatively without curing accelerators above 180 °C. The cured resins derived from terpendiphenol-based benzoxazines exhibited higher T<sub>g</sub>, because of the hindrance of molecular chain mobility by the rigid and bulky cyclohexane ring from terpen backbone. The cured resins showed superior heat resistance, electrical insulation and specially water resistance properties compared with the epoxy resins cured by a bisphenol A novalac resin or Ba.

Agag et al. [39] described the curing behavior of an epoxy resin and benzoxazine resin. The epoxy ring opened when they reacted with the hydroxyl groups that resulted from the ring opening of benzoxazines, and construct a network structure. For blends with equal functionality of oxirane to oxazine, the ring opening of benzoxazine and the partial curing of epoxy with hydroxyl functionality was indicated by a single exotherm at temperatures of about 240 °C in DSC thermograms. For the blends with higher molar ratio of epoxy, the homopolymerization of the residual epoxy resins with secondary hydroxyl groups, resulting from the ring opening of epoxide, [40] was observed by the second exotherm appears at 300 °C in the DSC plot.

In our previous study, a new class of PBZ was developed which exhibited extremely low surface free energies—even lower than that of pure Teflon ( $\gamma_s = 21 \text{ mJ/m}^2$ )—through strong intramolecular hydrogen bonding. [41-44] Furthermore, we applied the low surface free energy material polybenzoxazine as an efficient mold-release agent for silicon molds [45] and a stable superhydrophobic surface. [42] Typically, the surface free energy in PBZ system decreases initially and then increases steadily upon increasing the curing time, indicating that the surface free energy of PBZs is not stable during curing and annealing process. In order to overcome this problem, we designed the siloxane segment into benzoxazine to improve the stability of surface free energy during high temperature storage. [46] However, Liu [47] et al. found that the addition of soft segments, bis-propyl tetramethyl disiloxane, in benzoxazines usually results in lower  $T_g$  and poorer thermal properties. Ardhyanta et al. developed a PBa-PDMS hybrids system by sol-gel process to improve the  $T_g$  above to  $200^\circ\text{C}$ . [48] Poly(imide-siloxane) was selected to blend into PBa to increase  $T_g$  was also discussed by Takeichi. [49] An imide-containing structure which was incorporated into benzoxazine could improve the thermal properties of PBZs.

In this study, we have discovered that the siloxane-imide-containing segment into benzoxazine. It possesses a relatively low surface free energy and better thermal and UV resistant properties than those polybenzoxazines lacking siloxane group after thermal crosslinking. Furthermore, the surface free energy of the polymerized polybenzoxazines is more stable during high temperature thermal curing process.



## References

- [1] Holly, F. W.; Cope, A. C. *J. Am. Chem. Soc.* **1944**, *66*, 1875.
- [2] Scheriber, H. Ger, *Offen.* 2225504, **1973**; *Offen.* 2323936, **1973**.
- [3] Riess, G.; Schwob, J. M.; Guth, G.; Roche, M.; Lande, B. in “Advances in Polymer Science” (Eds B. M. Culbertson and J. E. Mcgrath), Plenum, New York, **1986**.
- [4] Ning, X.; Ishida, H. *J. Polym. Sci., Polym. Phys. Ed.* **1994**, *32*, 921.
- [5] Ishida, H. *J. Appl. Polym. Sci.* **1995**, *58*, 1751.
- [6] Burke, W. J.; Murdoch, K. C.; Ec, G. *J. Am. Chem. Soc.* **1954**, *76*, 1677.
- [7] Burke, W. J.; Glennie, E. L. M.; Weatherbee, C. *J. Org. Chem.* **1964**, *24*, 909.
- [8] Ghosh, N. N.; Kiskan, B.; Yagci, Y. *Porg. Polym. Sci.* **2007**, *32*, 1344.
- [9] Shen, S. B.; Ishida, H. *J. Appl. Polym. Sci.* **1996**, *61*, 1595.
- [10] Dunkers, J.; Ishida, H. *J. Polym. Sci. Part A: Polym. Chem.* **1999**, *37*, 1913.
- [11] Ning, X.; Ishida, H. *J. Polym. Sci., Part A: Polym. Chem.* **1994**, *32*, 1121.
- [12] Takeichi, T.; Komiya, I.; Takayama, Y. *Kyoka-Purasutikkus* (in Japanese) **1997**, *43*, 109.
- [13] Wang, Y. X.; Ishida, H. *Polymer* **1999**, *40*, 4563.
- [14] Macko, J. A.; Ishida, H. *Polymer* **2001**, *42*, 227.
- [15] Furukawa, N. *Benzoxazine-based thermosetting polymers and their manufacture, compositions, and heat- and fire-resistant dielectric cured products with low water absorption.* Jpn. Kokai Tokkyo Koho, **2004**, p18.
- [16] Wang, Y. X.; Ishida, H. *Polym. mater. sci. eng.* **1999**, *80*, 211.
- [17] Ishida, H.; Allen, D. J. *J. Polym. Sci., Part B: Polym. Phys.* **1996**, *34*, 1019.
- [18] Kim, H. D.; Ishida, H. *J. Appl. Polym. Sci.* **2001**, *79*, 1207.
- [19] Macko, J.; Ishida, H. *J. Polym. Sci., Part B: Polym. Phys.* **2000**, *38*, 2687.
- [20] Ishida, H.; Low, H. Y. *Macromolecules* **1997**, *30*, 1099.

- [21] Ishida, H.; Rodriguez, Y. *Polymer* **1995**, *36*, 3151.
- [22] Nair, C. P. R. *Prog. Polym. Sci.* **2004**, *29*, 401.
- [23] Agag, T.; Takeichi, T. *Macromolecules* **2001**, *34*, 7257.
- [24] Burke, W. J. *J. Am. Chem. Soc.* **1949**, *71*, 609.
- [25] Burke, W. J.; Bisshop, J. L.; Glennie, E. L. M.; Bauer, W. N. *J. Org. Chem.* **1965**, *30*, 3423.
- [26] Liu, J.; Ishida, H.; In: Salamone, J. C. *A new class of phenolic resins with ring-opening polymerization. The polymeric materials encyclopedia*. Florida: CRC Press **1996**, 484.
- [27] Andre, S.; Guida-Pietrasanta, F.; Rousseau, A.; Boutevin, B.; Caporiccio, G. *J. Polym. Sci., Part A: Polym. Chem.* **2000**, *38*, 2993.
- [28] Lin, K. F.; Lin, J. S.; Cheng, C. H. *J. Polym. Sci., Part A: Polym. Chem.* **1997**, *35*, 2469.
- [29] Liang, G. Z.; Gu, A. J. *Polym. J.* **1997**, *29*, 553.
- [30] Gouri, C.; Nair, C. P. R.; Ramaswamy, R. *High Perform. Polym.* **2000**, *12*, 497.
- [31] Agag, T.; Takeichi, T. *Macromolecules* **2003**, *36*, 6010.
- [32] Thanyalak Chaisuwan H. I. *J. Appl. Polym. Sci.* **2006**, *101*, 548.
- [33] Kasapoglu, F.; Cianga, I.; Yagci, Y.; Takeichi, T. *J. Polym. Sci., Part A: Polym. Chem.* **2003**, *41*, 3320.
- [34] Xiang, H.; ling, H.; Wang, J.; Song, L.; Gu, Y. *Polym. Compos.* **2005**, *26*, 563.
- [35] Lee, Y. H.; Allen, D. J.; Ishida, H. *J. Appl. Polym. Sci.* **2006**, *100*, 2443.
- [36] Ning, X.; Ishida, H. *J. Polym. Sci., Part A: Polym. Chem.* **1994**, *32*, 1121.
- [37] Russell, V. M.; Koenig, J. L.; Low, H. Y.; Ishida, H. *J. Appl. Polym. Sci.* **1998**, *70*, 1413.
- [38] Kimura, H.; Murata, Y.; Matsumoto, A.; Hasegawa, K.; Ohtsuka, K.; Fukuda, A. *J.*

- Appl. Polym. Sci.* **1999**, 74, 2266.
- [39] Agag, T.; Takeichi, T. *Perform. Polym.* **2002**, 14, 115.
- [40] Agag, T.; Takeichi, T. *Polymer* **1999**, 40, 6557.
- [41] Wang, Y. X.; Ishida, H. *J. Appl. Polym. Sci.* **2001**, 79, 2331.
- [42] Wang, C. F.; Wang, Y. T.; Tung, P. H.; Kuo, S. W.; Lin, C. H.; Sheen, Y. C. and Chang, F. C. *Langmuir* **2006**, 22, 8289.
- [43] Liao, C. S.; Wu, J. S.; Wang, C. F. and Chang, F. C. *Macromol Rapid Commun* **2008**, 29, 56.
- [44] Liao, C. S.; Wang, C. F.; Lin, H. C.; Chou, H. Y. and Chang, F. C., *J Phys Chem C* **2008**, 112, 16189.
- [45] Wang, C. F.; Chiou, S. F.; Ko, F. H.; Chen, J. K.; Chou, C. T.; Huang, C. F.; Kuo, S. W. and Chang, F. C. *Langmuir* **2007**, 23, 5868.
- [46] Chen, K. C.; Li, H. T.; Chen, W. B. and Huang, S. C. *11<sup>th</sup> Pacific Polymer Conference* **2009**.
- [47] Liu, Y. L.; Hsu, C. W. and Chou, C. I. *J Polym Sci Part A: Polym Chem* **2007**, 45, 1007.
- [48] Ardhyanta, H.; Wahid, M. H.; Sasaki, M.; Agag, T.; Kawauchi, T.; Ismail, H. and Takeichi, T. *Polymer* **2008**, 49, 4585.
- [49] Takeichi, T.; Agag, T. and Zeidam, R. *J Polym Sci Part A: Polym Chem* **2001**, 39, 2633.

## Chapter 2

### Synthesis of Siloxane-Imide-Containing Benzoxazines

Holly and Cope [1] first reported the condensation reaction of primary amines with formaldehyde and substituted phenols for the synthesis of well defined benzoxazine monomers. Benzoxazine monomers are typically synthesized using phenol, formaldehyde and amine (aliphatic or aromatic) as starting materials either by employing solution or solventless methods. Various types of benzoxazine monomer can be synthesized using various phenols and amines with different substitution groups attached. These substitution groups can provide additional polymerizable sites and also affect the curing process. Consequently, polymeric materials with desired properties may be obtained by tailoring the benzoxazine monomer. Mono-functional, di-functional and multifunctional benzoxazine monomers could be obtained from different designed starting materials. [2]

In this section, we prepared different molecular weight of di-functional siloxane-imide-containing benzoxazine monomers from synthesized siloxane-containing dihydroxyl precursors and aniline and paraformaldehyde.

#### 2.1 Synthesis of Siloxane-Imide-Containing Benzoxazine (BZ-A1)

##### 2.1.1 Materials and Characterization

1, 4-Dioxane and paraformaldehyde (95%) were purchased from TEDIA (USA) and Showa Chemicals (Japan), respectively. Ethyl acetate (99.9%) was used as received from Mallinckrodt, Inc. (USA). Aniline (99%), ethylene glycol ( $\geq 99\%$ ), and diiodomethane (99%) were obtained from Aldrich (USA). The bifunctional bisphenol

A-type benzoxazine (Ba, Figure 2-1) was purchased from Shikoku Chemicals (Japan).

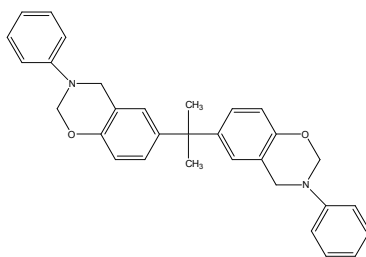


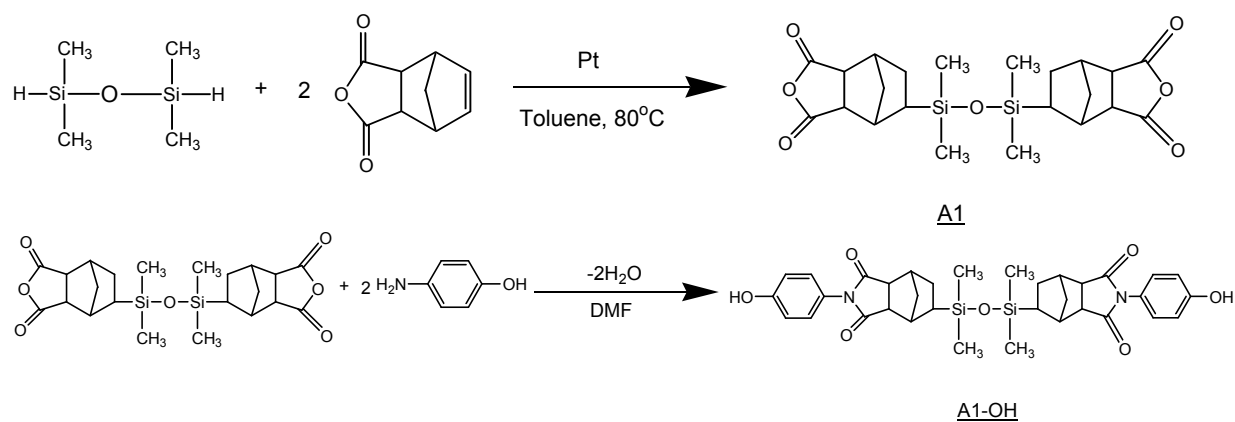
Figure 2-1. Structure of the bifunctional bisphenol A-type benzoxazine Ba.

FTIR spectra were recorded using a Nicolet Avatar 320 FTIR Spectrophotometer. The sample was prepared by casting the BZ-A1 monomer solution directly onto a potassium bromide plate and evaporated THF at 50 °C under vacuum. The spectrometer was operated in transmission mode utilizing the 32 scans at a resolution of 2 cm<sup>-1</sup>. <sup>1</sup>H NMR spectra were recorded using a Varian UNITY Inova-400NMR Spectrometer operating at a proton frequency of 400 MHz and CDCl<sub>3</sub> as the solvent. Molecular weights were determined using a TRIO-2000 liquid chromatograph/mass spectrometer and a DB-5MS column.

### 2.1.2 Synthesis of the siloxane-containing dihydroxyl (A1-OH)

The siloxane-imide-containing dianhydride A1 and the siloxane-containing dihydroxyl compound A1-OH were synthesized according to the method reported by Li et al. [3] (Scheme 2-1). The siloxane-imide-containing dianhydride (A1) (30g, 0.065 mol) was dissolved in 90ml of dimethyl-formamide (DMF), and 4-aminophenol (14.9g, 0.136mol) in 40ml of DMF was gradually added. The solution was stirred for 6 hrs at ice-bath conditions, followed by imidization using a Dean-Stark instrument at 130 °C reflux for 4 hrs. A 1-OH in solid powder was obtained after vacuum drying, and

it was recrystallized from isopropanol (38g, yield = 91%, mp = 123 °C).



Scheme 2-1. Preparation of the siloxane-imide-containing dianhydride (**A1**) and dihydroxyl compound (**A1-OH**)

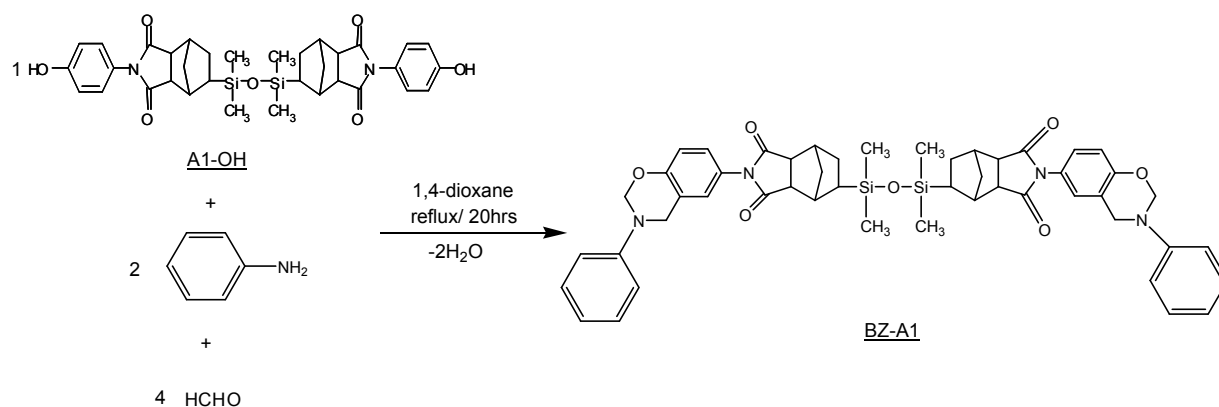
The chemical structure of the light brown powder, **A1-OH**, was confirmed from <sup>1</sup>H-NMR and FT-IR. <sup>1</sup>H-NMR (CDCl<sub>3</sub>, ppm) δ: 0.01-0.02 (m, 12H), 0.61 (m, 2H), 1.54-1.62 (m, 8H), 2.74 (m, 2H), 2.78 (m, 2H), 3.12-3.17 (m, 4H), 6.70-6.73 (d, 4H), 6.90-6.94 (d, 4H), 7.42 (s, 2H). FT-IR: imide 1789 and 1720 cm<sup>-1</sup>, OH 3100-3500 cm<sup>-1</sup> (yield: 88%)

### 2.1.3 Synthesis of the siloxane-imide-containing benzoxazine

#### *N,N'*-bis(*N*-phenyl-3,4-dihydro-2*H*-benzo[1,3]oxazine)-5,5'-bis(1,1',3,3'-tetramethyldisiloxane-1,3-diyl)-bis(norborane-2,3-dicarboximide) (**BZ-A1**)

Aniline (1.88 g, 0.02 mol) was added dropwise into a mixture of **A1-OH** (6.44 g, 0.01 mol), paraformaldehyde (1.26 g, 0.04 mol), and 1,4-dioxane (100 mL) in a 250-mL round-bottom flask equipped with a magnetic stirrer bar. (Scheme 2-2) The mixture was then heated under reflux at 115 °C for 20 hrs, and gradually became homogeneous and turning dark brown. The resulting mixture was filtered and the solvent was evaporated under vacuum. The residue was dissolved in ethyl acetate and

washed five times sequentially with 1 N aqueous NaOH and distilled water. Evaporation of the solvent and vacuum drying in an oven provided BZ-A1 as a brown powder (73.0%).



Scheme 2-2. Preparation of the siloxane-imide-containing benzoxazine monomer

#### BZ-A1 from A1 and A1-OH

BZ-A1 was prepared according to Scheme 2 and its chemical structure was confirmed using FT-IR and  $^1\text{H}$  NMR spectroscopies and liquid chromatography/mass spectrometry (LC-MS). The IR spectrum of BZ-A1 (Figure 2-2) displays characteristic absorptions of a benzoxazine structure at  $1498\text{ cm}^{-1}$  and  $1030\text{ cm}^{-1}$  (vibrations of the trisubstituted benzene ring),  $1328\text{ cm}^{-1}$  ( $\text{CH}_2$  wagging of the oxazine unit) and  $1230\text{ cm}^{-1}$  (asymmetric C–O–C stretching). The  $^1\text{H}$  NMR spectrum of BZ-A1 (Figure 2-3) displays aromatic protons at 6.60–7.40 ppm and characteristic peaks attributed to methylene units (oxazine Ar- $\text{CH}_2$ -N) at 5.30 and 4.60 ppm, respectively. LC-MS (Figure 2-4) provided a molecular weight of 881.1 g/mol, consistent with the calculated formula weight.

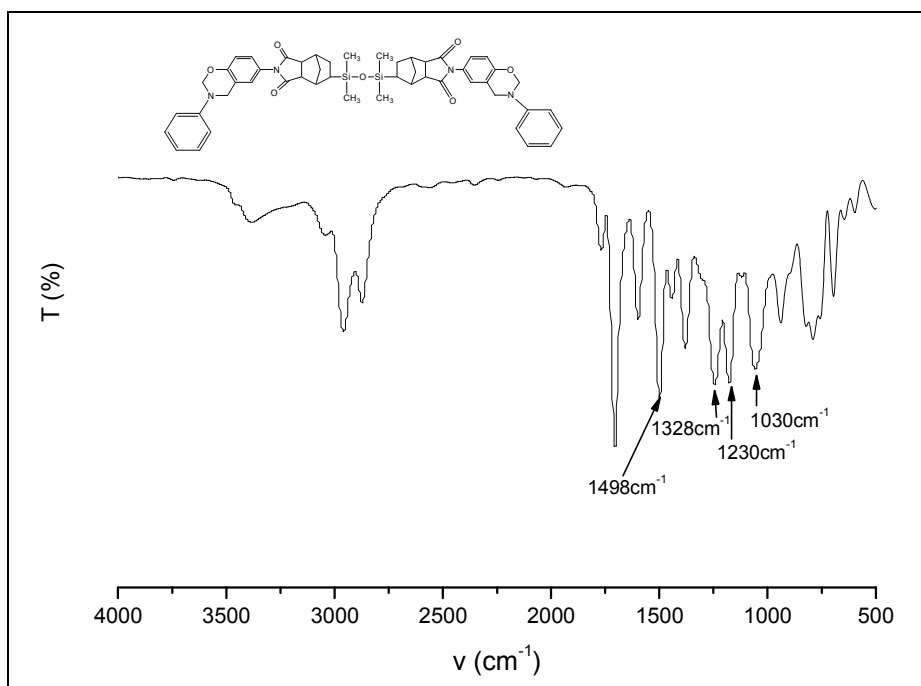


Figure 2-2. IR spectrum of the siloxane-imide-containing benzoxazine BZ-A1.

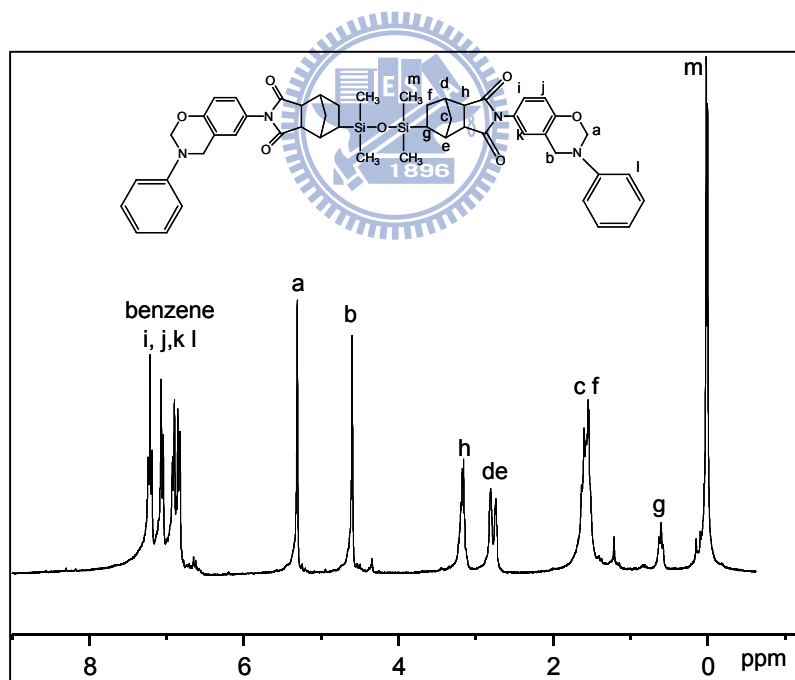


Figure 2-3.  $^1\text{H}$  NMR spectrum of the siloxane-imide-containing benzoxazine BZ-A1.



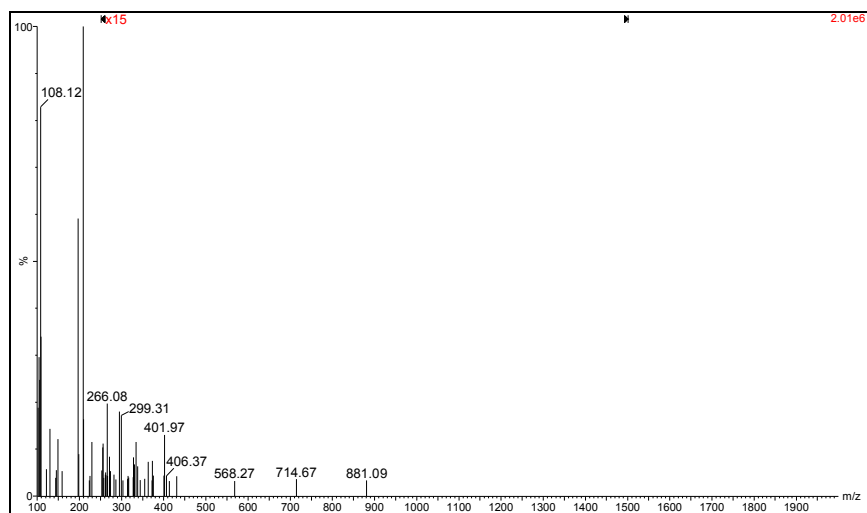


Figure 2-4. LC/Mass spectrum of the siloxane-imide-containing benzoxazine BZ-A1.



## 2.2 Synthesis of Siloxane-Imide-Containing Benzoxazine (BZ-A6)

### 2.2.1 Materials

5-Norbornene-2, 3-dicarboxylic anhydride (nadic anhydride) was purchased from Alfa Aesar (USA). Hydride-terminated polydimethylsiloxane, DMS-H03, was purchased from Gelest (USA) with molecular weight of ca. 400–500. Platinum divinyltetramethyldisiloxane complex was purchased from Gelest (USA). All chemicals were purified prior to use. 1,4-Dioxane and paraformaldehyde (95%) were purchased from TEDIA (USA) and Showa Chemicals (Japan), respectively. Ethyl acetate (EtOAc, 99.9%) was used as received from Mallinckrodt (USA). Aniline (99%), ethylene glycol (EG,  $\geq 99\%$ ), and diiodomethane (DIM, 99%) were obtained from Aldrich (USA).



### 2.2.2 Synthesis of dinoborane anhydride terminated polydimethylsiloxane (A6)

The synthesis of the siloxane-imide-containing dianhydride A1 has been reported in the literature. [3, 4] The higher-molecular-weight siloxane-imide-containing dianhydride, which is called A6, was prepared with reference to these previous methods. Pt catalyst (0.8 mL) was added dropwisely into a solution of nadic anhydride (82.1 g) in toluene (400 mL) in a three-neck round-bottom flask while stirring with a magnetic stirrer bar. DMS-H03 (112.5 g) was gradually added into the solution and then heated react to 70 °C for 48 hrs. The resulting mixture was filtered and the solvent was evaporated under vacuum. After the removal of residue nadic anhydride, A6 was obtained as a transparent liquid (yield: 75.0%). The chemical structure of the transparent liquid product, A6, was confirmed with  $^1\text{H-NMR}$  (Varian UNITY Inova-400NMR spectrometer) and FT-IR (Perkin Elmer, Spectrum one).  $^1\text{H-NMR}$

(CDCl<sub>3</sub>, 400 MHz)  $\delta$ : 0.03~0.05 ppm (12H, CH<sub>3</sub>-Si-CH<sub>3</sub>), 0.65 ppm (2H, -CH-Si-), 1.55~1.66 ppm (8H, cyclopentane CH<sub>2</sub>), 3.39~3.43 ppm (4H, -C(=O)). FT-IR (KBr): 1859 cm<sup>-1</sup>, 1778 cm<sup>-1</sup> (anhydride, C=O stretching), 1222 cm<sup>-1</sup> (C-Si stretching), 1078 cm<sup>-1</sup> (Si-O-Si stretching); no 1680 cm<sup>-1</sup> (norborane, C=C stretching) or 2150 cm<sup>-1</sup> (Si-H, stretching).

### 2.2.3 Imidization of siloxane-imide-containing dianhydride (A6-OH)

4-Aminophenol (5.3 g, 0.0484 mol) in DMF (30 mL) was added gradually to a stirred solution of the siloxane-imide-containing dianhydride A6 (16.5 g, 0.022 mol) in dimethylformamide (DMF, 30 mL) in a 250-mL round-bottom flask (Scheme 2-3). The solution was stirred for 6 hrs in an ice-bath and the imidization was performed using a Dean-Stark apparatus. A6-OH was obtained as a viscous dark brown liquid after vacuum drying (yield: 86.8%). <sup>1</sup>H-NMR (CDCl<sub>3</sub>)  $\delta$ : 0.03~0.08 ppm (12H, CH<sub>3</sub>-Si-CH<sub>3</sub>), 0.65 ppm (2H, -CH-Si-), 1.55~1.66 ppm (8H, cyclopentane CH<sub>2</sub>), 6.23 ppm (2H, aromatic C-OH), 6.73~6.96 ppm (8H, benzene). FT-IR (KBr): 1720 cm<sup>-1</sup> (imide), 3100~3500 cm<sup>-1</sup> (OH, broad band).

### 2.2.4 Synthesis of siloxane-imide-containing benzoxazine (BZ-A6)

Aniline (3.8 g, 0.04 mol) was added dropwisely into a mixture of A6-OH (18.95 g, 0.02 mole), paraformaldehyde (2.4 g, 0.08 mole), and 1,4-dioxane (120 ml) in a 250 ml round-bottom flask equipped with a magnetic stirrer bar (Scheme 2-4). The mixture was then heated under reflux at 115 °C for 20 hrs, gradually becoming homogeneous and turning dark brown. The resulting mixture was filtered and the solvent was evaporated under vacuum. The residue was dissolved in ethyl acetate and washed five times sequentially with 0.5 N aqueous NaOH and distilled water. Evaporation of the

solvent and vacuum drying in an oven provided BZ-A6 as a viscous dark brown liquid product (yield: 87.7%).  $^1\text{H-NMR}$  ( $\text{CDCl}_3$ ) (Figure 2-5)  $\delta$ : 6.70~7.30 ppm (aromatic protons), 5.35 ppm ( $\text{OCH}_2\text{N}$ ), 4.65 ppm ( $\text{Ar-CH}_2\text{-N}$ ). FT-IR (KBr) (Figure 2-6):  $1256\text{ cm}^{-1}$  ( $\text{C-O-C}$ , stretching),  $1178\text{ cm}^{-1}$  ( $\text{C-N-C}$ , stretching),  $1307\text{ cm}^{-1}$  ( $\text{CH}_2$ , wagging of oxazine),  $1502\text{ cm}^{-1}$  (trisubstituted benzene ring).

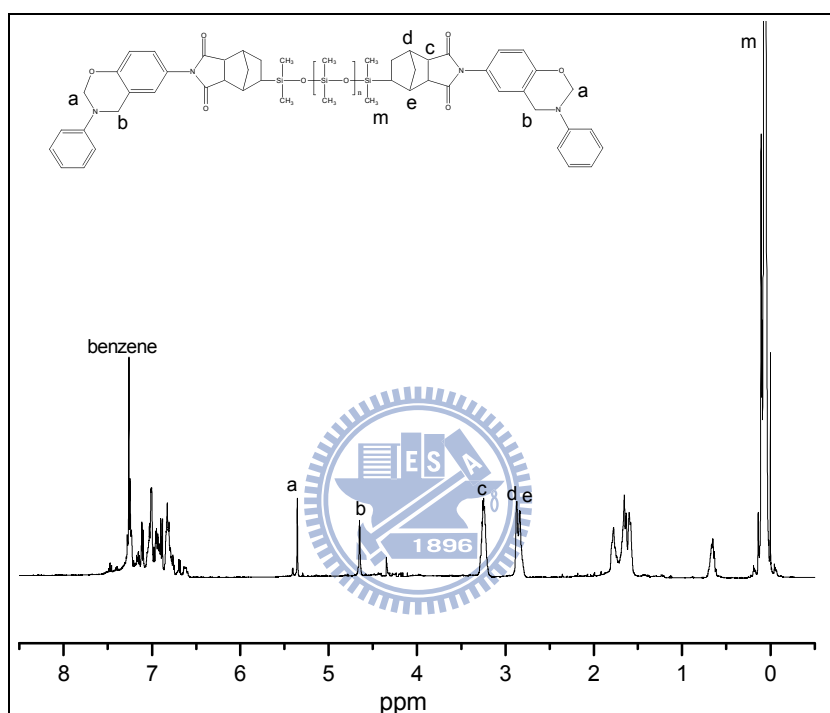


Figure 2-5.  $^1\text{H-NMR}$  spectrum of the siloxane-imide-containing benzoxazine BZ-A6.

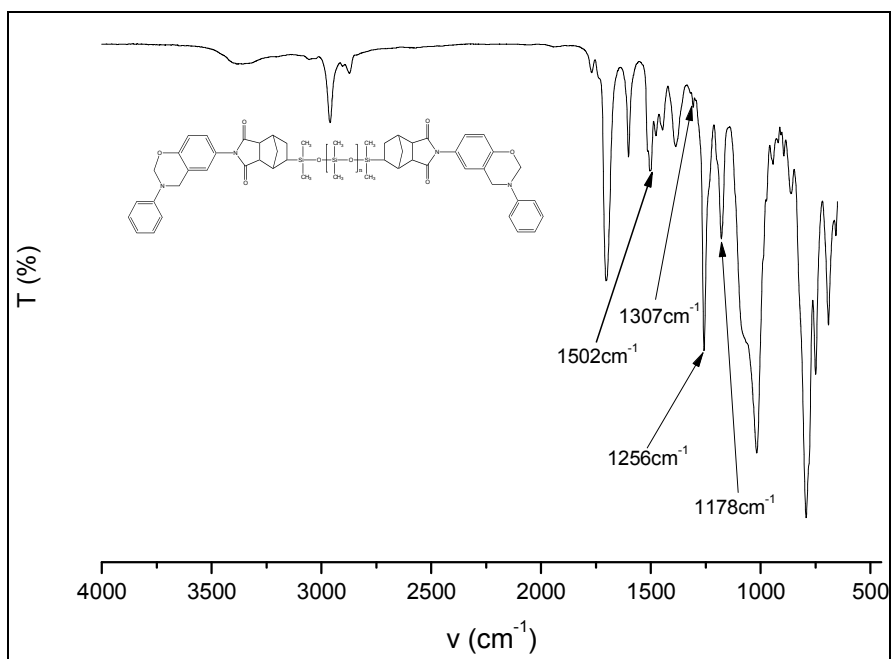
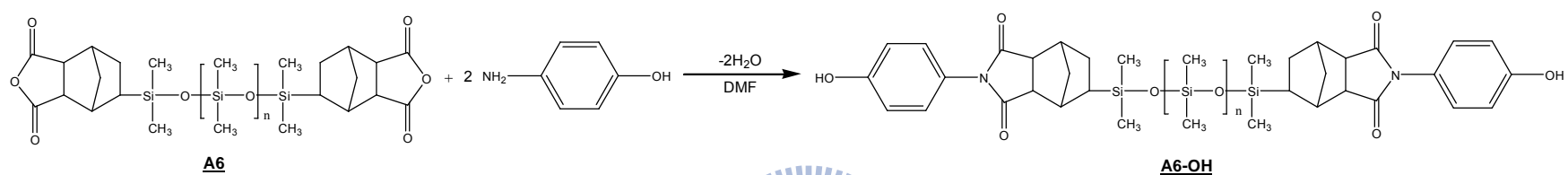
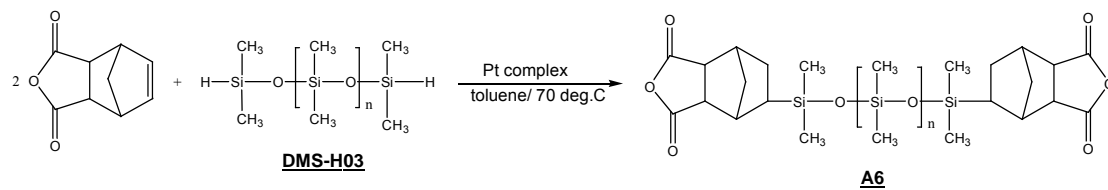
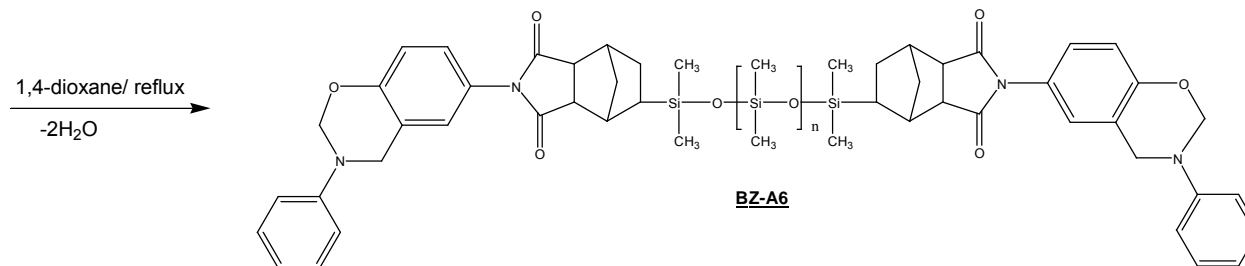
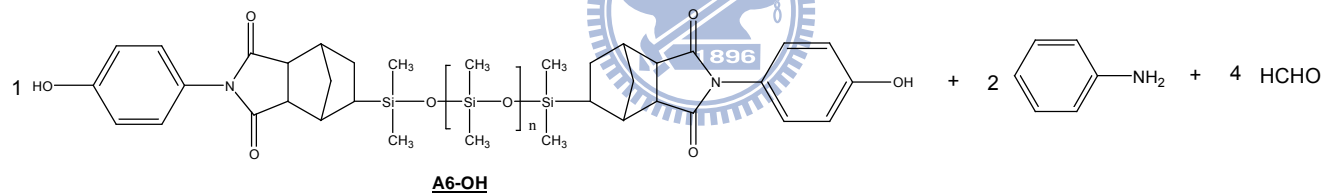


Figure 2-6. FT-IR spectrum of the siloxane-imide-containing benzoxazine BZ-A6.





Scheme 2-3. Syntheses of compounds A6 and A6-OH



Scheme 2-4. Preparation of compound BZ-A6

## References

- [1] Holly, F. W.; Cope, A. C. *J. Am. Chem. Soc.* **1944**, *66*, 1875.
- [2] Ghosh, N. N.; Kiskan, B.; Yagci, Y. *Porg. Polym. Sci.* **2007**, *32*, 1344.
- [3] Li, H.T; Chang H.R.; Wang, M. W; and Lin, M. S. *Polym Int* **2005**, *54*, 1416.
- [4] Eddy, V. J; Hallgren, J. E. and Robert, E. *J Polym Sci Part A: Polym Chem* **1990**, *28*, 2417.



## Chapter 3

### Curing Behavior of Siloxane-Imide-Containing Benzoxazines

To understand the polymerization reaction of benzoxazines, an understanding of the chemical structure of its oxazine ring is very important. The ring opening of the benzoxazine was first discussed by Burke et al. [1] In the reaction of 1,3-dihydrobenzoxazine with a phenol, having both *ortho* and *para* position free, it was found that aminoalkylation occurred preferentially at the free *ortho* position to form a Mannich base bridge structure, along with small amount reaction at *para* position. A cross-linked network structured polybenzoxazines, with higher Tg and degradation temperature, can be obtained when benzoxazines undergo polymerization. It has been observed that during synthesis of a difunctional benzoxazine (from bisphenol A, formaldehyde and aniline) form by the subsequent reactions between the rings and ortho position of bisphenol A hydroxyl groups. These free phenolic hydroxyl structure containing dimers and oligomers trigger the monomer to be self-initiated towards polymerization and crosslinking reactions. [2] The curing behavior of siloxane-imide-containing benzoxazines, BZ-A1 and BZ-A6, are discussed in this section.

#### 3.1 Curing behavior of the siloxane-imide-containing benzoxazine BZ-A1

Typically, benzoxazines undergo exothermic ring opening reactions at ca. 200–250 °C, which can be monitored using DSC. DSC was performed using a TA Instrument DSC-Q10 apparatus operated at a heating rate of 10 °C/min under a N<sub>2</sub>



atmosphere. The gas flow rate was 40ml/ min. Benzoxazine samples of approximately 5 mg were scanned in hermetic aluminum sample pans. The reaction point of the bisphenol A–type benzoxazine Ba is 228.7 °C; the energy of the exothermic ring opening reaction is 296.0 J/g (Figure 3-1). The thermogram of BZ-A1 in Figure 3-1 reveals a ring opening exothermic reaction having an onset temperature at 194.9 °C and a peak point at 232.7 °C. The exothermic energy of BZ-A1 is 173.7 J/g; i.e., it is lower than that of Ba, presumably due to molecular weight effect, molecular weight of BZ-A1 (879 g/mol) is significantly higher than that of Ba (462 g/mol). The PBZs of Ba (PBa) and BZ-A1 (PBZ-A1) were then cured in an oven under the curing conditions listed in Table 3-1.

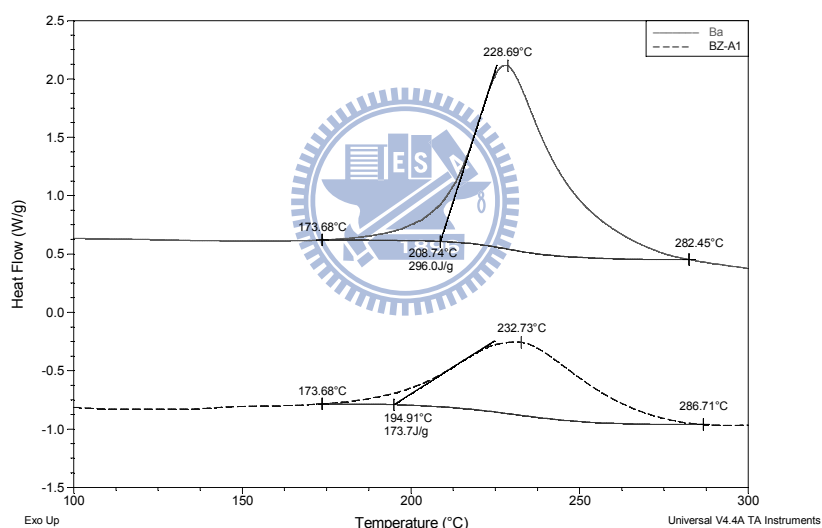


Figure 3-1. DSC thermograms of Ba and BZ-A1.

Table 3-1. Curing conditions for PBZs

Benzoxazine	Ba	BZ-A1
Curing conditions	200 °C/2 hrs + 230 °C/2 hrs	
	200 °C /2 hrs + 230 °C/4 hrs	
	200 °C /2 hrs + 230 °C/6 hrs	

PBZs usually exhibit good thermal properties after polymerization. [3] The glass transition temperature of PBZ-A1 after cross-linking was 186.1 °C (Figure 3-2), which is substantially higher than that of typical PBZs (PBa:  $T_g = 150.0$  ). [4] In general, the longer and flexible of siloxane segments in the matrix structure results in lower of  $T_g$  ( $T_g$  from  $\tan \delta$  peak of CP-F-Bz/BATMS-Bz-100 is 116 ) as discussed by Liu et al. [5] Our PBZ-A1 structure features both siloxane and imide segments in the benzoxazine monomer where the imide segment tends to raise the glass transition temperature.

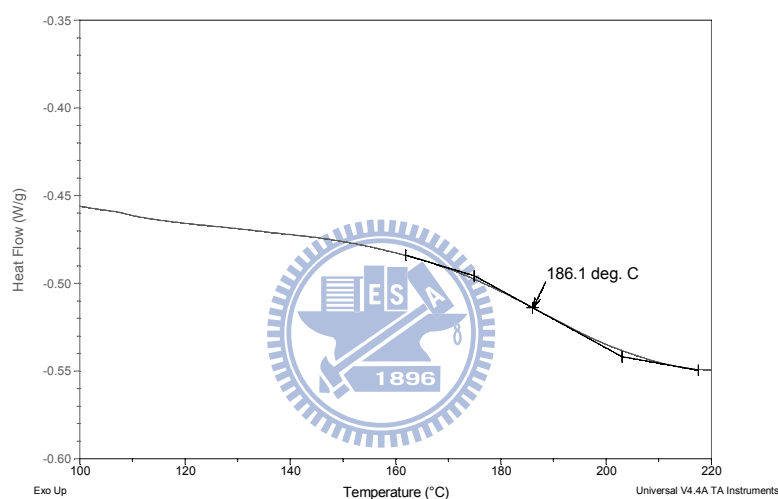


Figure 3-2. Glass transition temperature ( $T_g$ ) of PBZ-A1, determined from the DSC trace.

### 3.2 Curing behavior of the siloxane-imide-containing benzoxazine BZ-A6

In general, benzoxazines undergo exothermic ring opening at temperatures of ca. 200–250 °C [6-9] which can be monitored using DSC. The thermogram of BZ-A6 in Figure 3-3 reveals a ring opening exothermic reaction having an onset temperature at 153.7 °C and a peak maximum at 214.2 °C with exothermic energy of 57.9 J/g. After curing at 200 for 2 hrs, the reaction heat is decreased to be 37.9 J/g from 57.9 J/g. We performed the polymerization of BZ-A6 using a two-step process; the first step

involved benzoxazine ring opening at 200 °C and the second involved post curing at a 230 °C. PBZs were cured in an oven under the curing conditions listed in Table 3-2.

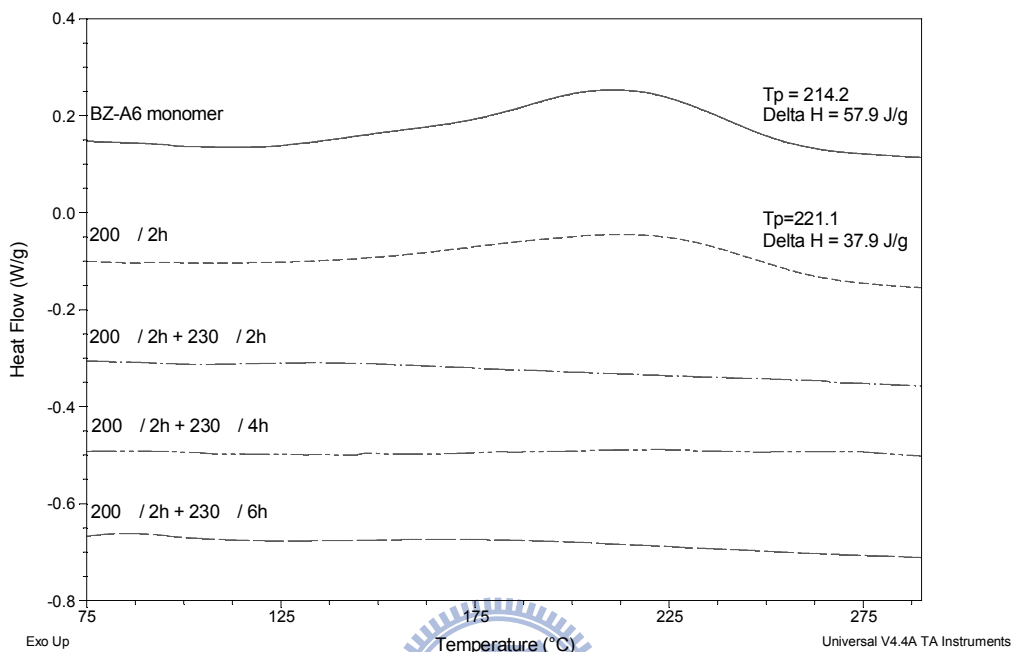


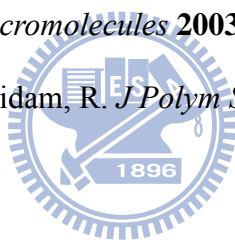
Figure 3-3. DSC thermograms of BZ-A6 monomer and polymerized BZ-A6 (after curing).

Table 3-2. Curing conditions for PBZs

Benzoxazine	Ba	BZ-A1	BZ-A6
Curing conditions	200 °C/2 hrs + 230 °C/2 hrs		
	200 °C/2 hrs+ 230 °C/4 hrs		
	200 °C/2 hrs+ 230 °C/6 hrs		

## References

- [1] Burke, W. J.; Bishop, J. L.; Glennie, E. L. M.; Bauer, W. N. *J. Org. Chem.* **1965**, *30*, 3423.
- [2] Ning, X.; Ishida, H. *J. Polym. Sci., Part A: Polym. Chem.* **1994**, *32*, 1121.
- [3] Ghosh, N. N.; Kiskan, B. and Yagci, Y. *Prog Polym Sci* **2007**, *32*, 1344.
- [4] Ishida, H. and Allen, D. J. *J Polym Sci Part B: Polym Phys* **1996**, *34*, 1019.
- [5] Liu, Y. L.; Hsu, C. W. and Chou, C. I. *J Polym Sci Part A: Polym Chem* **2007**, *45*, 1007.
- [6] Chen, K. C.; Li, H. T.; Chen, W. B.; Liao, C. H.; Sun, K. W. and Chang, F. C. *Polym Int* in press
- [7] Takeichi, T.; Kano, T and Agag, T. *Polymer* **2005**, *46*, 12172.
- [8] Agag, T. and Takeichi, T. *Macromolecules* **2003**, *36*, 6010.
- [9] Takeichi, T.; Agag, T. and Zeidam, R. *J Polym Sci Part A: Polym Chem* **2001**, *39*, 2633.



## Chapter 4

### Thermal/ Mechanical Properties of Siloxane-Imide-Containing Polybenzoxazines

The physical, mechanical and thermal properties of polybenzoxazines are primarily decided by the nature of the diphenol and diamine. The properties of polybenzoxazines are shown to compare very favorably with those of conventional phenolic and epoxy resins. DMA reveals that these candidate resins for composite applications possess high modulus and glass transition temperatures. Long-term immersion studies indicate that they have low water absorption and low saturation compact. Impact, tensile and flexural properties are also good. [1] BZs are cured usually in the temperature window of 160-220 °C. The polymer exhibit T<sub>g</sub> in the range 160-340 °C depending on the structure, and have higher stability. The high TGA decomposition onset temperature and char yield are attributed to the very strong intramolecular H-bonding between phenolic OH and the Mannich bridge. [2]

In this section, we discussed the thermal and mechanical properties of polymerized siloxane-imide-containing PBZ-A1 and PBZ-A6.

#### 4.1 Thermal stability of the poly-siloxane-imide-containing benzoxazine PBZ-A1

##### 4.1.1 Materials and Characterization

The bifunctional bisphenol A-type benzoxazine (Ba, Figure 4-1) was purchased from Shikoku Chemicals (Japan). The siloxane-imide-containing benzoxazine, BZ-A1, was synthesized from the according method in chapter 2, the structure is shown in

Figure 4-2. DSC was performed using a TA Instrument DSC-Q10 apparatus operated at a heating rate of 10 °C/min under a N<sub>2</sub> atmosphere. The gas flow rate was 40ml/ min. Benzoxazine samples of approximately 5 mg were scanned in hermetic aluminum sample pans. TGA was performed using a TA Instrument TGA-Q500 apparatus operated at a heating rate of 20 °C/min under an atmosphere of N<sub>2</sub> or air, respectively. An energy dispersive system (EDS) was used for element test, which was recorded using an LEO-1530 FE-SEM system.

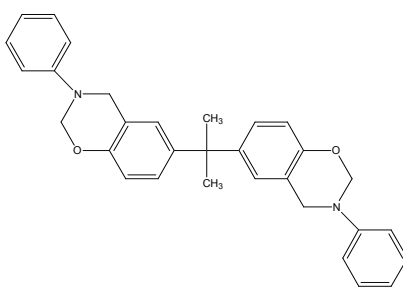


Figure 4-1. Structure of the bifunctional bisphenol A-type benzoxazine Ba.

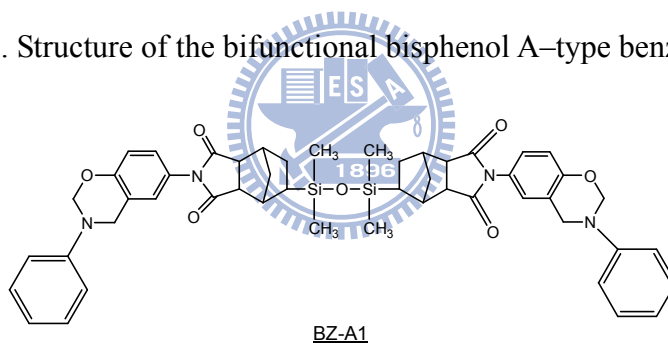


Figure 4-2. Structure of the BZ-A1.

#### 4.1.2 TGA of the poly-siloxane-imide-containing benzoxazine PBZ-A1

PBZs usually exhibit good thermal properties after polymerization. [3] The glass transition temperature of PBZ-A1 after cross-linking was 186.1 °C (Figure 4-3), which is substantially higher than that of typical PBZs (PBa:  $T_g = 150.0$  ). [4] In general, the longer and flexible of siloxane segments in the matrix structure results in lower of  $T_g$  ( $T_g$  from  $\tan \delta$  peak of CP-F-Bz/BATMS-Bz-100 is 116 ) as discussed by Liu et al. [5] Our PBZ-A1 structure features both siloxane and imide segments in the

benzoxazine monomer where the imide segment tends to raise the glass transition temperature.

Bisphenol-A is one of the phenolic compounds often used as the starting material for the synthesized of polybenzoxazines. PBa shows high decomposed temperature ( $T_{5\%}$  c.a. 300-330 °C) and high char yield (c.a. 30-42 %) from TGA. [3, 6-9] Liu et al. [5] investigated that siloxane-containing polybenzoxazine, CP-F-Bz/BATMS-Bz-100, has  $T_d$  at 369 °C in air. Figure 4-4 displays TGA thermograms recorded in air and results are summarized in Table 4-1. The 5% and 10% weight loss temperatures ( $T_{5\% \text{ loss}}$  and  $T_{10\% \text{ loss}}$ , respectively) for PBZ-A1 cured at 200 °C/ 2hrs and 230 °C/ 2hrs were 380.1 °C and 441.1 °C, respectively, which are both higher than those of PBa or siloxane-containing polybenzoxazine. The PBZ-A1 shows higher thermal stability than PBa because of the presence of the siloxane-imide-containing segment. In Liu et al. siloxane-containing polybenzoxazine TGA study, they found high thermal stability silica layers formation during the thermal oxidation process and the layer structured protect the polybenzoxazine. [10] PBa-PDMS hybrids was investigated that introduced PDMS into PBa results in the improvement of thermal stability of the hybrid. [11] The better thermal stability of PBZ-A1 with higher decomposed temperature and high char amount is come from siloxane and imide group.

In contrast, the presence of siloxane-imide groups improved the thermo-oxidative stability of the benzoxazine by increasing the char yield to 10–12 wt% in air. This char yield is close to the content of inorganic content (Si–O–Si, 8.2%) in the BZ-A1 structure. EDS analysis was employed to analyze the elemental composition of the PBZ-A1 residue after TGA testing in air. Figure 4-5 displays an image of the residue from PBZ-A1 and its EDS data. The silicone content in the residue was significantly higher than those of C and O atom, the residue from PBZ-A1 after TGA testing in air

was primarily inorganic in nature. Thus, the siloxane units of BZ-A1 provide an inorganic content in its structure, therefore, improve its thermo-stability properties after cross-linking.

The same phenomena occurred in the TGA thermograms recorded under a N<sub>2</sub> atmosphere (Figure 4-6, Table 4-2). The 5% weight loss temperature of PBa was ca. 328–337 °C under the N<sub>2</sub> atmosphere, whereas that of PBZ-A1 was significantly higher (ca. 355–362 °C). The temperatures for 5 and 10 wt% losses of PBZ-A1 were both higher than those for PBa. PBZ-A1 also featured a high weight residue after high temperature decomposition. The char yield of PBZ-A1 after curing at 200 °C for 2 hrs and then 230 °C for 2 hrs was high (48.0 %), i.e., it was improved by the presence of the siloxane-imide groups. It appears that the PBZ-A1 has the potential use as flame-retardant material.

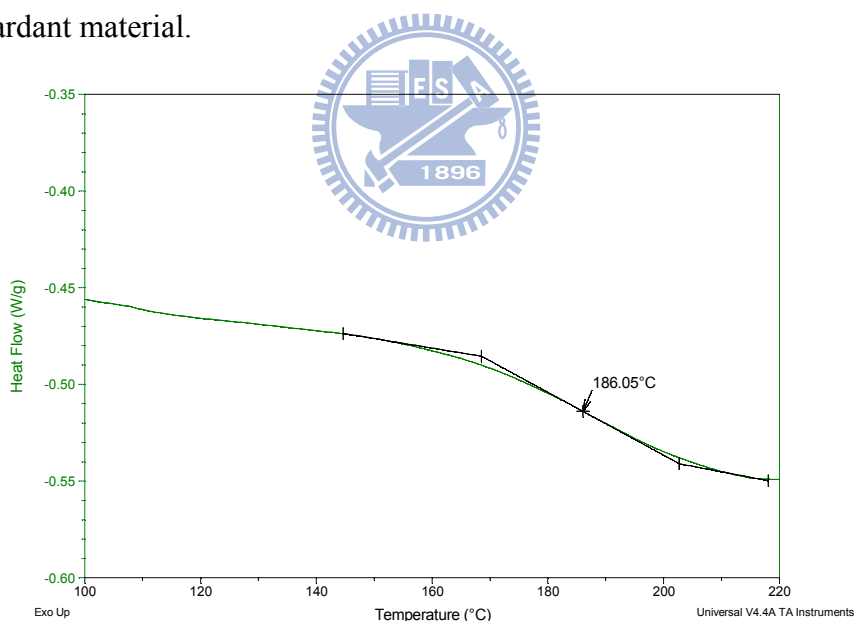


Figure 4-3. Glass transition temperature ( $T_g$ ) of PBZ-A1, determined from the DSC trace.



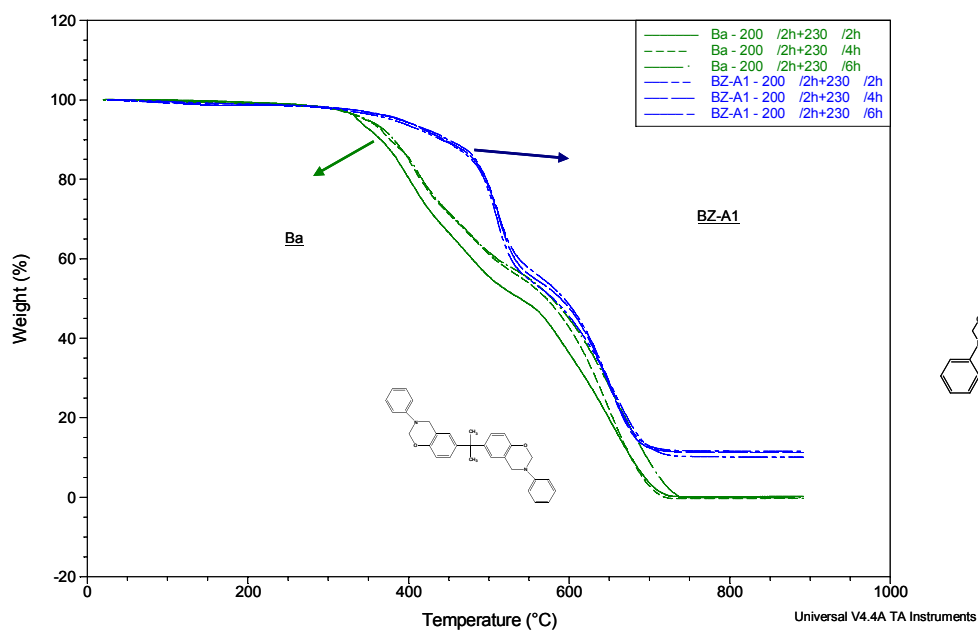


Figure 4-4. TGA thermograms of PBa and PBZ-A1 (in air).

Table 4-1. Thermostabilities of the cured PBZs PBa and PBZ-A1 (in air)

Polymer	Curing Conditions	T <sub>5% loss</sub> (°C)	T <sub>10% loss</sub> (°C)	T <sub>d</sub> (°C)	Char Yield at 850 °C
PBa	200 °C/2 hrs + 230 °C/2 hrs	337.3	365.5	349.3	0.2%
	200 °C / 2 hrs + 230 °C/4 hrs	347.0	376.8	346.4	-0.3%
	200 °C / 2 hrs + 230 °C/6 hrs	349.1	382.1	357.9	-0.1%
PBZ-A1	200 °C/2 hrs + 230 °C/2 hrs	380.1	441.1	472.2	10.1%
	200 °C / 2 hrs + 230 °C/4 hrs	389.4	444.2	480.7	11.3%
	200 °C / 2 hrs + 230 °C/6 hrs	392.0	449.3	478.1	12.0%

T<sub>5% loss</sub>: Temperature at which the weight loss was 5%.

T<sub>10% loss</sub>: Temperature at which the weight loss was 10%.

T<sub>d</sub>: Decomposition temperature, onset point temperature.

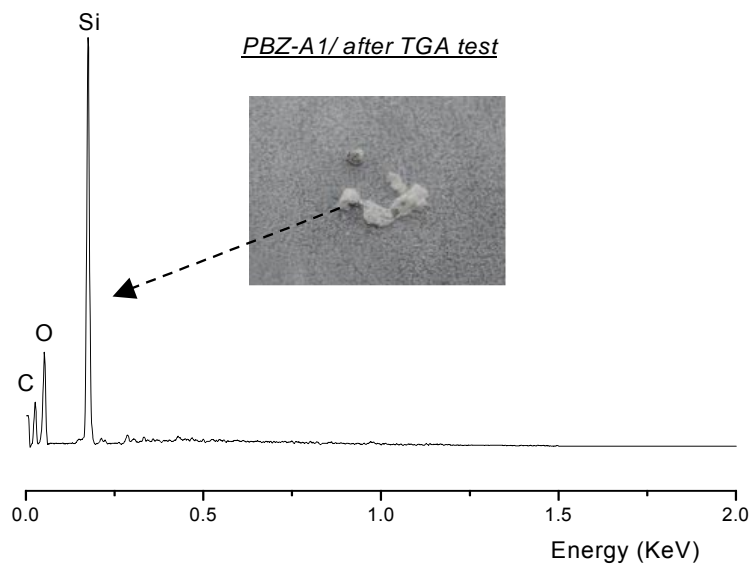


Figure 4-5. Residue and EDS analysis of PBZ-A1 after TGA testing.

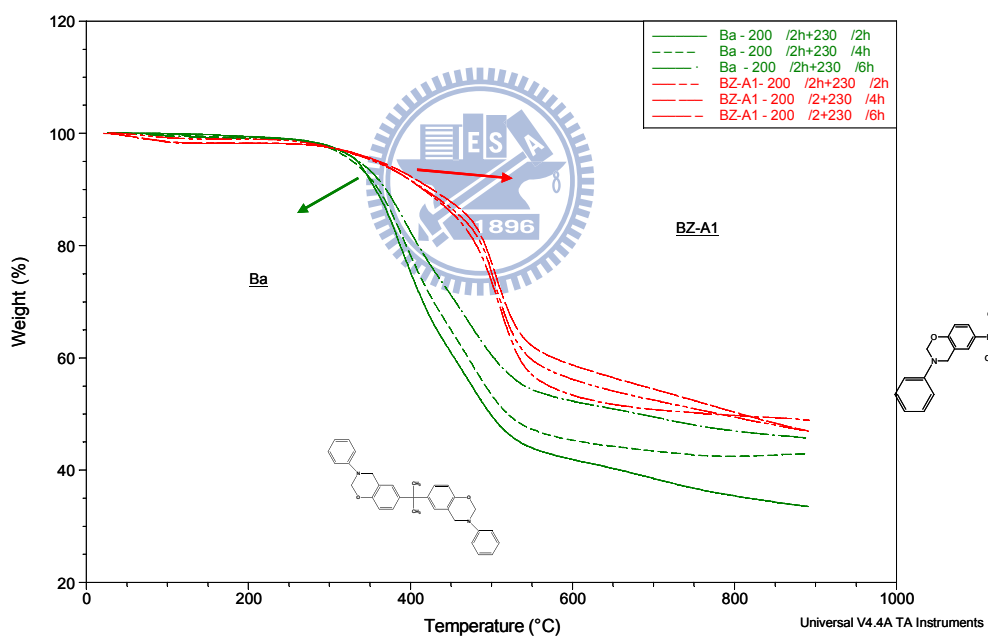


Figure 4-6. TGA thermograms of Ba and BZ-A1 (under N<sub>2</sub>).

Table 4-2. Thermostabilities of the cured PBZs PBa and PBZ-A1 (under N<sub>2</sub>)

Polymer	Curing Conditions	T <sub>5% loss</sub> (°C)	T <sub>10% loss</sub> (°C)	T <sub>d</sub> (°C)	Char Yield at 850 °C
PBa	200 °C/2 hrs + 230 °C/2 hrs	334.6	356.8	344.2	34.3%
	200 °C /2 hrs + 230 °C/4 hrs	328.8	360.7	342.7	42.7%
	200 °C /2 hrs + 230 °C/6 hrs	336.5	369.8	341.6	46.3%
PBZ-A1	200 °C/2 hrs + 230 °C/2 hrs	355.7	417.8	452.9	48.0%
	200 °C /2 hrs + 230 °C/4 hrs	361.5	427.2	448.4	48.4%
	200 °C /2 hrs + 230 °C/6 hrs	358.5	415.8	446.5	49.3%

T<sub>5% loss</sub>: Temperature at which the weight loss was 5%.

T<sub>10% loss</sub>: Temperature at which the weight loss was 10%.

T<sub>d</sub>: Decomposition temperature, onset point temperature.

## 4.2 Thermal stability of the poly-siloxane-imide-containing benzoxazine PBZ-A6

### 4.2.1 Materials and Characterization

The bifunctional bisphenol A-type benzoxazine (Ba, Figure 4-1) was purchased from Shikoku Chemicals (Japan). The siloxane-imide-containing benzoxazine, BZ-A6, was synthesized from the according method in chapter 2, the structure is shown in Figure 4-7. DSC was performed using a TA Instrument DSC-Q10 apparatus operated at a heating rate of 10 °C/min under a N<sub>2</sub> atmosphere. The gas flow rate was 40ml/ min. Benzoxazine samples of approximately 5 mg were scanned in hermetic aluminum sample pans. TGA was performed using a TA Instrument TGA-Q500 apparatus operated at a heating rate of 20 °C/min under an atmosphere of N<sub>2</sub> or air, respectively.

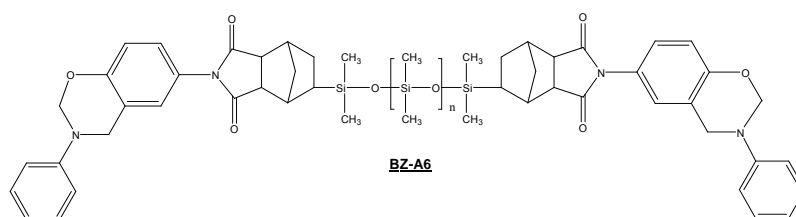


Figure 4-7. Structure of the BZ-A6.

#### 4.2.2 TGA of the poly-siloxane-imide-containing benzoxazine PBZ-A6

Polybenzoxazines usually exhibit good thermal properties. [3] Figure 4-7 displays TGA thermograms recorded under air atmosphere. No residue remained after burning PBa at high temperature, the char was almost zero at 850 °C. The char yield of PBZ-A1 at 850 °C was 10–11 wt% and the elemental analysis confirmed that the residue was inorganic silicon oxide. [12] PBZ-A6 exhibited a higher char yield of 16–17 wt%, presumably due to the longer siloxane chain in the BZ-A6 backbone than that in BZ-A1. Thus, the char yield increased upon increasing the siloxane content in the polymer. The PBa started to decomposed,  $T_{5\% \text{ loss}}$ , around 330-350 and it was obviously that PBZ-A1 has higher decomposed temperature to 380-395 from the result in Figure 4-8. Polybenzoxazine which contained the siloxane-imide segment in the main-chain, PBZ-A1 and PBZ-A6, could improve the thermal stability. The highest  $T_{5\% \text{ loss}}$  was observed in the PBZ-A6 curve. The weight residue of PBZ-A6 is 16-18wt% at 850 under air atmosphere, which is list in Table 4-3. It was obviously that the char yield is higher than that of shorter siloxane containing PBZ-A1 (10-12 wt%) or the conventional bisphenol A type polybenzoxazine, PBa (almost 0%). It was indicated that longer siloxane chain could make further improvements in the thermal stability since the more siloxane containing was incorporated into the main chain of PBZ-A6.

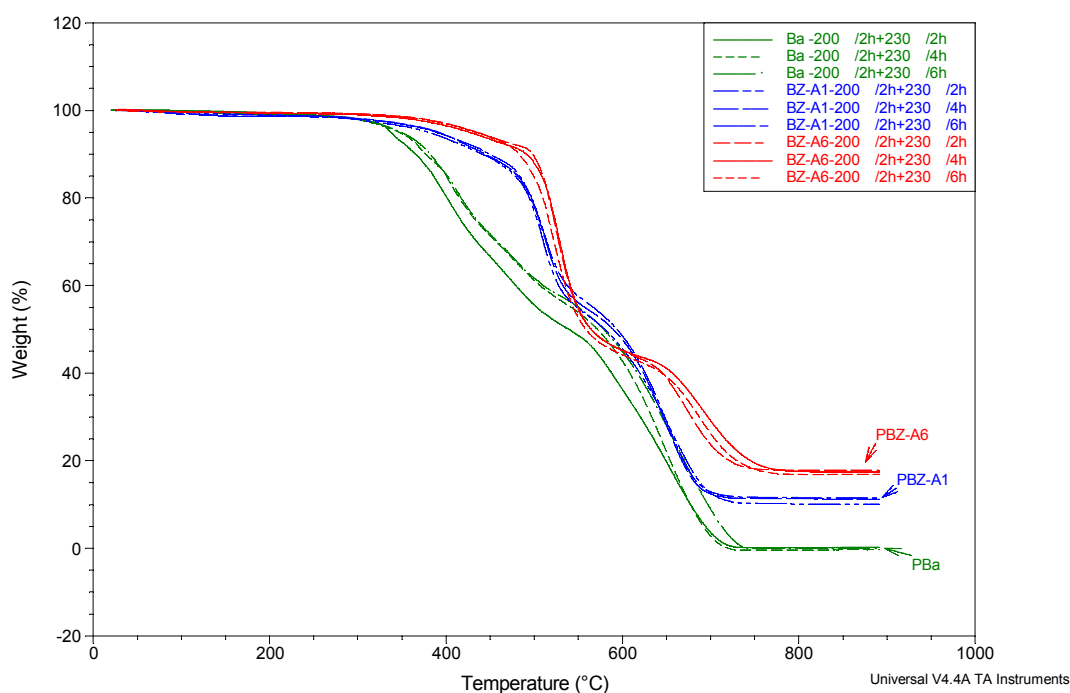


Figure 4-8. TGA thermograms of PBa, PBZ-A1 and PBZ-A6 (in air).

Table 4-3. Thermostability of cured polybenzoxazine PBa, PBZ-A1 and PBZ-A6 (in air)

Polymers	Curing Condition		T <sub>5% loss</sub> ( )	T <sub>10% loss</sub> ( )	T <sub>d</sub> ( )	Char Yield at 850
	1 <sup>st</sup> step @ 200	2 <sup>nd</sup> step @ 230				
PBa	2 hrs	2 hrs	337.3	365.5	349.3	0.2%
		4 hrs	345.0	376.8	346.4	-0.3%
		6 hrs	349.1	381.5	357.9	-0.1%
PBZ-A1	2 hrs	2 hrs	380.1	441.1	472.2	10.1%
		4 hrs	389.4	444.2	480.7	11.3%
		6 hrs	392.0	449.3	478.1	11.6%
PBZ-A6	2 hrs	2 hrs	435.4	497.9	498.3	17.8%
		4 hrs	426.7	491.0	498.6	17.4%
		6 hrs	433.3	482.4	491.5	16.9%

T<sub>5% loss</sub>: The temperature for which the weight loss is 5%.

T<sub>10% loss</sub>: The temperature for which the weight loss is 10%.

T<sub>d</sub>: The decomposed temperature

TGA analysis has revealed that PBa exhibits high decomposition temperature ( $T_{5\%}$ , ca. 300–330 °C) and high char yield (ca. 30–42%). [3, 6-8] In a previous study, we found that PBZ-A1 exhibited superior thermal properties relative to that of PBa. [12] Figure 4-9 displays TGA thermograms recorded under  $N_2$  atmosphere and Table 4-4 summarizes the results. The 5 and 10% weight loss temperatures ( $T_{5\% \text{ loss}}$  and  $T_{10\% \text{ loss}}$ , respectively) for PBZ-A6 (437.1 and 481.3 °C, respectively) were the highest among the polymers investigated in this study. The thermal decomposition temperature of PBZ-A6 was in the range 460–471 °C. PBZ-A1 and PBZ-A6 exhibited higher thermal stability than PBa because of the presence of the siloxane-imide-containing segment. Furthermore, the siloxane content of PBZ-A6 is higher than that of PBZ-A1 and the decomposition temperature of PBZ-A6 was higher accordingly. The siloxane-imide-containing PBZs also featured high weight residues after TGA. The highest char yield was 50.9% from PBZ-A6 due to the presence of longer siloxane-imide group. PBZ-A6 exhibited good thermal stability, the highest decomposition temperature, and the highest char yield. It appears that incorporating siloxane and imide moieties into the benzoxazine main chain can significantly enhance the thermal properties of PBZs, providing the potential to be used as flame-retardant materials.

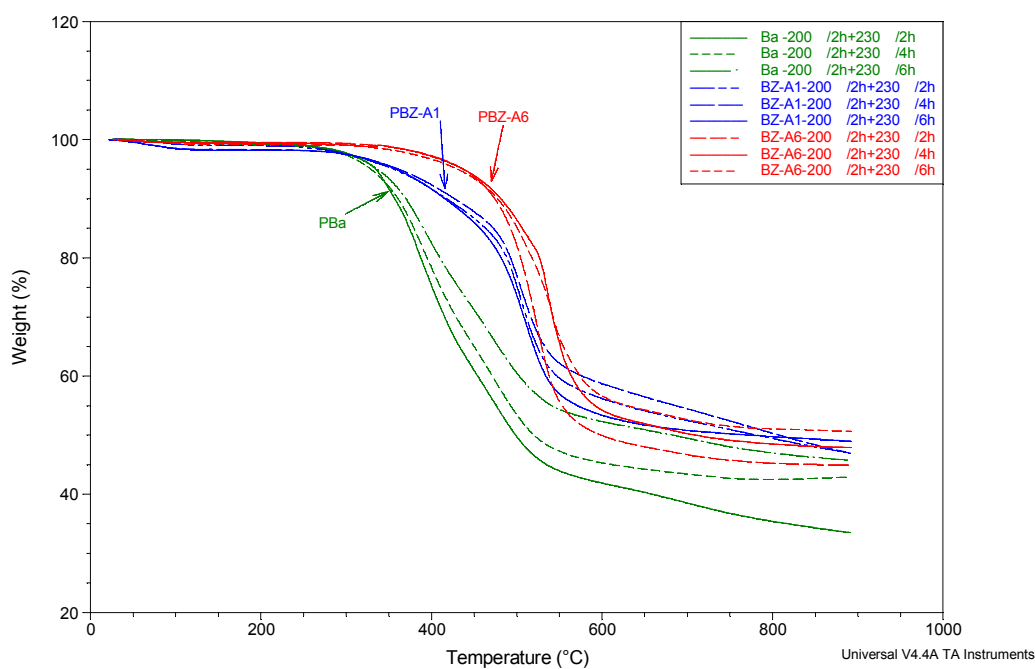


Figure 4-9. TGA thermograms of PBa, PBZ-A1 and PBZ-A6 (in N<sub>2</sub>).

Table 4-4. Thermostability of cured PBZ PBa, PBZ-A1, and PBZ-A6 (in N<sub>2</sub>)

Polymer	Curing Conditions		T <sub>5% loss</sub> (°C)	T <sub>10% loss</sub> (°C)	T <sub>d</sub> (°C)	Char Yield at 850 °C
	1 <sup>st</sup> step @ 200	2 <sup>nd</sup> step @ 230				
PBa	2 hrs	2 hrs	334.6	356.8	344.2	34.3%
		4 hrs	328.8	360.7	342.7	42.7%
		6 hrs	336.5	369.8	341.6	46.3%
PBZ-A1	2 hrs	2 hrs	355.7	417.8	452.9	48.0%
		4 hrs	361.5	427.2	448.4	48.4%
		6 hrs	358.5	415.8	446.5	49.3%
PBZ-A6	2 hrs	2 hrs	437.1	474.2	471.0	45.1%
		4 hrs	437.2	481.3	459.9	48.1%
		6 hrs	430.6	477.4	463.7	50.9%

T<sub>5% loss</sub>: Temperature at which the weight loss reached 5%.

T<sub>10% loss</sub>: Temperature at which the weight loss reached 10%.

T<sub>d</sub>: Decomposition temperature

### 4.2.3 DMA of the poly-siloxane-imide-containing benzoxazine PBZ-A6

Figure 4-10 displays DMA thermograms of the PBZ-A6 under three curing conditions and results are summarized in Table 4-5. The curing profiles revealed that the storage modulus at room temperature was 600–800 MPa which is much lower than conventional PBa's. In general, a higher shear storage modulus in the rubbery state indicates a polymer having a high crosslinking density [5]. The storage modulus reached the highest value after longer post curing time at rubbery state which was indicated at 200 and 220 in Table 4-5. Thus, a longer curing time improved the crosslinking density as would be expected. These results are consistent with the fact that PBZ-A6 exhibited the highest  $T_g$  (186.4 °C) of the studied polymers. From a previous study [11] the storage modulus of the brittle PBa was found to be ca. 3.2 GPa at room temperature and  $T_g$  (derived from  $\tan \delta$ ) of 174 °C.

In generally, it is difficult to obtain free-standing PBZ films without adding plasticizers. Since the siloxane-imide-modified benzoxazine PBZ-A6 exhibits superior flexibility and toughness, PBZ-A6 readily formed a free-standing, bendable film after polymerization at a thickness of ca. 200  $\mu\text{m}$  (Figure 4-11). Notably, the PBZ-A6 film exhibited not only excellent flexibility but also a high value of  $T_g$  due to the presence of the rigid imide-norborane rings in the PBZ. DMA results revealed that the presence of siloxane and imide moieties can significantly improve the flexibility and toughness of PBZs without sacrificing high glass transition temperature.



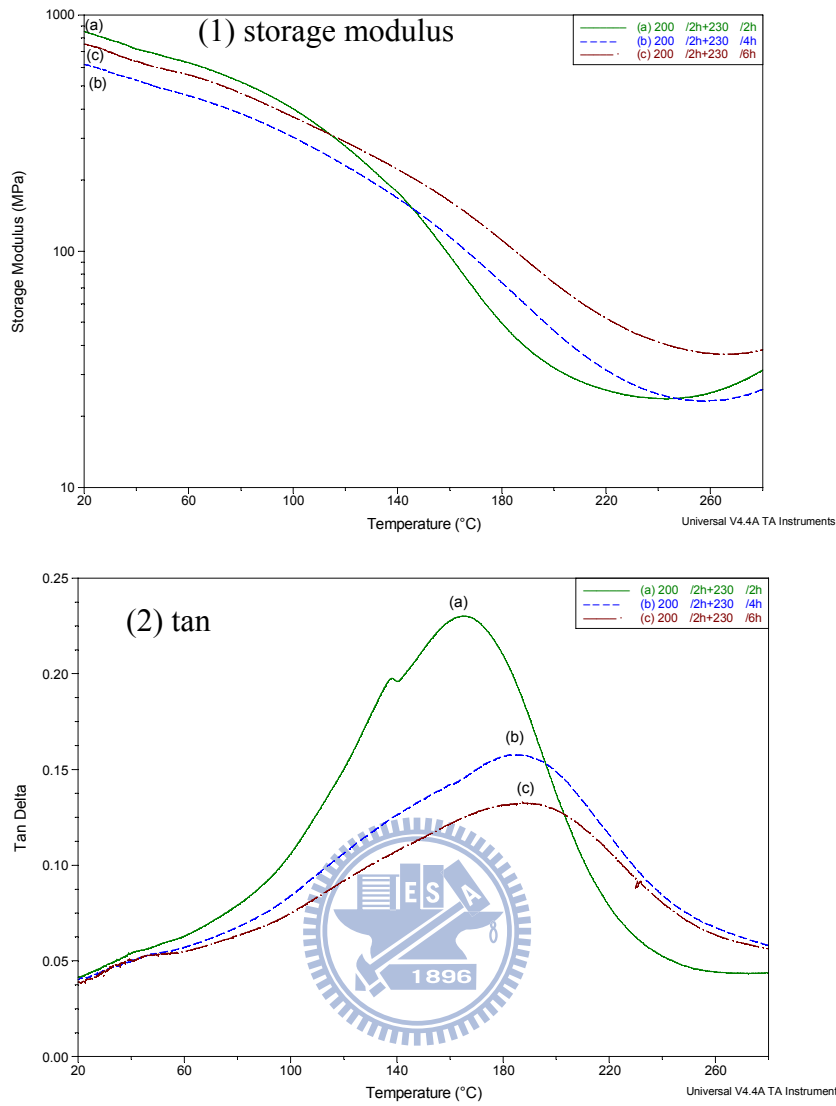


Figure 4-10. DMA thermograms of PBZ-A6: (1) storage modulus (2)  $\tan \delta$

Table 4-5. Thermal mechanical analysis data for PBZ-A6

sample	Curing conditions		Storage modulus (MPa)				$T_g$ from $\tan \delta$ peak (°C)
	1 <sup>st</sup> step @ 200	2 <sup>nd</sup> step @ 230	@ 25 °C	@ 180 °C	@ 200 °C	@ 220 °C	
(a)	2hrs	2hrs	816.2	47.0	32.1	25.8	166.2
(b)		4hrs	595.8	73.6	46.0	31.4	184.0
(c)		6hrs	729.5	111.3	73.7	52.0	186.4

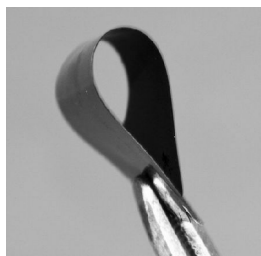


Figure 4-11. Photograph of a thin film of PBZ-A6, a siloxane-imide-containing PBZ.



## References

- [1] Nair, C. P. Reghunadhan *Prog. Polym. Sci.* **2004**, *29*, 401.
- [2] Shen, S. B. and Ishida, H. *Polym. Comp.* **1996**, *17*, 710.
- [3] Ghosh, N. N.; Kiskan, B.; Yagci, Y. *Porg. Polym. Sci.* **2007**, *32*, 1344.
- [4] Ishida, H. and Allen, D. J. *J Polym Sci Part B: Polym Phys* **1996**, *34*, 1019.
- [5] Liu, Y. L.; Hsu, C. W. and Chou, C. I. *J Polym Sci Part A: Polym Chem* **2007**, *45*, 1007.
- [6] Hemvichian, K. and Ishida, H. *Polymer* **2002**, *43*, 4391.
- [7] Agag, T. and Takeichi, T. *Macromolecules* **2003**, *36*, 6010.
- [8] Takeichi, T.; Kano, T. and Agag, T. *Polymer* **2005**, *46*, 12172.
- [9] Choi, S. W.; Ohba, S.; Brunovska, Z.; Hemvichian, K. and Ishida, H. *Polymer Degradation and Stability* **2006**, *91*, 1166.
- [10] Liu, Y. L.; Chiu, Y. C. and Wu, C. S. *J Appl Polym Sci* **2003**, *87*, 404.
- [11] Ardhyanta, H.; Wahid, M. H.; Sasaki, M.; Agag, T.; Kawauchi, T.; Ismail, H. and Tachechi, T. *Polymer* **2008**, *49*, 4585.
- [12] Chen, K. C.; Li, H. T.; Chen, W. B.; Liao, C. H.; Sun, K. W. and Chang, F. C. *Polym Int* in press

## Chapter 5

# Extremely Low Surface Free Energy and UV Stability of Siloxane-Imide-Containing Polybenzoxazines

### 5.1 Introduction of Surface Free Energy

#### 5.1.1 Interfacial Thermodynamics

The interface (surface) is a region of finite thickness (usually less than 0.1  $\mu\text{m}$ ) in which the composition and energy vary continuously from one bulk phase to other. The pressure (force field) in the interfacial zone is therefore non-homogeneous, having a gradient perpendicular to the interfacial boundary. In contrast, the pressure in a bulk phase is homogeneous and isotropic. Consequently, no net energy is expended in reversibly transporting the matter within a bulk phase. However, a net energy is required to create an interface by transporting from the bulk phase to the interfacial zone. The reversible work required to create a unit surface area is the surface free energy, that is

$$\gamma = \left( \frac{\partial G}{\partial A} \right)_{T, P, n} \quad (5.1)$$

where  $\gamma$  is the surface free energy,  $G$  the Gibbs free energy of the total system,  $A$  the interfacial area,  $T$  the temperature,  $P$  the pressure, and  $n$  the total number of moles of matter in the system.

The work required to separate reversibly the interface between two bulk phases  $\alpha$  and  $\beta$  from their equilibrium separation to infinity is the work of adhesion.

$$W_a = W_{\alpha\beta} = \gamma_\alpha + \gamma_\beta - \gamma_{\alpha\beta} \quad (5.2)$$

Where  $W_a$  is the work of adhesion,  $\gamma_\alpha$  the surface free energy of phase  $\alpha$ ,  $\gamma_\beta$  the surface free energy of phase  $\beta$ , and  $\gamma_{\alpha\beta}$  the interfacial energy between phase  $\alpha$  and  $\beta$  (Figure 5-1).

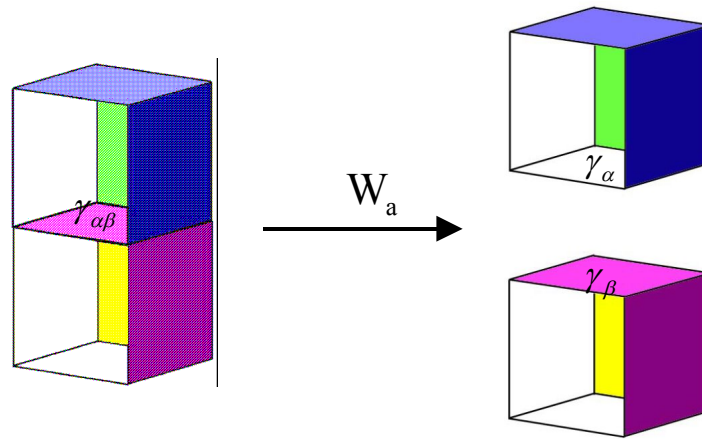


Figure 5-1. Work of adhesion.

This was apparently first purpose by Dupré. [1] When the two phase are identical, the reversible work is the work of cohesion (Figure 5-2),

$$W_c = W_{jj} = \gamma_j + \gamma_j - 0 = 2\gamma_j \quad (5.3)$$

where  $W_c$  is the work of cohesion for phase  $j$ .

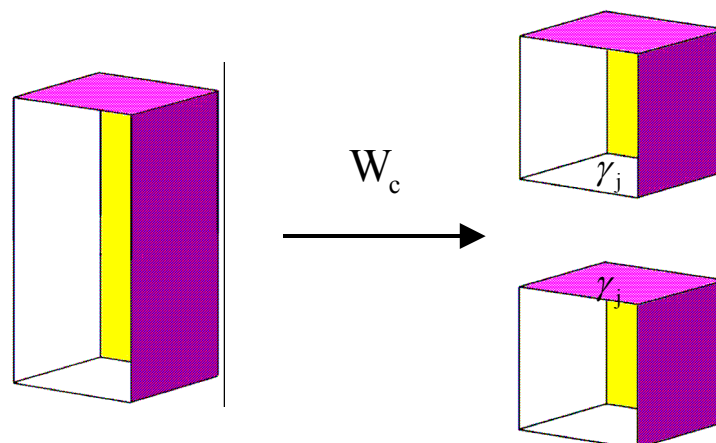


Figure 5-2. Work of cohesion.

The work of adhesion is the decrease of Gibbs free energy per unit area when an

interface is formed from two individual surfaces. Thus, the greater the interfacial attraction, the greater the work of adhesion will be. Rearrangement of Eq. (5.1) gives

$$\gamma_{\alpha\beta} = \gamma_{\alpha} + \gamma_{\beta} - W_a \quad (5.4)$$

indicating that the greater the interfacial attraction, the smaller the interfacial energy will be. The works of adhesion can be related to the cohesion theoretically. Thereby, the interfacial energy can be linked to the properties of the two individual phases.

Thermodynamic discussions of adhesion in solid-liquid systems should be carried out in terms of surface free energy rather than surface tension. Discussions that involve the shape of liquid-gas or liquid-liquid interfaces can be carried out either in terms of surface tension or surface free energy.

### 5.1.2 Contact Angle Equilibrium: Young Equation

A liquid in contact with a solid will exhibit a contact angle (Figure 5-3). If the system is at rest, a static contact angle is obtained. If the system is in motion, a dynamic contact angle is obtained. Here, static contact angles are discussed. A system at rest may be in stable equilibrium (the lowest energy state), or in meta stable equilibrium (an energy through separated from neighboring states by energy barriers).

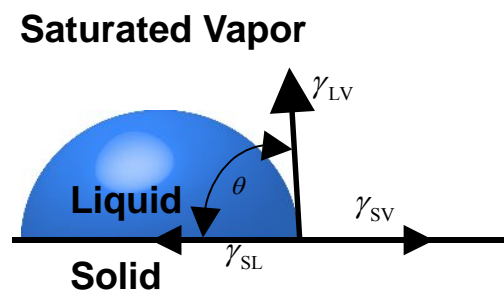


Figure 5-3. Contact angle equilibrium on a smooth, homogeneous, planar, and rigid surface.

Stable equilibrium will be obtained if the solid surface is ideally smooth,

homogeneous, planar, and nondeformable; the angle formed is the equilibrium contact angle,  $\theta$ .

On the other hand, if the solid surface is rough or compositionally heterogeneous, the system may reside in one of many stable states; the angle formed is a metastable contact angle. The amount of mechanical energy in the liquid drop (such as vibrational energy) determines which metastable state is to be occupied. Therefore, metastable contact angle vary with drop volume, external mechanical energy (such as vibration), and how the angle is formed (whether by advancing or receding the liquid front on the solid). The stable equilibrium contact angle may sometimes (but rarely) be observed on a rough or heterogeneous surface. This equilibrium angle corresponds to the lowest energy state.

The angle formed by advancing the liquid front on the solid is termed advancing contact angle,  $\theta_a$  (Figure 5-4). The angle formed by receding the liquid front on the solid is termed receding contact angle,  $\theta_r$  (Figure 5-5).

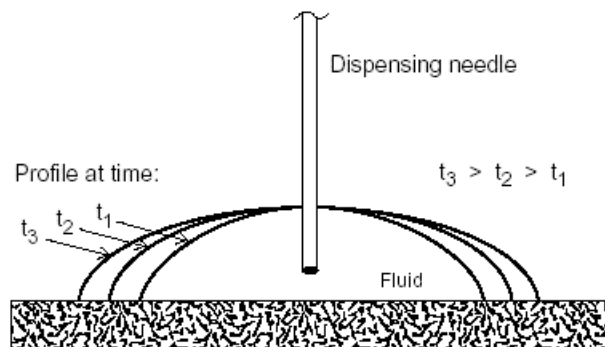


Figure 5-4. Advancing contact angle.

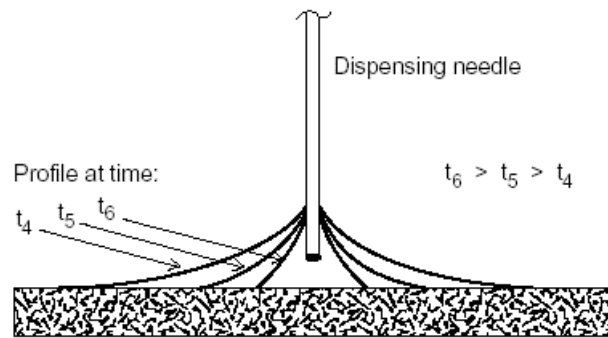


Figure 5-5. Receding contact angle.

Advancing contact angle are usually greater than receding contact angle when the system is in a metastable state. On the other hand, the advancing and the receding angles are identical when equilibrium angles are formed. Many real surfaces are rough or heterogeneous. Thus, variable contact angles are often observed. This has previously led to concern as to whether a true thermodynamic quality. The origin of variable contact angle has now been clearly established and the thermodynamic status of contact angle ascertained.

The equilibrium contact angle (abbreviated  $\theta$  here) for liquid drop on an ideally smooth, homogeneous, planar, and nondeformable surface (Figure 5-3) is related to the various interfacial tension by

$$\gamma_{LV} \cos \theta = \gamma_{SV} - \gamma_{SL} \quad (5.5)$$

where  $\gamma_{LV}$  is the surface tension of the liquid in equilibrium with its saturated vapor,  $\gamma_{SV}$  the surface free energy of the solid in equilibrium with the saturated vapor of the liquid, and  $\gamma_{SL}$  the interfacial tension between the solid and the liquid. This is known as the Young equation. Young [2] described the relation in words, and did not attempt to prove it. Several proofs were offered later by others. [3-5]

Many real surfaces are rough or heterogeneous. A liquid drop resting on such a



surface may reside in the stable equilibrium (the lowest energy state), or in a metastable equilibrium (energy trough separated from neighboring states by energy barriers). The equilibrium contact angle  $\theta_e$  corresponds to the lowest energy state for a system. On an ideally smooth and compositionally homogeneous surface, the equilibrium contact angle is the Young's angle  $\theta_Y$ , which is also the microscopic local contact angle on any rough or heterogeneous surface, hence also known as the intrinsic contact angle  $\theta_0$ . The fact that  $\theta_0$  equals  $\theta_Y$  has been proved theoretically as the condition for minimization of system free energy.

The equilibrium contact angle on a rough surface is Wenzel's angle  $\theta_w$ . The equilibrium contact angle on a heterogeneous surface is Cassie's angle  $\theta_c$ . These angles correspond to the lowest energy state, but are often not observed experimentally. Instead, the system often resides in a metastable state, exhibiting a metastable contact angle. In this case, advancing and receding angles are different, known as hysteresis (H). The different  $\theta_a - \theta_r$  is the extent of hysteresis.

### 5.1.3 Determination of Surface Free Energy

The surface free energy of a solid polymer cannot be measured directly, as reversible formation of its surface is difficult. Many indirect methods have been proposed, including the polymer melt (temperature dependence) method, Good-Girifalco Method, Owens, Wendt, and Kaelble's Method (Two-Liquid Geometric Method), Wu's Method (Two-Liquid Harmonic Method), Lifshitz-van der Waals Acid-Base Theory (Three-Liquid Acid-Base Method), critical surface tension and others.

### **Good–Girifalco Method**

Good and Girifalco in the 1950s proposed the following equation to describe the surface energy of interfacial phase systems: [6-8]

$$\gamma_{ab} = \gamma_a + \gamma_b - 2\Phi(\gamma_a\gamma_b)^{1/2} \quad (5.6)$$

The subscripts a and b refer to the two phases, which may be liquid or solid.  $\Phi$  is a constant between interfaces of a system and is defined as:

$$-\frac{\Delta F_{ab}^a}{(\Delta F_a^c \Delta F_b^c)^{1/2}} = \Phi \quad (5.7)$$

where  $\Delta F_{ab}^a$  = the free energy of adhesion for the interface between phases A and B, per  $\text{cm}^2$ ,  $= \gamma_{ab} - \gamma_a - \gamma_b$  and  $\Delta F_n^c$  = free energy of cohesion for phase N  $= 2\gamma_n$ .

Equation (5.6) can be rewritten as the well known Good and Girifalco equation:

$$\gamma_{SL} = \gamma_S + \gamma_{LV} - 2\Phi(\gamma_S\gamma_{LV})^{1/2} \quad (5.8)$$

Combined equations 5.5 and 5.8 yield:

$$\gamma_{LV}(1 + \cos \theta) = 2\Phi(\gamma_S\gamma_{LV})^{1/2} \quad (5.9)$$

or

$$\gamma_S = \frac{\gamma_{LV}(1 + \cos \theta)^2}{4\Phi^2} \quad (5.10)$$

Suppose the value of  $\Phi$  is known for a pair of the testing solid and liquid,  $\gamma_S$  can be calculated from contact angle data with eq. (5.10). In the zeroth order approximation, Good and Girifalco suggested that  $\Phi$  was equal to unity.

### **Fowkes' Method**

Fowkes [9,10] proposed that “the surface tensions are a measure of the attractive forces between surface layers and liquid phase, and that such forces and their contribution to the free energy are additive.” He designated, in the case of the surface

tension of water, the surface tension could be considered the sum of contributions from dispersion forces ( $\gamma^d$ ) and dipole interactions, mainly hydrogen bonds ( $\gamma^h$ ):

$$\gamma_{\text{H}_2\text{O}} = \gamma_{\text{H}_2\text{O}}^d + \gamma_{\text{H}_2\text{O}}^h \quad (5.11)$$

where superscript h refers to hydrogen bonding, and d to dispersion. In addition, at the interface between a liquid and solid, as Fowkes pointed out, the interfacial molecules are attracted by the bulk liquid from one side and from the other side by the intermolecular forces between the two phases. Fowkes defined the dispersion force contribution to surface tension of the solid in terms of the interaction with the dispersion forces of the liquid. As a result, the Young–Good–Girifalco equation can be modified as:

$$\gamma_{SL} = \gamma_S + \gamma_{LV} - 2(\gamma_S^d \gamma_{LV}^d)^{1/2} \quad (5.12)$$

Combine eqs. (5.5) and (5.12) results in:

$$\gamma_{LV}(1 + \cos \theta) = 2(\gamma_S^d \gamma_{LV}^d)^{1/2} \quad (5.13)$$

Strictly speaking, eq. (5.13) provides a method to estimate the value of  $\gamma_S^d$ , but not total  $\gamma_S$ , from a single contact angle measurement, where only dispersion forces operate in the liquid, such as a hydrocarbon liquid. The  $\gamma_S^d$  of any solid can be determined using a “dispersion force only” liquid.

### **Owens, Wendt, and Kaelble’s Method (Two-Liquid Geometric Method)**

Owens and Wendt [11] and Kaelble [12] extended Fowkes’ equation to a more general form:

$$\gamma_{SL} = \gamma_S + \gamma_{LV} - 2(\gamma_S^d \gamma_{LV}^d)^{1/2} - 2(\gamma_S^p \gamma_{LV}^p)^{1/2} \quad (5.14)$$

Combine eqs. (5.5) and (5.14) yield:

$$\gamma_{LV}(1 + \cos \theta) = 2(\gamma_S^d \gamma_{LV}^d)^{1/2} + 2(\gamma_S^p \gamma_{LV}^p)^{1/2} \quad (5.15)$$

where superscript d refers to a dispersion (nonpolar) component, and p refers to a polar (nondispersion) component, including all the interactions established between the solid and liquid, such as dipole– dipole, dipole-induced dipole and hydrogen bonding, etc.

Since  $\gamma_S$  is the sum of surface tension components contributed from dispersion and polar parts:

$$\gamma_S = \gamma_S^d + \gamma_S^p \quad (5.16)$$

Equations (5.14) and (5.15) provide a method to estimate surface tension of solids.

Using two liquids with known  $\gamma_L^d$  and  $\gamma_L^p$  for contact angle measurements, one could easily determine  $\gamma_S^d$  and  $\gamma_S^p$  by solving the following two equations:

$$\begin{aligned} \gamma_{LV1}(1 + \cos \theta_1) &= 2(\gamma_S^d \gamma_{LV1}^d)^{1/2} + 2(\gamma_S^p \gamma_{LV1}^p)^{1/2} \\ \gamma_{LV2}(1 + \cos \theta_2) &= 2(\gamma_S^d \gamma_{LV2}^d)^{1/2} + 2(\gamma_S^p \gamma_{LV2}^p)^{1/2} \end{aligned} \quad (5.17)$$

The values of  $\gamma_L^d$  and  $\gamma_L^p$  of reference liquids have been provided by Kaelble.

### **Wu's Method (Two-Liquid Harmonic Method)**

This method uses the contact angle  $\theta$  of two testing liquids and the harmonic-mean equation. The results agree remarkable well with the liquid homolog method, polymer melt method, and the equation of state method.

Based on “harmonic” mean and force addition, Wu proposed the following equations: [13, 14]

$$\gamma_{SL} = \gamma_S + \gamma_{LV} - \frac{4\gamma_S^d \gamma_{LV}^d}{\gamma_S^d + \gamma_{LV}^d} - \frac{4\gamma_S^p \gamma_{LV}^p}{\gamma_S^p + \gamma_{LV}^p} \quad (5.18)$$

Equation (5.18) can be written as follows with the aid of eq. (5.5):

$$\gamma_{LV}(1 + \cos \theta) = \frac{4\gamma_S^d \gamma_{LV}^d}{\gamma_S^d + \gamma_{LV}^d} + \frac{4\gamma_S^p \gamma_{LV}^p}{\gamma_S^p + \gamma_{LV}^p} \quad (5.19)$$

Equations (5.18) and (5.19) provide a method to estimate surface tension of solids. Using two liquids with known  $\gamma_L^d$  and  $\gamma_L^p$  for contact angle measurements, one could easily determine  $\gamma_S^d$  and  $\gamma_S^p$  by solving the following two equations:

$$\begin{aligned} \gamma_{LV1}(1 + \cos \theta) &= \frac{4\gamma_S^d \gamma_{LV1}^d}{\gamma_S^d + \gamma_{LV1}^d} + \frac{4\gamma_S^p \gamma_{LV1}^p}{\gamma_S^p + \gamma_{LV1}^p} \\ \gamma_{LV2}(1 + \cos \theta) &= \frac{4\gamma_S^d \gamma_{LV2}^d}{\gamma_S^d + \gamma_{LV2}^d} + \frac{4\gamma_S^p \gamma_{LV2}^p}{\gamma_S^p + \gamma_{LV2}^p} \end{aligned} \quad (5.20)$$

Wu [13] claimed that this method applied accurately between polymers and between a polymer and an ordinary liquid.

### **Lifshitz–van der Waals Acid-Base Theory (Three-Liquid Acid-Base Method)**

Van Oss et al. has proposed a methodology that represents both Fowkes–Owens–Wendt–Kaelble and Wu. This methodology introduces a new meaning of the concepts, “apolar” and “polar,” the later cannot be represented by a single parameter such as  $\gamma^p$ .

As shown in eq. (5.11), surface tension  $\gamma$  could be divided into an apolar component and a hydrogen bonding component or (more generally) acidbase interaction. One may follow Fowkes’ approach [15, 16] and separate surface energy into several components as:

$$\gamma = \gamma^d + \gamma^{\text{dip}} + \gamma^{\text{ind}} + \gamma^h + \dots \quad (5.21)$$

$$\gamma = \gamma^d + \gamma^{AB} \quad (5.22)$$

where the superscripts, d, dip, ind, and h refer to (London) dispersion, (Keesom) dipole– dipole, (Debye) induction, and hydrogen bonding forces, respectively. And the

superscript AB refers to the acid-base interaction.

By regrouping components, van Oss and Good expressed the surface energy as:

$$\gamma = \gamma^{LW} + \gamma^{AB} \quad (5.23)$$

$$\gamma^{LW} = \gamma^d + \gamma^{dip} + \gamma^{ind} \quad (5.24)$$

where LW stands for Lifshitz–van der Waals. Because a hydrogen bond is a proton-sharing interaction between an electronegative molecule or group and an electropositive hydrogen, a hydrogen bonding is an example of Lewis acid (electron acceptor) and Lewis base (electron donor). Van Oss et al., [17-23] therefore, treated hydrogen bonding as Lewis acid-base interactions. In addition, van Oss et al. [17- 19] created two parameters to describe the strength of Lewis acid and base interactions:

$\gamma^+$  = Lewis acid parameter of the surface free energy

$\gamma^-$  = Lewis base parameter of the surface free energy

$$\gamma^{AB} = 2\sqrt{\gamma^+\gamma^-} \quad (5.25)$$



Based on these definitions, a material is classified as a bipolar substance if both its  $\gamma^+$  and its  $\gamma^-$  are greater than 0 ( $\gamma^{AB} \neq 0$ ). In other words, it has both nonvanishing  $\gamma^+$  and  $\gamma^-$ . A monopolar material is one having either an acid or a base characters, which means either  $\gamma^+ = 0$  and  $\gamma^- > 0$  or  $\gamma^+ > 0$  and  $\gamma^- = 0$ . An apolar material is neither an acid nor a base (both its  $\gamma^+$  and its  $\gamma^-$  are 0). For both monopolar and apolar materials, their  $\gamma^{AB} = 0$ . Therefore, according to the Fowkes notation, the criterion for a substance to be apolar, is,  $\gamma^{AB} = 0$ . This is not true in the van Oss and Good’s methodology.

How do we calculate these surface energy parameters? van Oss, Good, and their coworkers, have developed a “three-liquid procedure” (Equation 5.26) to determine

$\gamma_s$  by using contact angles techniques and a traditional matrix scheme.

$$\begin{aligned}\gamma_{LV1}(1 + \cos \theta_1) &= 2(\sqrt{\gamma_S^{LW} \gamma_{LV1}^{LW}} + \sqrt{\gamma_S^+ \gamma_{LV1}^-} + \sqrt{\gamma_S^- \gamma_{LV1}^+}) \\ \gamma_{LV2}(1 + \cos \theta_2) &= 2(\sqrt{\gamma_S^{LW} \gamma_{LV2}^{LW}} + \sqrt{\gamma_S^+ \gamma_{LV2}^-} + \sqrt{\gamma_S^- \gamma_{LV2}^+}) \\ \gamma_{LV3}(1 + \cos \theta_3) &= 2(\sqrt{\gamma_S^{LW} \gamma_{LV3}^{LW}} + \sqrt{\gamma_S^+ \gamma_{LV3}^-} + \sqrt{\gamma_S^- \gamma_{LV3}^+})\end{aligned}\quad (5.26)$$

In short, to determine the components of  $\gamma_s$  of a polymer solid, it was recommended [24, 25] to select three or more liquids from the reference liquids table, with two of them being polar, the other one being apolar. Moreover, the polar pairs—water and ethylene glycol, and water and formamide— were recommended to give good results, while apolar liquids are either diiodomethane or a-bromonaphthalene. Because the LW, Lewis acid, and Lewis base parameters of  $\gamma_{LV1}$ ,  $\gamma_{LV2}$ , and  $\gamma_{LV3}$  are available, one can determine the LW, Lewis acid, and base parameters of  $\gamma_s$  by solving these three equations simultaneously.

#### 5.1.4 Surface Free Energy of Polymer

##### Molecular-Weight Dependence

The surface free energy of homologous series tends to increase, while the surface entropy tends to decrease, with increasing molecular weight. At infinite molecular weight, both the surface free energy and the surface entropy are, however, finite. The surface free energy of homologous series varies linearly with  $M_n^{-2/3}$ , [26, 27]

$$\gamma = \gamma_\infty - \frac{k_e}{M_n^{2/3}} \quad (5.27)$$

where  $\gamma_\infty$  is the surface free energy at infinite molecular weight and  $k_e$  is a constant.

This equation fits the data for n-alkanes with standard deviations in  $\gamma$  about 0.05 dyne/cm, and for prefluoroalkanes, polyisobutylenes, polydimethylsiloxanes, and polystyrenes with standard deviations in  $\gamma$  about 0.2 dyne/cm (Table 5-1).

Table 5-1. Numerical constant for molecular weight dependence of surface free energy.

Polymers	Temp.	$\gamma_{\infty}$ dyne/cm	$k_e$	$\sigma^a$
n-alkanes	20	37.81	385.9	0.03
Polyisobutylenes	24	35.62	382.7	0.34
Polydimethylsiloxanes	20	21.26	166.1	0.09
Prefluoroalkanes	20	25.85	682.8	0.30
Polystyrenes	176	29.97	372.7	0.08
Poly(ethylene oxide)- dimethyl ether	24	44.35	342.8	0.44

<sup>a</sup> $\sigma$  is the standard deviations in  $\gamma$

The surface free energy variation decreases with increasing molecular weight. The  $k_e$  values in Table 2-1 indicate that  $\gamma$  will be smaller than  $\gamma_{\infty}$  by less than 1 dyne/cm when the molecular weight is greater about 3000. Accordingly, for instance, the surface free energy of poly(vinyl acetate) melts having molecular weight 11,000-120,000 are found to be practically independent of molecular weight (Figure 5-6). [28]



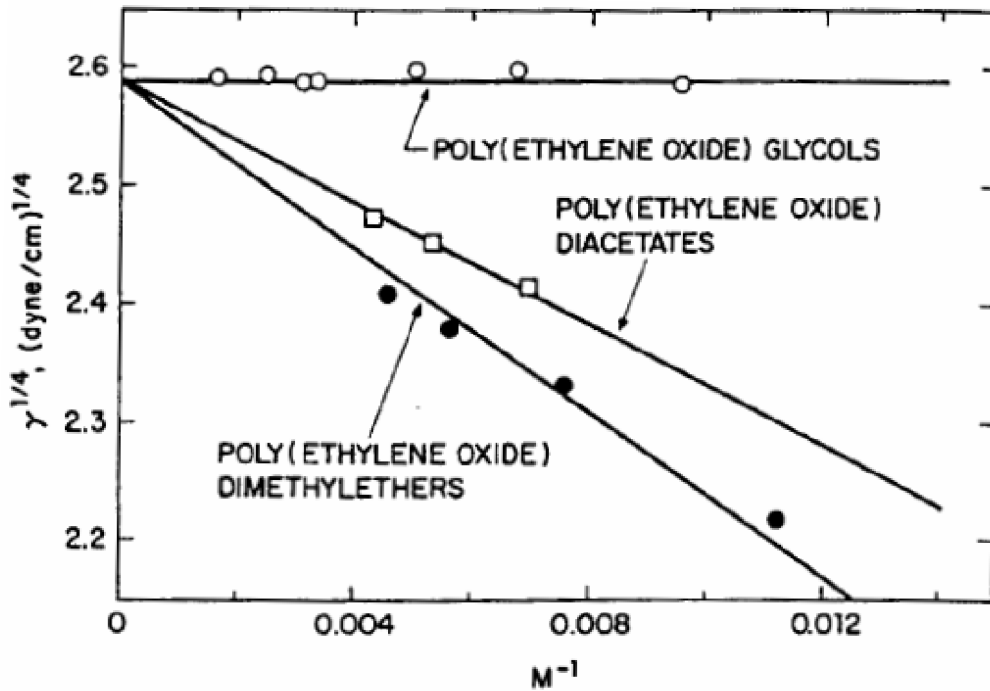
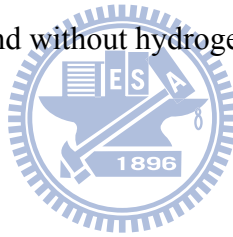


Figure 5-6. Comparison of surface energy and molecular weight between polymers with and without hydrogen bonds.



### Effects of Phase Transitions

At the crystal-melt transition, the surface free energy of crystalline phase  $\gamma^c$  is related to that of the amorphous phase  $\gamma^a$  by [29]

$$\gamma^c = \left( \frac{\rho_c}{\rho_a} \right)^n \gamma^a \quad (5.28)$$

where  $\rho_c$  is the crystalline density,  $\rho_a$  the amorphous density, and  $n$  the Macleod's exponent (Table 5-2).

Table 5-2. Macleod's exponent for some polymers

Polymers	Macleod's exponent
Polychloroprene	4.2
Poly(methyl methacrylate)	4.2
Poly(n-butyl methacrylate)	4.2
Polystyrene	4.4
Poly(vinyl acetate)	3.2
Poly(ethylene oxide)	3.0
Polybutylene	4.1
Polypropylene	3.2
Polyethylene, linear	3.2
Polyethylene, branched	3.3
polydimethylsiloxane	3.5

Thus, at the crystal-melt transition, the surface free energy changes discontinuously, since the density is discontinuous. As  $\rho_c$  is usually greater than  $\rho_a$ , the crystalline phase will have higher surface free energy than amorphous phase. For instance, polyethylene has  $n = 3.2$ ,  $\gamma^a = 35.7$  dyne/cm, and  $\rho_a = 0.855$  g/ml at 20

. The crystalline density  $\rho_c$  is 1.000 g/ml. Thus  $\gamma^c$  is calculated by eq. (5.28) to be 58.9 dyne/cm, which compares rather well with an experimental value of 53.6 dyne/cm. [30] Semicrystalline polymers tend to be covered with an amorphous surface layer. As the amorphous phase has lower surface free energy, it tends to migrate to the surface.

### **Copolymers and Blends**

Low-energy components in copolymers or blends tend to preferentially adsorb on the surface, just as in small-molecule liquids, as this will lower the free energy of the system.

### Random Copolymers

The surface free energy of a random copolymer usually follows the linear relation [31]

$$\gamma = x_1\gamma_1 + x_2\gamma_2 \quad (5.29)$$

where  $\gamma$  is the surface free energy and  $x$  is the mole fraction. The subscripts 1 and 2 refer to the components 1 and 2, respectively. Such behavior is shown for random copolymers of ethylene oxide and propylene oxide in Figure 5-7.

### Block and Graft Copolymers

However, block and graft copolymers show considerable surface activity of the lower energy component, when the lower-energy blocks or grafts are sufficient long that they can accumulate and orient on the surfaces independently of the rest of the molecule.

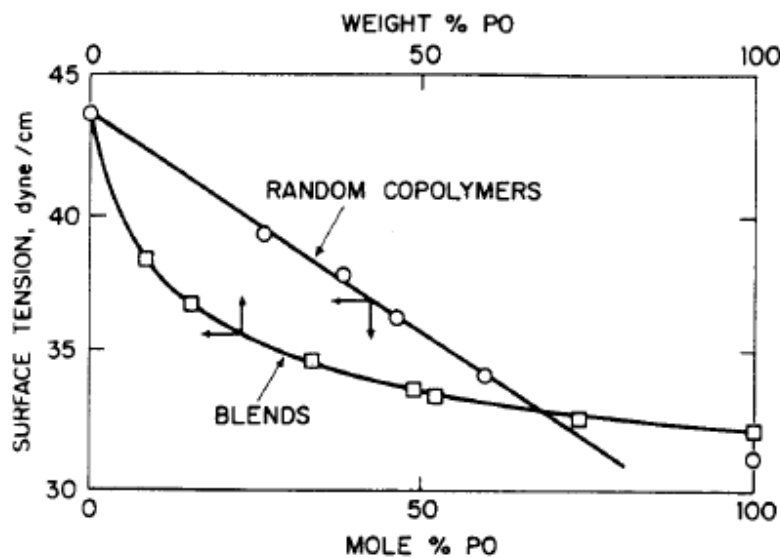


Figure 5-7. Linear additivity of surface tension of random copolymers of ethylene oxide and propylene oxide, and surface-active behavior of blends of poly(ethylene oxide) (PEG 300) and poly(propylene oxide) (PPG 425). [31]

For instance, pronounced surface activity is observed for ABA block copolymers of ethylene oxide (A block, higher surface free energy) and propylene oxide (B block, lower surface free energy) (Figure 5-8). [31]

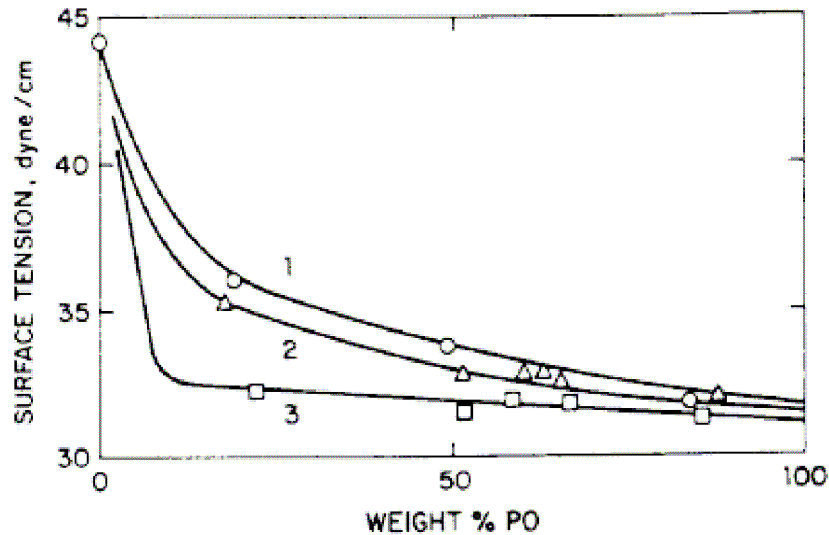


Figure 5-8. Surface tension versus composition for ABA block copolymers of ethylene oxide (A block) and propylene oxide (B block). Degree of polymerization are (1) DP = 16, (2) DP = 30, (3) DP = 56. [31]

### Blends of Polymers

Blends of both compatible and incompatible polymers show pronounced surface activity, incompatible blends being more pronounced than compatible blends. The surface activity of an incompatible blends is further complicated by heterogeneous phase structure.

Surface activity of compatible blend of poly(ethylene oxide) and poly(propylene oxide) is shown in Figure 5-9. [31] The surface activity increases with increasing molecular weight, apparently because of increased in compatibility.

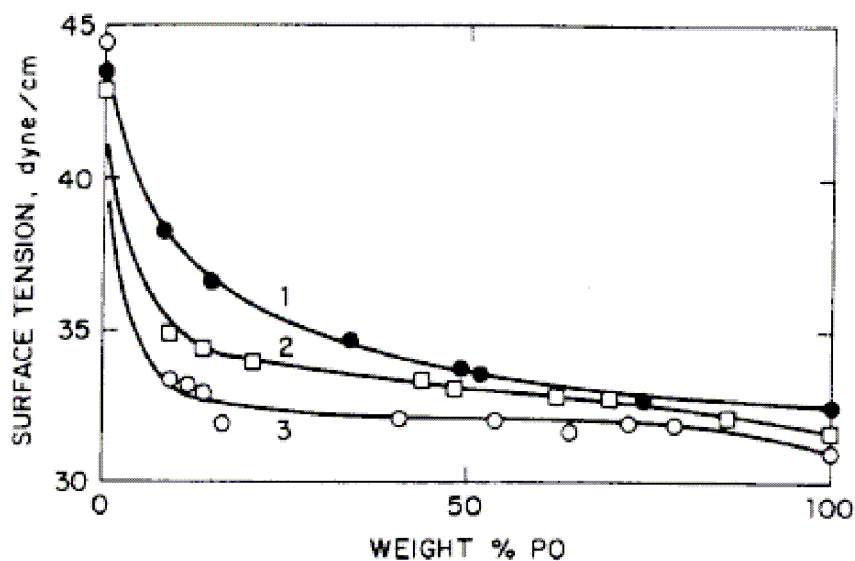


Figure 5-9. Surface tension of blends of compatible homopolymers. (1) poly(ethylene oxide) (PEG 300) + poly(propylene oxide) (PPG 425), (2) PPG 2025 + polyepichlorohydrin (PECH 1500), (3) PPG 400 + PECH 2000. [31]

## 5.2 Superhydrophobic Surfaces

Conventionally, superhydrophobic surfaces have been produced mainly in two ways. One is to create a rough structure on a hydrophobic surface ( $CA > 90^\circ$ ), and the other is to modify a rough surface by materials with low surface energy. Up to now, many methods have been developed to produce rough surfaces, including solidification of melted alkylketene dimmer (AKD, a kind of wax), [32] plasma polymerization/etching of polypropylene (PP) in presence of polytetrafluoroethylene (PTFE), [33] microwave plasma-enhanced chemical vapor deposition (MWPE-CVD) of trimethylmethoxysilane (TMMOS), [34] anodic oxidization of aluminum, [35] immersion of porous alumina gel films in boiling water, [36] mixing of a sublimation material with silica or boehmite, [37] phase separation, [38] and molding [39]. For example, the superhydrophilic surface [40] with a water contact angle (CA) of almost  $0^\circ$  generated by UV irradiation has been successfully used as a transparent coating

with antifogging and self-cleaning properties (Figure 5-10).

To obtain superhydrophobic surfaces, coating with low-surface-free-energy materials such as fluoroalkylsilane (FAS) is often necessary. [35-39] While a water CA has commonly been used as a criterion for the evaluation of hydrophobicity of a solid surface, this alone is insufficient to assess the sliding properties of water droplets on the surface. [41] A fully superhydrophobic surface should exhibit both high CA and low sliding angle, where sliding angle can also be expressed as the difference between advancing and receding contact angle (hysteresis).

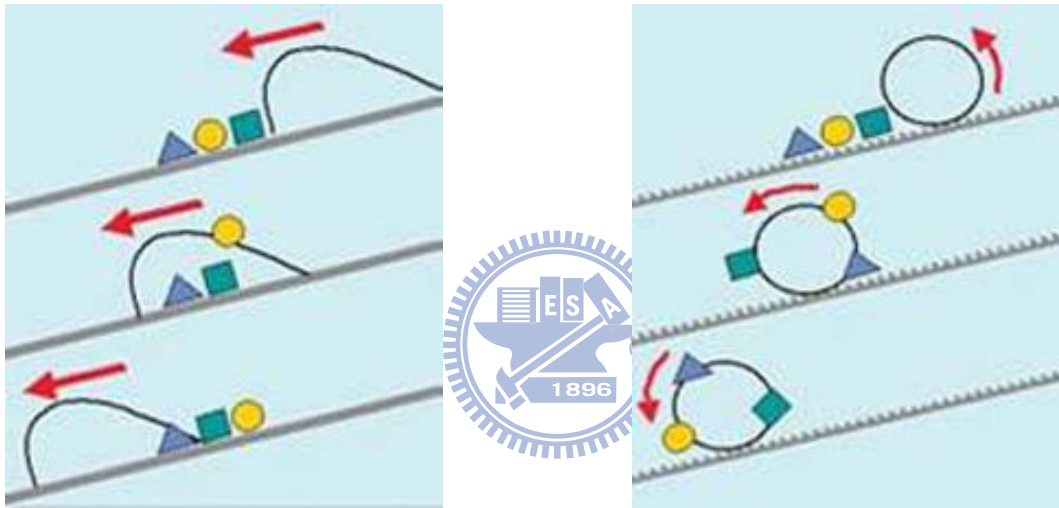


Figure 5-10. (Left) Surfaces without self-cleaning. (Right) Surfaces with self-cleaning.

### 5.2.1 Natural Examples

Several natural materials exhibit super-hydrophobicity, with advancing contact angles between  $150^\circ$  and  $165^\circ$ . Neinhuis and Barthlott reported that this is the case for the leaves of about 200 plants, including asphodelus, eucalyptus, euphorbia, Indian Cress, Lady's Mantle, lotus and tulipa (Figure 5-11). [42-44] These surfaces have generally three common features: (a) they are coated by an epicuticular film of wax, or by wax crystalloids, making them hydrophobic (Young contact angle greater than  $90^\circ$ ); (b) they are decorated by textures such as bumps, at a scale of typically  $10\mu\text{m}$ ; (c) a

secondary texture, of much smaller size (about  $1\mu\text{m}$  in many cases) and different morphology (often hairs) is superimposed on the first one. [42-44]

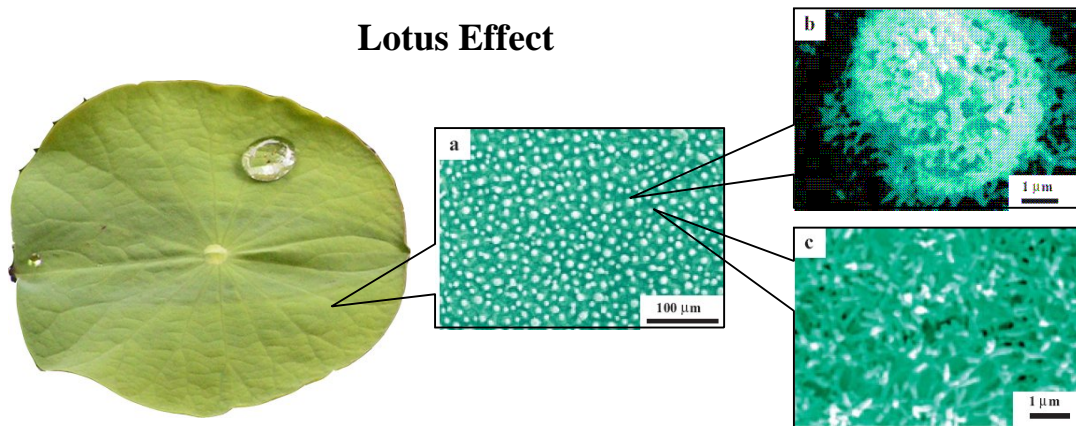


Figure5-11. Water droplets on lotus. [42]

Similarly, animals can be super-hydrophobic, owing to micro-structures at a scale between 100 nm and several micrometres. This is the case for example for water strider legs (Figure 5-12), butterfly wings (and indeed lepidopter means ‘having wings with scales’) (Figure 5-13), duck feathers and some bugs. [45-47] In many cases, this is a strategy for allowing a safe interaction with water: a duck coming out of water immediately de-wets, and water striders are supported by the surface of a pond. Butterflies close their wings during the night, and dew condensation between the wings would stick them together if they were wettable.

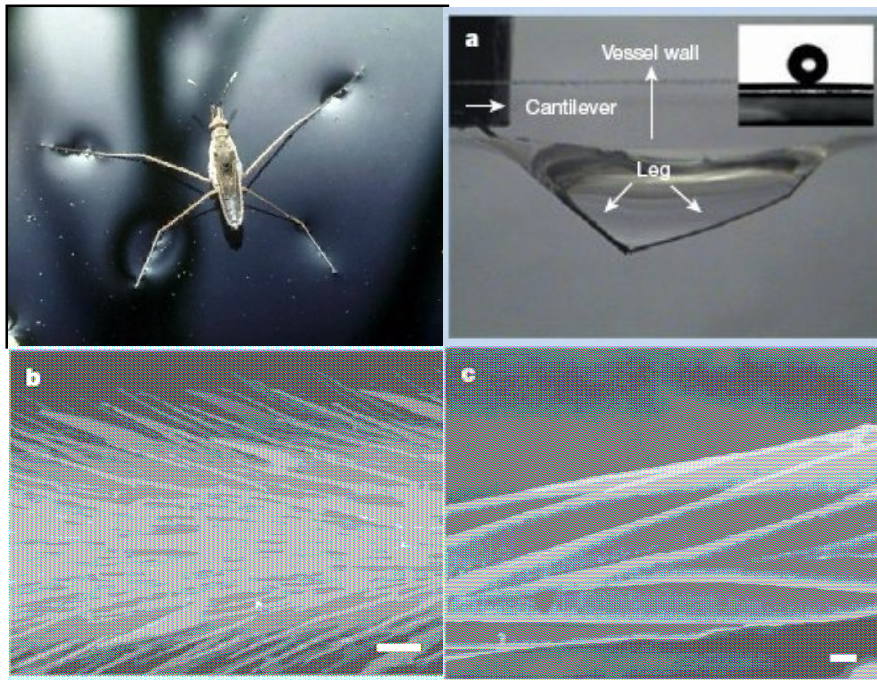


Figure 5-12. The non-wetting leg of a water strider. (a) Typical side view of a maximal-depth dimple (4.38 mm) just before the leg pierces the water surface. Inset, water droplet on a leg; this makes a contact angle of  $167.6^\circ$ . (b), (c), Scanning electron microscope images of a leg showing numerous oriented spindly microsetae (b) and the fine nanoscale grooved structures on a seta (c). Scale bars: b,  $20\ \mu\text{m}$ ; c,  $200\ \text{nm}$ .

As a conclusion, all these natural materials clearly show that the hydrophobicity of a solid is enhanced by textures. We further examine what the mechanisms are of this effect and propose partial answers to the (open) question of why double structures are often present. But we first describe how many synthetic super-hydrophobic materials have been developed (in particular in the past few years) and discuss their properties.



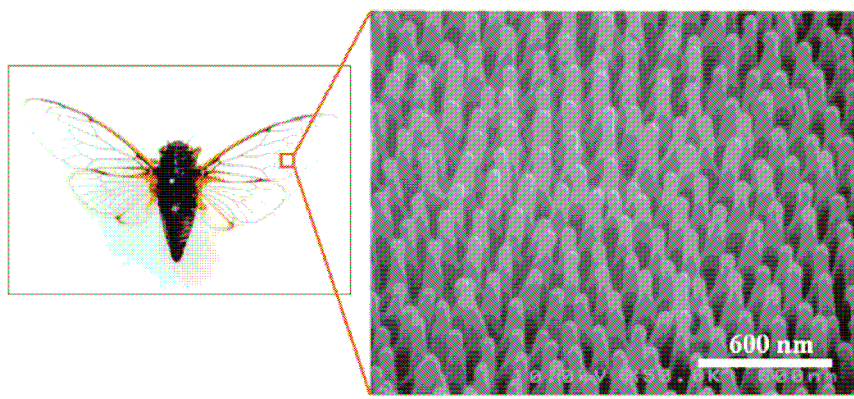


Figure 5-13. FE-SEM micrograph of the wing surface of *Cicada orni* with regularly aligned nanostrips.

### 5.2.2 Synthetic Substrates

Many synthetic materials have been developed like these natural examples in order to obtain water-repellency. Some applications are quite obvious: stone, wood and concrete need to be protected from the effects of rain. In other cases (fabrics), we need enhanced water-proofing. One can also try to get rid of droplets which affect the transparency of glass (window panes, windshields, greenhouses) or reflection (mirror). It is also expected (or hoped) that a water-repellent substrate will be anti-frost and anti-dew. But one of the most important properties of these substrates is their ability to let liquids move very quickly on them: this can be extremely interesting in microfluidic devices, where we often desire a reduction of the friction associated with a flow. This also explains why these materials are often referred to as self-cleaning: raindrops are efficiently removed, taking with them the dirt particles which were deposited on the solids [48]. We can see the same phenomenon when pouring liquid nitrogen on the ground: the very mobile drops take with them the dust present on the surface, the particles lowering interfacial energy by adsorbing at the interface. Many of the plants which are super-hydrophobic indeed look cleaner because of this effect—

which could be one of the reasons for the reverence of the lotus in India.

One method to improve the liquid repellency of a surface is to combine a suitable chemical structure (surface energy) with a topographical microstructure (roughness); previous attempts have included preparing fractal surface (Figure 5-14), [32] plasma treating polymer surfaces, [49,50] preparing gel-like roughened polymers through solvent processing (Figure 5-15), [51] preparing roughened block copolymers through solvent processing (Figure 5-16) [52], and densely packing aligned carbon nanotubes [53-55]. Both super-hydrophobic and super-amphiphobic surfaces can result from increased surface roughness; this effect occurs naturally on the lotus leaf, for example. [43,56] The surfaces of these leaves possess a micron-level roughness covered with nano-sized crystals of wax; [54] the water contact angles of these leaves can be as high as  $160^\circ$  because air is trapped between the water droplets and the wax crystals at the plant surface to minimize the contact area. [57]

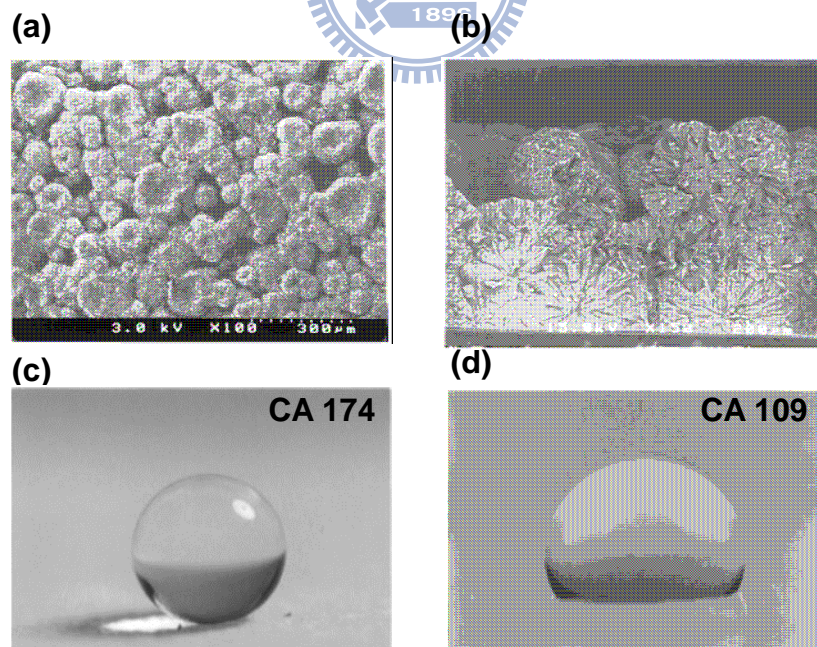


Figure 5-14. SEM images of the fractal alkylketene dimmer (AKD) surface: (a,) top view, (b) cross section. Water droplet on AKD surfaces: (c) fractal AKD surface; (d) flat AKD surface. [32]

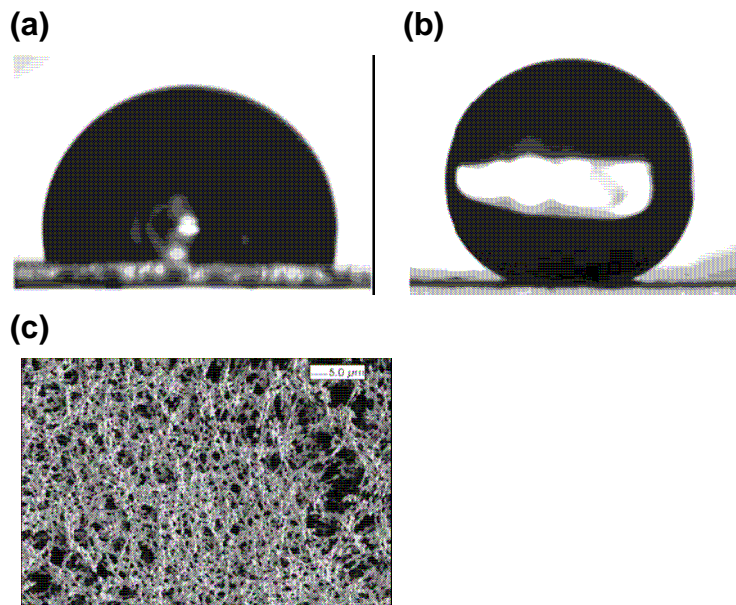


Figure 5-15. The profile of a water drop on (a) a smooth i-PP surface ( $CA = 104^\circ$ ), (b) a superhydrophobic i-PP coating on a glass slide ( $CA = 160^\circ$ ). (c) SEM picture of a superhydrophobic i-PP film. [51]

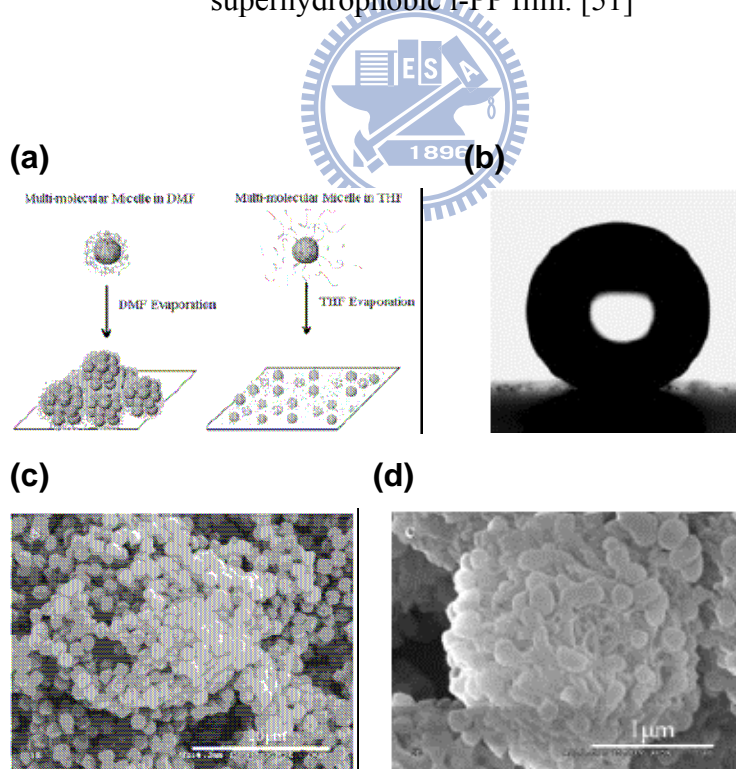
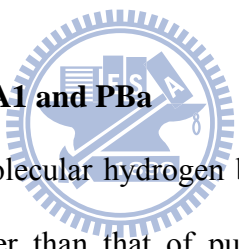


Figure 5-16. (a) Illustration of the solvent effect on the morphologies of PP-PMMA copolymer surface. (b) The profile of a water drop on superhydrophobic polymer surface. (c) SEM images of superhydrophobic polymer. (d) Enlarged view of (c). [52]

Whatever its nature, natural or artificial, regularly patterned or highly disordered, a structured hydrophobic material is super-hydrophobic. This property a priori sounds interesting, since it should provide a strong reduction of adhesion of the drops—but the situation is not that simple: we saw that in some cases the hysteresis of the contact angle can be extremely small, which defines a slippery surface, but that in other cases this quantity can be large, which implies a sticky state (in spite of a very high contact angle), of less obvious practical interest. We now give some hints about the mechanisms responsible for these different effects, and stress in particular that indeed two different super-hydrophobic states can exist and even coexist.

### **5.3 Surface behavior of siloxane-imide-containing polybenzoxazines**

#### **5.3.1 Surface behavior of PBZ-A1 and PBA**



PBZs feature strong intramolecular hydrogen bonds and result in extremely low surface free energies, even lower than that of pure Teflon. [58] A fraction of the intramolecular hydrogen bonds in the as-cured sample tends to convert into intermolecular hydrogen bonds upon thermal treatment, thereby resulting in increased hydrophilicity and wettability. To broaden the applications of PBZs, benzoxazine monomers possessing less sensitive toward thermal treatment are required.

The surface behaviors during curing process of the siloxane-imide-containing monomer (PBZ-A1) and bisphenol A-containing bifunctional benzoxazine monomer (PBA) were characterized after spin-coating with thicknesses of ca. 150 nm. Table 5-3 lists the advancing contact angles and standard deviations of three different testing liquids on the surfaces of PBA and PBZ-A1 films with various curing and annealing times. Due to the advancing contact angle is relatively less sensitive to surface

roughness and heterogeneity than the receding angle, advancing angle data have been commonly used to calculate surface and interfacial tension components. [24, 59] At a curing and annealing temperature of 230 °C, the contact angles for both PBa and PBZ-A1 from all testing liquids increased initially during the first hour but decreased steadily thereafter (Figure 5-17). In the PBa system, curing at 230 °C for 1 hr resulted in the highest contact angles for all three tested liquids: 106.1° for water, 82.5° for ethylene glycol, and 84.3° for diiodomethane. In the PBZ-A1 system, similar trends were observed by curing and annealing at 230 °C, except that the contact angles were all higher than those for the PBa system. Curing at 230 °C for 1 hr also provided the highest contact angles for all three of the testing liquids: 108.8° for water, 85.4° for ethylene glycol, and 86.8° for diiodomethane. The contact angle for water on PBa was initially 105.9° but decreased dramatically to 13.7° after curing for 24 hrs. In contrast, the contact angle for water on PBZ-A1 was initially 106.7°, reached 108.8° after curing for 1 hr, and decayed very slowly to 84.0° after curing for 24 hrs. Indeed, the contact angles for water on PBZ-A1 were all higher than those on PBa at all curing time, suggesting that the good thermo-stability of the siloxane-imide-containing segment in BZ-A1 is able to improve the stability of its surface free energy during curing and annealing at high temperatures for long periods of time.

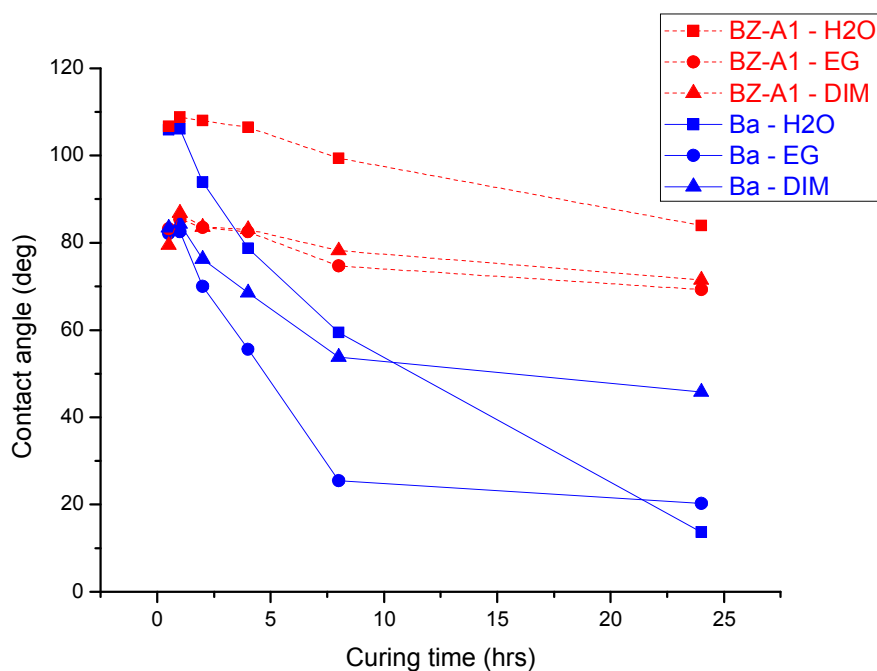


Figure 5-17. Contact angles of polybenzoxazines during different curing time at 230 °C.

Table 5-3. Surface free energies of the cured and annealed PBa and PBZ-A1

Polymer	Curing conditions		Contact angle (°)			Surface free energy $\gamma_s$ (mJ/m <sup>2</sup> )
	Temperature (°C)	Time (h)	Water (H <sub>2</sub> O)	Ethylene Glycol (EG)	Diiodomethane (DIM)	
PBa	230	0.5	105.9	82.1	83.4	17.0
		1	106.1	82.5	84.3	16.6
		2	93.9	70.0	76.3	22.5
		4	78.8	55.6	68.6	30.0
		8	59.4	25.5	53.8	43.6
		24	13.7	20.3	45.8	42.6
PBZ-A1	230	0.5	106.7	83.2	79.5	18.5
		1	108.8	85.4	86.8	15.1
		2	108.0	83.5	83.6	16.6
		4	106.5	82.5	83.1	17.0
		8	99.4	74.7	78.2	20.4
		24	84.0	69.3	71.5	24.6

The van Oss and Good's three-liquid method [17] was employed to calculate the

surface free energy ( $\gamma_s$ ) and results are summarized in Table 5-3. When the curing temperature for the PBa system was 230 °C, the surface free energy decreased initially and then increased steadily with curing time (Figure 5-18). The lowest surface free energy (16.6 mJ/m<sup>2</sup>) was obtained when curing at 230 °C for 1 hr and then increased to 42.6 mJ/m<sup>2</sup> upon increasing the curing or annealing time. In this system, curing at 230 °C for 1 hr provided the lowest surface free energy of 15.1 mJ/m<sup>2</sup>—a value that is even lower than that of Teflon [60] (21 mJ/m<sup>2</sup>) and PBa (16.6 mJ/m<sup>2</sup>), determined by using same liquids. The low surface free energy of PBZ-A1 may come from the combination of benzoxazine group and siloxane-containing segments. The incorporation of the siloxane segment in benzoxazine improves thermal stability while maintains its low surface free energy after high temperature thermal annealing for periods of time.

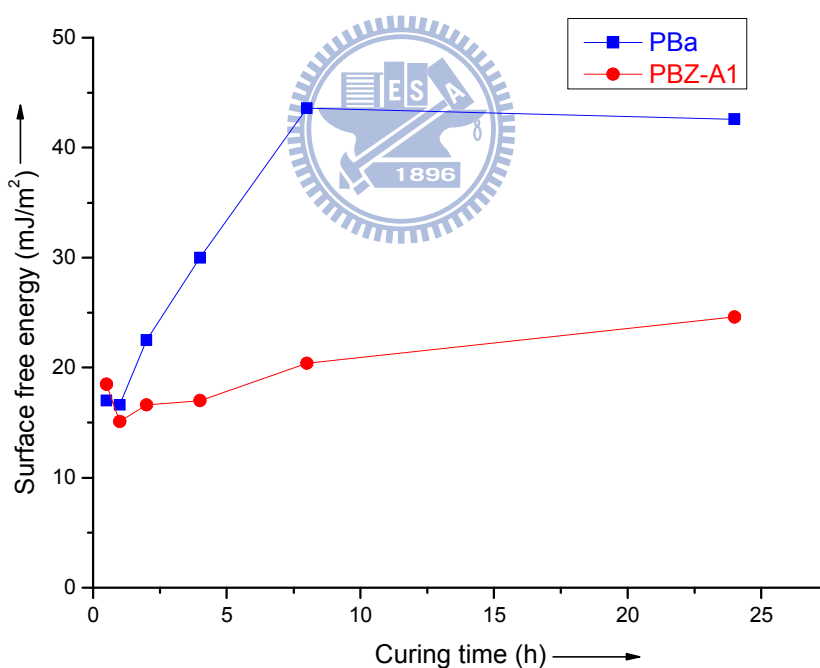


Figure 5-18. Surface free energies of PBZs after various curing and annealing hours at

230 .

### 5.3.2 Surface behavior and thermal resistant of PBZ-A6, PBZ-A1 and PBa

Since PBZs feature strong intramolecular hydrogen bonds, they exhibit extremely low surface free energies, even lower than that of pure Teflon. [58] We compared the surface behavior during the curing process of the siloxane-imide-containing monomers PBZ-A6 and PBZ-A1 and the bisphenol A-containing bifunctional benzoxazine monomer PBa after spin-coating to a thickness of ca. 150 nm. Table 5-4 lists the advancing contact angles and standard deviations of three different testing liquids on the surfaces of the PBZ films after subjecting to various curing and annealing times. Since the advancing contact angle is relatively less sensitive to surface roughness and heterogeneity than the receding angle, advancing angle data are commonly used to calculate surface and interfacial tension components. [24, 59] Under curing and annealing temperature at 230 °C, the water contact angles for those three PBZ films (PBa, PBZ-A1, PBZ-A6) were all higher than 100° during the first hour, indicating hydrophobic properties. For all three systems, curing at 230 °C for 1 hr provided the highest contact angles for the three tested liquids. Notably, the contact angles for the PBZ-A6 system (113.7° for water, 93.9° for EG, and 92.3° for DIM) were all higher than those of the PBa and PBZ-A1 systems.



Table 5-4. Advancing contact angles and corresponding surface free energies for PBZ films prepared from Ba, BZ-A1, and BZ-A6

Polymers	Curing conditions		Contact angle (°)			Surface free energy $\gamma_s$ (mJ/m <sup>2</sup> )
	Temperature (°C)	Time (hrs)	Water (H <sub>2</sub> O)	Ethylene Glycol (EG)	Diiodomethane (DIM)	
PBa	230	1	106.1	82.5	84.3	16.6
		2	93.9	70.0	76.3	22.5
		4	78.8	55.6	68.6	30.0
		8	59.4	25.5	53.8	43.6
		24	13.7	20.3	45.8	42.6
PBZ-A1	230	1	108.8	85.4	86.8	15.1
		2	108.0	83.5	83.6	16.6
		4	106.5	82.5	83.1	17.0
		8	99.4	74.7	78.2	20.4
		24	84.0	69.3	71.5	24.6
PBZ-A6	230	1	113.7	93.9	92.3	12.4
		2	112.2	89.0	86.8	14.7
		4	111.9	88.7	86.8	14.7
		8	110.9	88.2	86.8	14.8
		24	108.3	82.3	84.3	16.2

We employed van Oss and Good's three-liquid method [17] to calculate the surface free energies ( $\gamma_s$ ) of the systems and results are summarized in Table 5-4. The two siloxane-imide-containing benzoxazine systems produced lower surface free energies. The lower surface free energy of PBZ-A6 ( $\gamma_s = 12.4$  mJ/m<sup>2</sup>) can be attributed to the dual effects; forming intramolecular hydrogen bonds after ring opening of the benzoxazine and introducing a high content of low-surface-free-energy dimethylsiloxane chains. In a previous study, we found that the incorporation of a

siloxane segment into a benzoxazine is able to improve the thermal stability while maintaining its low surface free energy after high-temperature thermal annealing for various periods of time. [61] Figure 5-19 reveals that the surface free energy of the PBa increased from 16.6 mJ/m<sup>2</sup> after the first hour curing to 42.6 mJ/m<sup>2</sup> after thermal annealing for 24 hrs. The thermal stability in terms of surface free energy was significantly improved when siloxane segments were incorporated: the surface free energies of PBZ-A1 and PBZ-A6 increased to only 24.6 and 16.2 mJ/m<sup>2</sup> after similar thermal annealing for 24 hrs. Such thermal stability improvement in surface free energy of PBZ-A6 is from the combination of the benzoxazine groups and the presence of the longer siloxane-containing segments. The high char yield of PBZ-A6 (16–17 wt% in air at 850 °C) confirms its high content of siloxane-containing units. Thus, the incorporation of the siloxane segments in benzoxazines improves the thermal stability while maintaining low surface free energy after thermal annealing at high temperatures for lengthy periods of time.

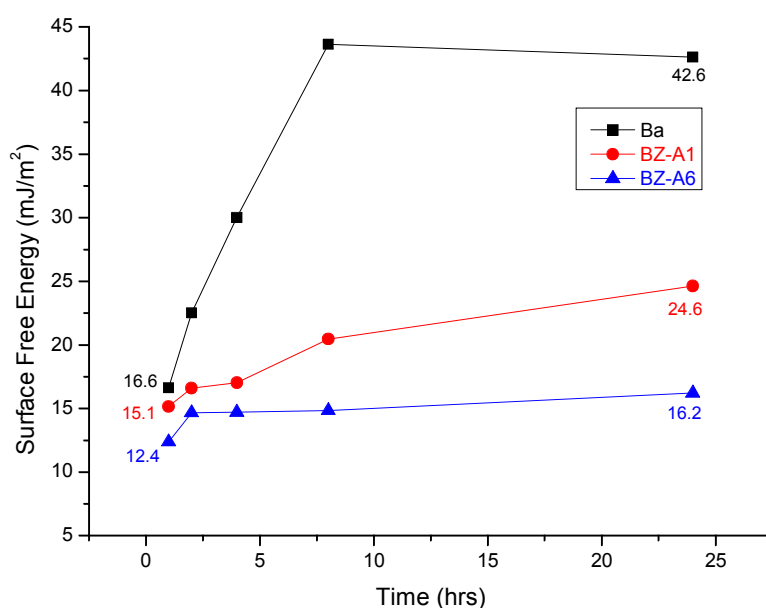


Figure 5-19. Surface free energies of PBZs after curing and annealing at 230 °C.

### 5.3.3 Surface behavior and ultraviolet resistant of PBZ-A6, PBZ-A1 and PBa

Next, we examined the UV resistance properties of the PBZs. Figure 5-20 presents the variation in water contact angles after exposure to UV-A radiation. The water contact angles of PBa, PBZ-A1, and PBZ-A6 films cured at 230 °C for 1 hr were all greater than 100°, indicating that they all possess hydrophobic surfaces. The water contact angle of PBa dramatically decreased to 12.1° from 106.1° after 24 hrs UV-A exposure, and dropped to 5.1° after 100 hrs of exposure. In a previous study<sup>15</sup>, we found that a fraction of the intramolecular hydrogen bonds of the as-cured samples converted into intermolecular hydrogen bonds after UV exposure, thereby resulting in increased hydrophilicity. For the siloxane-imide-containing PBZ-A1, the water contact angle was maintained at 107.1° after 24 hrs of UV-A exposure, but it decreased to 42.5° after 168 hrs. Notably, PBZ-A6 maintained its hydrophobic properties; the water contact angle remained at 103.4° after UV-A exposure for 500 hrs. Figure 5-21 displays the surface free energy (calculated using van Oss and Good's three-liquid method) of PBZ-A6 during UV-A exposure. We observed similar trend in contact angle data when using EG and DIM as solvents, the contact angles of these two solvents decreased only less than 10% after 500 hrs of UV-A exposure. The surface free energy of PBZ-A6 remained extremely low at 16.5 mJ/m<sup>2</sup> after UV exposure for 500 hrs.

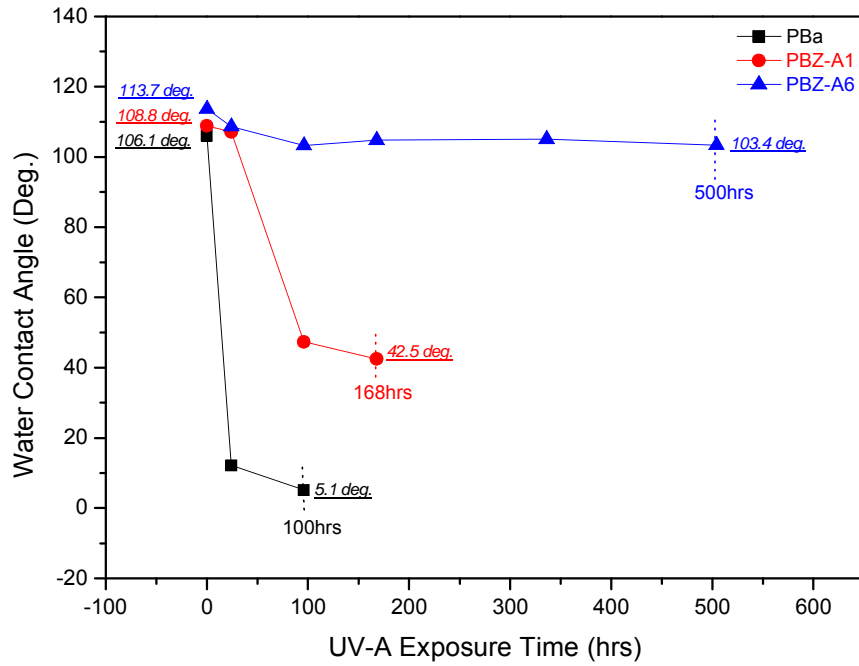


Figure 5-20. Water contact angles of PBZ films after UV-A exposure for various periods of time.

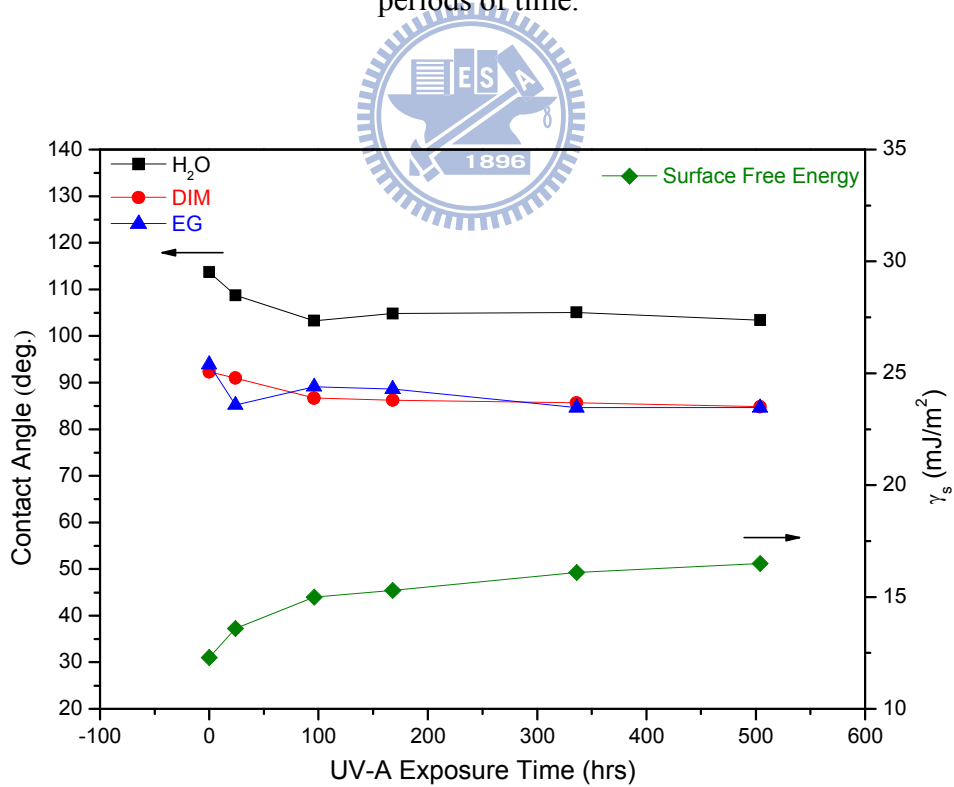


Figure 5-21. UV resistant behavior of PBZ-A6 film.

## References

- [1] Dupré, A., *Theorie mécanique de la chaleur*, Paris, **1869**, p.368.
- [2] Young, T., *Phil Trans. R. Soci. Lond.* **1805**, 95, 65.
- [3] Michaelis, A. S.; Dean, S. W., *J. Phys. Chem.* **1962**, 66, 34.
- [4] Baily, G. L. J. *Proc. 2nd Int. Congr. Surf. Act.*, **1957**, 3, 189.
- [5] Poynting, J. H.; Thompson, J. J. *A Textbook of Physics: Properties of Matter*, 8th ed., Charles Griffin, London, **1920**.
- [6] Girifalco, L. A.; Good, R. J. *J. Phys. Chem.* **1957**, 61, 904.
- [7] Good, R. J.; Girifalco L. A.; Kraus, G. *J Phys. Chem.* **1957**, 62, 1418.
- [8] Good, R. J.; Girifalco, L. A. *J. Phys. Chem.* **1960**, 64, 561.
- [9] Fowkes, F. W. in Contact Angle, *Wettability and Adhesion, Advances in Chemistry Series 43*, R. F. Gould, Ed., American Chemical Society, Washington, DC, **1964**, p. 99.
- [10] Fowkes, F. W. in Adhesion and Adsorption of Polymers, *Polymer Science and Technology*, vol. 12A, L. H. Lee, Ed., Plenum Press, New York, **1980**, p. 43.
- [11] Owens, D. K.; Wendt, R. C. *J. Appl. Polym. Sci.* **1969**, 13, 1741.
- [12] Kaelble, D. H. *J. Adhesion* **1970**, 2, 50.
- [13] Wu, S. *J. Polym. Sci., Part C* **1971**, 34, 19.
- [14] Wu, S. in Adhesion and Adsorption of Polymers, *Polymer Science and Technology*, vol. 12A, L. H. Lee, Ed., Plenum Press, New York, **1980**, p. 53.
- [15] Fowkes, F. M.; Mostafa, M. A. *Int. Eng. Chem. Prod. Res. Dev.* **1978**, 17, 3.
- [16] Fowkes, F. M.; McCarthy, D. C.; Mostafa, M. A. *J. Colloid Interface Sci.* **1980**, 78, 200.
- [17] van Oss, C. J.; Chaudhury, M. K.; Good, R. J. *Chem. Rev.* **1988**, 88, 927.
- [18] van Oss, C. J.; Ju, L.; Chaudhury, M. K.; Good, R. J. *J. Colloid Interface Sci.*

- 1989**, 128, 313.
- [19] van Oss, C. J.; Good, R. J. *J. Macromol. Sci.-Chem.* **1989**, A26, 1183.
- [20] van Oss, C. J. *J. Dispers. Sci. Technol.* **1990**, 11, 491.
- [21] van Oss, C. J.; Arnold, K.; Good, R. J.; Gawrisch, K.; Ohki, S. *J. Macromol. Sci.-Chem.* **1990**, A27, 563.
- [22] van Oss, C. J.; Good, R. J.; Busscher, H. J. *J. Dispers. Sci. Technol.* **1990**, 11, 75.
- [23] van Oss, C. J.; Giese, R. F.; Jr.; Good, R. J. *Langmuir* **1990**, 6, 1711.
- [24] Good, R. J.; van Oss, C. J. in *Modern Approaches to Wettability*, M. E. Schrader and G. I. Loeb, Eds., Plenum Press, New York, **1992**, p. 1.
- [25] Good, R. J. in *Contact Angle, Wetting, and Adhesion*, K. L. Mittal, Ed., VSP, **1993**, p. 3.
- [26] LeGrand, D. G.; Gaines, G. L.; Jr. *J. Colloid Interface Sci.* **1969**, 31, 162.
- [27] LeGrand, D. G.; Gaines, G. L.; Jr. *J. Colloid Interface Sci.* **1973**, 42, 181.
- [28] Wu, S. *J. Colloid Interface Sci.* **1969**, 31, 153.
- [29] Wu, S. *J. Macromol. Sci.* **1974**, C10, 1.
- [30] Schonhorn, H.; Ryan, F. W. *J. Phys. Chem.* **1966**, 70, 3811.
- [31] Rastogi, A. K.; St. Pierre, L. E. *J. Colloid Interface Sci.* **1969**, 31, 168.
- [32] Onda, T.; Shibuichi, S.; Satoh, N.; Tsujii, K. *Langmuir* **1996**, 12, 2125.
- [33] Chen, W.; Fadeev, A. Y.; Hsieh, M. C.; Oner, D.; Youngblood, J.; McCarthy, T. J. *Langmuir* **1999**, 15, 3395.
- [34] Wu, Y.; Sugimura, H.; Inoue, Y.; Takai, O. *Chem. Vap. Deposition* **2002**, 8, 47.
- [35] Tsujii, K.; Yamamoto, T.; Onda, T.; Shibuchi, S. *Angew. Chem. Int. Ed. Engl.* **1997**, 36, 1011.
- [36] Tadanaga, K.; Katata, N.; Minami, T. *J. Am. Ceram. Soc.* **1997**, 80, 3213.
- [37] Nakajima, A.; Fujishima, A.; Hashimoto, K.; Watanabe, T. *Adv. Mater.* **1999**, 11,

1365.

- [38] Nakajima, A.; Abe, K.; Hashimoto, K.; Watanabe, T. *Thin Solid Films* **2000**, *376*, 140.
- [39] Bico, J.; Marzolin, Quéré, C. D. *Europhys. Lett.* **1999**, *47*, 220.
- [40] Wang, R.; Hashimoto, K.; Fujishima, A.; Chikuni, M.; Kojima, E.; Kitamura, A.; Shimohigoshi, M.; Watanabe, T. *Nature* **1997**, *388*, 431.
- [41] Miwa, M.; Nakajima, A.; Fujishima, A.; Hashimoto, K.; Watanabe, T. *Langmuir* **2000**, *16*, 5754.
- [42] Neinhuis, C.; Barthlott, W. *Ann. Bot.* **1997**, *79*, 667.
- [43] Neinhuis, C.; Barthlott, W. *Planta* **1997**, *202*, 1.
- [44] Otten, A.; Herminghaus, S. *Langmuir* **2004**, *20*, 2405.
- [45] Wagner, T.; Neinhuis, C.; Barthlott, W. *Acta Zool.* **1996**, *3*, 213.
- [46] Lee, W.; Jin, M. K.; Yoo, W. C.; Lee, J. K. *Langmuir* **2004**, *20*, 7665.
- [47] Gao, X.; Jiang, L. *Nature* **2004**, *432* 36.
- [48] Blossey, R. *Nat. Mater.* **2003**, *2*, 301.
- [49] M. Morra, E. Occhiello, F. Garbassi, *Langmuir* **1989**, *5*, 872.
- [50] Woodward, I.; Schofield, W. C. E.; Roucoules, V.; Badyal, J. P. S. *Langmuir* **2003**, *19*, 3432.
- [51] Erbil, H. Y.; Demirel, A. L.; Avcı, Y.; Mert, O. *Science* **2003**, *299*, 1377.
- [52] Xie, Q.; Fan, G.; Zhao, N.; Guo, X.; Xu, J.; Dong, J.; Zhang, L.; Zhang, Y.; Han, C. C. *Adv. Mater.* **2004**, *16*, 302.
- [53] De Gennes, P. G. *Rev. Mod. Phys.* **1985**, *57*, 827.
- [54] Feng, L.; Li, S.; Li, Y.; Li, H.; Zhang, L.; Zhai, J.; Song, Y.; Liu, B.; Jiang, L.; Zhu, D. *Adv. Mater.* **2002**, *14*, 1857.
- [55] Li, H.; Wang, X.; Song, Y.; Liu, Y.; Li, Q.; Jiang, L.; Zhu, D. *Angew. Chem. Int.*

*Ed.* **2001**, *40*, 1743.

[56] Neinhuis, C.; Barthlott, W. *New Phytologist* **1998**, *138*, 91.

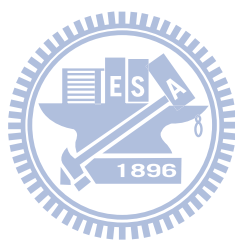
[57] Herminghaus, S. *Europhys. Lett.* **2000**, *52*, 165.

[58] Wang, C. F.; Su, Y. C.; Kuo, S. W.; Huang, C. F.; Sheen, Y. C. and Chang, F. C.  
*Angew Chem Int Ed* **2006**, *45*, 2248.

[59] Drelich, J.; Miller, J. D. and Good, R. J. *J Colloid Interface Sci* **1996**, *179*, 37.

[60] Takei, Y. G.; Aoki, T.; Sanui, K.; Ogata, N.; Sakurai, Y. and Okano, T.  
*Macromolecules* **1994**, *27*, 6163.

[61] Chen, K.C.; Li, H.T.; Chen, W. B.; Liao, C, H.; Sun, K. W. and Chang, F. C.;  
*Polym Int* accepted





## Chapter 6

# New Thermosetting Resin from Siloxane-Containing Benzoxazine and Epoxy Resin

### ABSTRACT

Siloxane-imide-containing benzoxazine, BZ-A6, was copolymerized with siloxane-epoxy, GT-1000. The curing behavior of the copolymers was studied using DSC and FT-IR, which indicated a lower curing temperature of 150 °C. The activation energy ( $E_a$ ) of BZ-A6/ GT-1000 copolymer is 59.4 KJ/mol. from Kissinger method. The siloxane benzoxazine-epoxy mixture exhibited higher thermal stability, exhibited higher char yield as 44.6% and higher decomposed temperature at 364.9 °C. Moreover, the water contact angle of the BZ-A6/ GT-1000 copolymer is more stable than the conventional bisphenol A type benzoxazine-epoxy, Ba/ DGEBA, during the UV exposure process, indicating that the benzoxazine-epoxy mixture is more suitable to apply as a hydrophobic material with UV resistant requirement. There are wide applications of siloxane benzoxazine-epoxy mixture since its lower curing temperature and good temperature- and UV- resistant properties.

**Keywords:** benzoxazine, siloxane, epoxy, copolymer, thermal stability, UV stability, DSC kinetic

## 6.1 Introduction

Polybenzoxazine which is synthesized by the ring-opening polymerization of cyclic benzoxazine monomer has been developed as a new type phenolic resin. [1-3] Polybenzoxazines have excellent thermal and non-flammable properties like traditional phenolic resins, and they also have excellent properties that are not found in the traditional phenolic resins, such as molecular design flexibility, low moisture absorption and no by product release upon curing. [2, 3, 4-8]

In our previous study, a new class of PBZ was developed which exhibited extremely low surface free energies—even lower than that of pure Teflon—through strong intramolecular hydrogen bonding. [9-12] Furthermore, we applied the low surface free energy material polybenzoxazine as an efficient mold-release agent for silicon molds<sup>13</sup> and a stable superhydrophobic surface. [10] Typically, the surface free energies of PBZ systems increase steadily upon increasing the thermal curing time and UV exposure time, indicating that PBZs lose stability during thermal treatment or UV exposure, mainly due to the formation of carbonyl-containing species during UV exposure. [12, 14] To overcome this problem, we designed the siloxane segment into benzoxazine to improve the stability of surface free energy during high temperature storage. [15, 16] A longer siloxane segment was introduced into the benzoxazine BZ-A6, and examined to have better thermal stability and UV resistance than those polybenzoxazines lacking the siloxane group after thermal crosslinking. [17]

Epoxy resins have been widely used in those applications required thermosetting characteristics. However, the hardeners used for the epoxy resins including amines and anhydrides, have some drawbacks such as high toxicity or low UV stability. [18] Copolymerization of the polybenzoxazine precursor with an epoxy may allow the network structure to achieve a higher crosslink density and have been studied. In a

number of previous works, benzoxazines and epoxy resins copolymerization have been discussed and reported to be potential effective for thermal and mechanical properties. [19-22] The curing kinetic of benzoxazine system was first investigated by Ishida et al [23] to understand the curing process. The activation energy of benzoxazine resin, Ba, was calculated to be 116 KJ/ mol by Kissinger's method. The kinetic of copolybenzoxazine and benzoxazine-epoxy novolac resin are also discussed in our previous study [24] and by Jubsilp et al [25], respectively.

The present study reports the copolymer properties of siloxane-benzoxazine and siloxane-epoxy. The curing reaction was examined by DSC and FT-IR, the thermal properties was studied by TGA and the UV stability was also discussed.



## 6.2 Experimental

### 6.2.1 Materials

The bifunctional bisphenol A-type benzoxazine (Ba, Figure 6-1) was purchased from Shikoku Chemicals (Japan). Diglycidyl ether of bisphenol-A epoxy resin (DGEBA, Epon 828, epoxy equivalent weight: 190) was obtained from Shell Chemical Company. Phenylmethylsiloxane-co-dimethylsiloxane)-tricyclidyl ether terminated (GT-1000, epoxy equivalent weight: 340) was purchased from Groud Tek Advance Material Science Co., Ltd. (Taiwan). 1,4-Dioxane and paraformaldehyde (95%) were purchased from TEDIA (USA) and Showa Chemicals (Japan), respectively. Ethyl acetate (99.9%) was used as received from Mallinckrodt, Inc. (USA). Tetrahydrofuran (99%) and aniline (99%) were obtained from Aldrich (USA). The chemical structures of these compounds are shown in Figure 6-1.

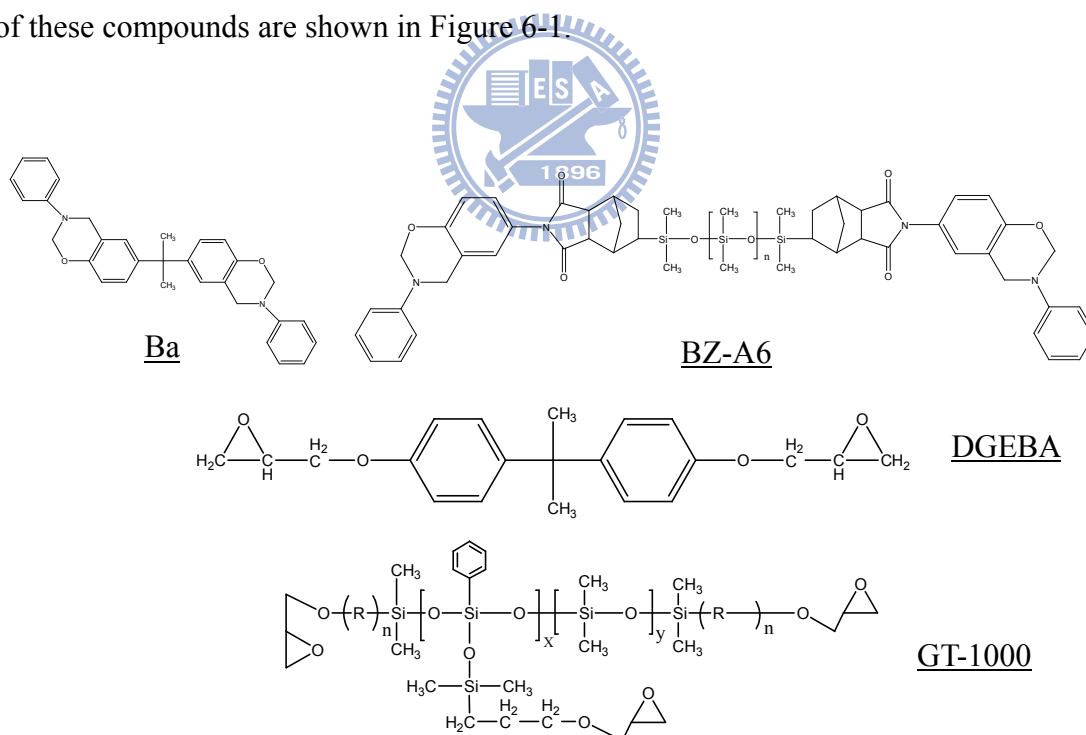


Figure 6-1. Structure of bi-functional bisphenol A type benzoxazine (Ba), siloxane-imide-containing benzoxazine (BZ-A6) and siloxane-containing epoxy (GT-1000).

### 6.2.2 Synthesis of siloxane-imide-containing benzoxazine (BZ-A6)

Siloxane-imide-containing benzoxazine, BZ-A6 (Figure 6-1), was synthesized according to our previous method. [17] Aniline (3.78 g, 0.04 mol) was added dropwise into a mixture of A6-OH (18.95 g, 0.02 mole), paraformaldehyde (2.44 g, 0.08 mole), and 1, 4-dioxane (120 ml) in a 250 ml round-bottom flask equipped with a magnetic stirrer bar. The mixture was then heated under reflux at 115 °C for 20 hrs, gradually becoming homogeneous and turning dark brown. The resulting mixture was filtered and the solvent evaporated under vacuum. The residue was dissolved in ethyl acetate and washed five times sequentially with 0.5 N aqueous NaOH and distilled water. Evaporation of the solvent and vacuum drying in an oven provided BZ-A6 was obtained as a viscous dark brown liquid product (yield: 87.7%). [17]

### 6.2.3 Curing conditions of neat resin

Samples containing 50 eq.% of benzoxazine and 50 eq.% of epoxy mixture, BZ-A6/GT-1000 and Ba/DGEBA, were prepared and cured at a specified temperature in the oven. The curing reaction of BZ-A6/GT-1000 copolymer was 150 °C for 2 hrs and 180 °C for 2hrs. No external catalyst was used in these experiments. The curing condition was determined as 200 °C for 2 hrs and 230 °C for 2hrs of Ba/ DGEBA copolymer from the results of model reaction.

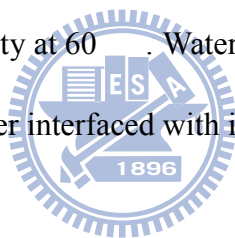
### 6.2.4 Preparation of polybenzoxazine film

Benzoxazine/ epoxy copolymers (Ba/ DGEBA and BZ-A6/ GT-1000) were mixed in THF solution at room temperature, respectively. The solution was filtered through a 0.2 μm syringe filter before spin-coating onto a glass slide (100 mm × 100 mm × 1 mm). 1 mL of the appropriate monomer solution was spin-coated onto a glass slide

using a spinner operating at 1500 rpm for 45 s. Then the samples were subjected to the above described curing schedule.

### 6.2.5 Characterization

Differential scanning calorimetry (DSC) was performed on TA Instrument DSC-Q10 with a heating rate of 10 / min. under nitrogen atmosphere. Thermogravimetric analysis (TGA) was performed on TA Instrument TGA-Q500 with a heating rate of 20 / min. under a nitrogen and an air atmosphere, respectively. TGA was used to study the thermal decomposition of the siloxane-containing benzoxazine/ epoxy resin copolymers. Ultraviolet resistant properties were investigated from QUV accelerated weathering tester under UVA-351 nm wave length and 0.89 W/m<sup>2</sup> irradiation intensity at 60 . Water contact angle goniometry at 25 °C using a Krüss GH-100 Goniometer interfaced with image-capture software by injecting a 5 μL liquid drop.



## 6.3 Results and discussion

### 6.3.1 Curing behavior of benzoxazine with epoxy resin

It is known that benzoxazine exhibit exothermic ring opening reaction around 200-250 °C, which could be monitored by DSC. Benzoxazine-epoxy curing characteristics were obtained by DSC analysis. The DSC of Ba/ DGEBA samples was shown in Figure 6-2(a), heating rate of 10 °C/min. was selected here. In the spectrum, Ba/ DGEBA indicated an exothermic peak at 250.0 °C, and the onset of cure at 227.9

with the total heat of reaction ( $\Delta H$ ) is 304.9 J/g. This is the region where thermal opening of benzoxazine ring takes place and gives phenolic resin and further the epoxy and benzoxazine co-curing reaction happens. [26-28] Figure 6-2(b) is the thermal scanning curve of the copolymerized Ba/ DGEBA after 200 °C/2hrs and 230 °C/2hrs curing. It unveiled that the copolymerization was almost completed since there was no residual reaction heat.

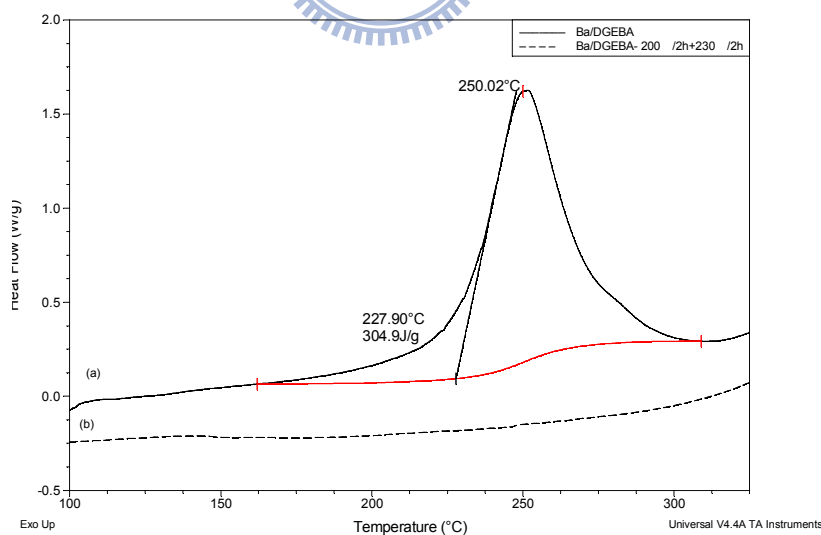


Figure 6-2. DSC thermogram of (a) Ba/ DGEBA copolymer and (b) copolymerized Ba/ DGEBA.

The novel copolymer system of siloxane-imide-containing benzoxazine (BZ-A6)

and siloxane-containing epoxy resin (GT-1000), BZ-A6/ GT-1000 was also checked the curing behavior by DSC, shown in Figure 6-3(a). In the spectrum, BZ-A6/ GT-1000 indicated an exothermic peak at 210.6 °C, and the onset of cure at 142.3 °C with the total heat of reaction (ΔH) is 105.2 J/g. Since the novel copolymer system exhibited much lower curing temperature and less reaction energy, the curing condition was selected as 150 °C / 2hrs and 180 °C / 2hrs and the dynamic DSC curve, Figure 6-3(b), was confirmed that the BZ-A6/ GT-1000 copolymerization proceed to less reaction energy.

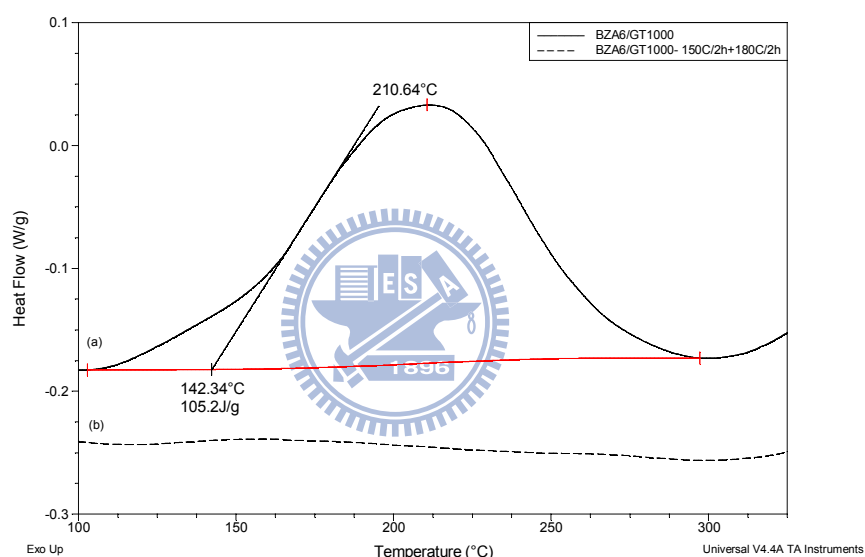


Figure 6-3. DSC thermogram of (a) BZ-A6/ GT-1000 copolymer and (b) copolymerized BZ-A6/ GT-1000.

Ring-opening of the benzoxazine ring at elevated temperatures provides phenolic structures. It was shown in Figure 6-4 that these phenolic hydroxyl groups can react with epoxy resins. The tertiary amine was produced in the backbone of the phenolic resin from the ring-opening of the benzoxazine ring. These tertiary amine groups can catalyzed homopolymerization of epoxy groups. [19, 22, 29, 30]



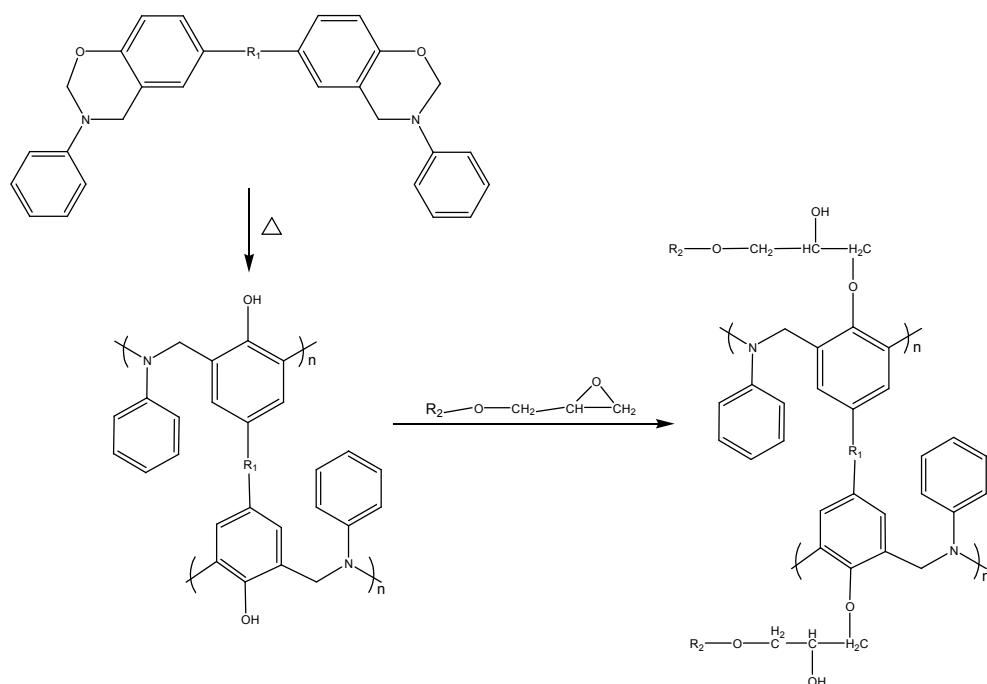


Figure 6-4. Ring-opening reaction of benzoxazine with epoxy.

### 6.3.2 FT-IR Characterization of copolymerization

To investigate the curing reaction of benzoxazine-epoxy copolymer in detail, FT-IR measurement was carried out. FT-IR spectrums of the copolymer of Ba/DGEBA are shown in Figure 6-5. The absorption at  $1234\text{ cm}^{-1}$  assigned to the asymmetric C-O-C stretching of the benzoxazine ring structure and the absorption at  $913\text{ cm}^{-1}$  and  $864\text{ cm}^{-1}$  were assigned to be the epoxy ring, shown in Figure 6-5(a). The benzoxazine ring is start to disappear at the beginning first hour at  $200\text{ }^\circ\text{C}$ , and the epoxide peaks appears to have almost completely disappeared after post curing at  $230\text{ }^\circ\text{C}$ . After curing at  $200\text{ }^\circ\text{C}$  for 2hrs and  $230\text{ }^\circ\text{C}$  for 2hrs, both absorption of benzoxazine and epoxy rings are disappeared, Figure 6-5(e). We realized that the benzoxazine and epoxy ring opened, and the curing reaction proceeded without any curing accelerators. For the BZ-A6/GT-1000 system, the similar copolymerization phenomena even in lower curing condition can be observed from FT-IR spectrum,

Figure 6-6. During polymerization, the oxazine rings open and the absorption at  $1234\text{ cm}^{-1}$  of asymmetric C-O-C stretching from the benzoxazine ring is started to disappear at the beginning first hour at  $150^\circ\text{C}$ . After curing at  $150^\circ\text{C}$  for 2hrs and  $180^\circ\text{C}$  for 2hrs, both absorption of benzoxazine and epoxy rings are disappeared, Figure 6-6(e).

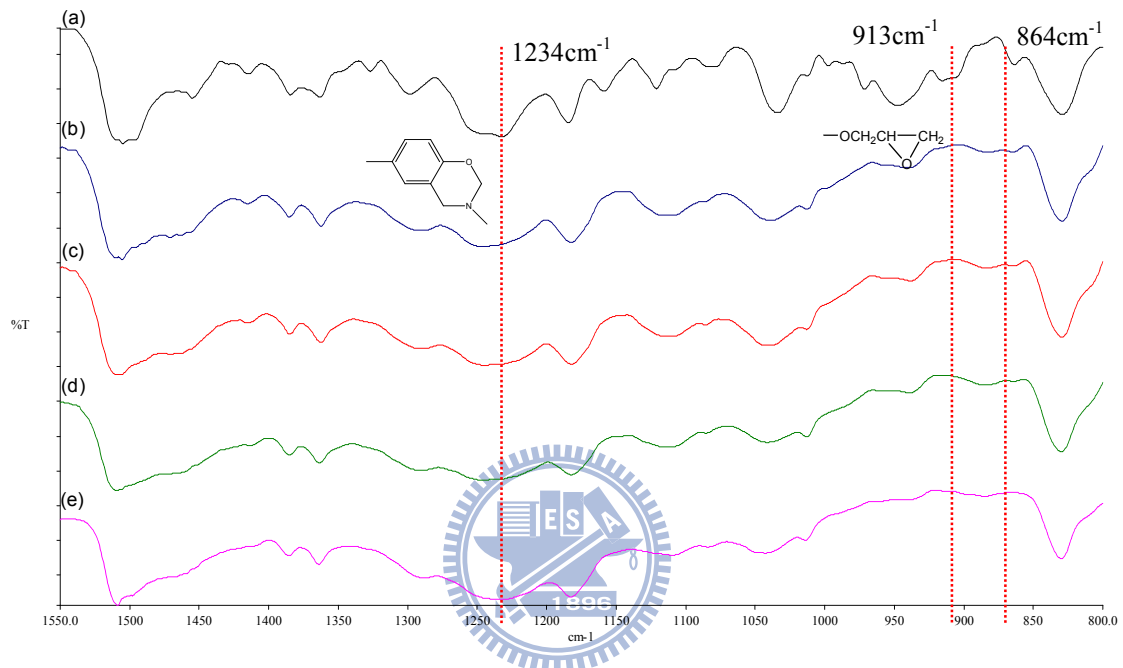


Figure 6-5. FT-IR spectrum of Ba/ DGEBA copolymer (a) before reaction (b)  $200^\circ\text{C} / 1\text{h}$  (c)  $200^\circ\text{C} / 2\text{h}$  (d)  $200^\circ\text{C} / 2\text{h} + 230^\circ\text{C} / 1\text{h}$  (e)  $200^\circ\text{C} / 2\text{h} + 230^\circ\text{C} / 2\text{h}$ .

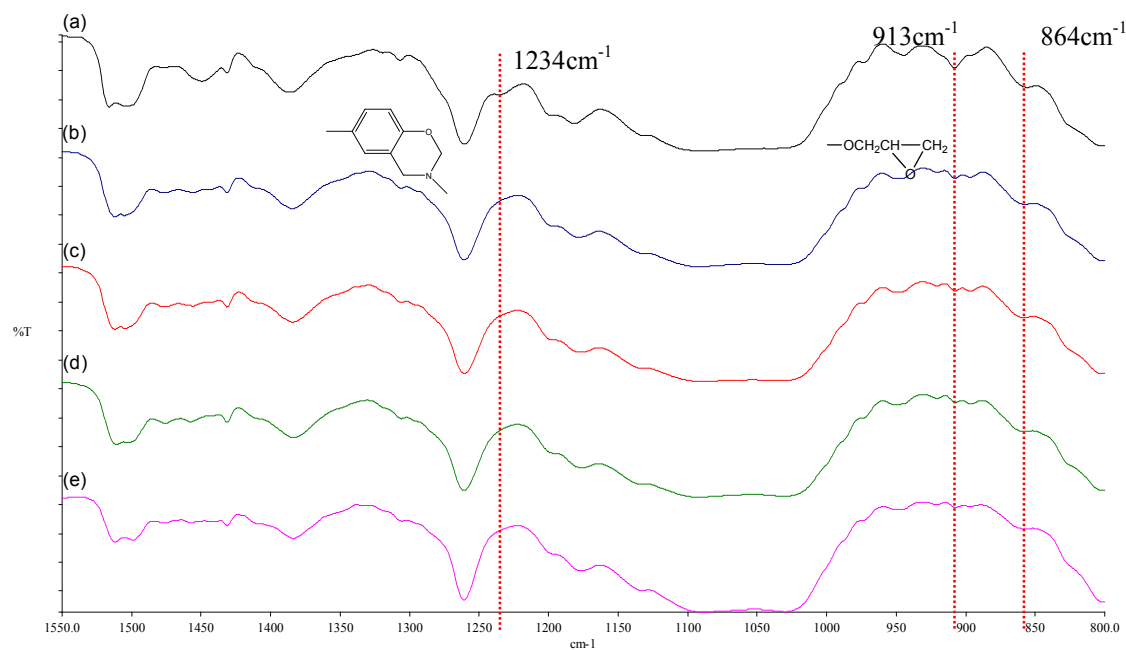


Figure 6-6. FT-IR spectrum of BZ-A6/ GT-1000 copolymer (a) before reaction (b) 150 / 1h (c) 150 / 2h (d) 150 / 2h + 180 / 1h (e) 150 / 2h + 180 / 2h.

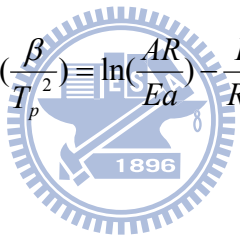
The curing of copolymer networks is a variety of the reaction. It can be observed that the ring opening of the benzoxazine appears first at lower temperature. Then the epoxy appears to be reacting with the phenolic hydroxyl groups after the ring opening polymerization makes them available. The reaction of benzoxazine-benzoxazine is at lower temperatures and benzoxazine-epoxy is at higher temperatures.

### 6.3.3 Scanning DSC studies

The polymerization behavior of benzoxazine-epoxy copolymer was examined by using differential scanning calorimetry (DSC). Kinetic analysis can be performed mostly using three kinetic models [31]: the Kissinger [32] and Flynn-Wall-Osawa [33] methods are suitable for dynamic kinetic analysis, while the Kamal method [34] is suitable for isothermal kinetic analysis (autocatalytic model). Non-isothermal analysis of Kissinger method is used in this experiment. The heating rate was carried out at 5,

10, 15 and 20 / min. from 40 to 325 in a constant flow of nitrogen of 50 ml/min. and integrated the area of exothermic peak.

Figure 6-7 shows the DSC exothermic peaks from these different dynamic heating rates of Ba/ DGEBA copolymer. A faster heating rate (20 / min.) results in a higher maximum temperature ( $T_p=259.8$  ) since the sample has a shorter time to react and to release the heat of reaction. In addition, lower the heating rate results in larger exothermic heat per unit weight which are summarized in Table 6-1. Based on the Kissinger method, the activation energy can be obtained while the maximum reaction rate is zero under a constant heating rate condition. The resulting relation can be expressed by the following equation.  $\beta=dT/ dt$  is a constant heating rate,  $T_p$  is the maximum exothermic temperature, and  $R$  is the universal gas constant.

$$\ln\left(\frac{\beta}{T_p^2}\right) \equiv \ln\left(\frac{AR}{Ea}\right) - \frac{Ea}{RT_p}$$


By plotting

$$\ln\left(\frac{\beta}{T_p^2}\right)$$

versus

$$\frac{1}{T_p}$$

which gives the activation energy without a specific assumption of the conversion-dependent function, the slope is calculated and shown in Figure 6-8 and the activation energy,  $Ea$ , of Ba/ DGEBA copolymer is 113.5 KJ/ mol. (Table 6-1)

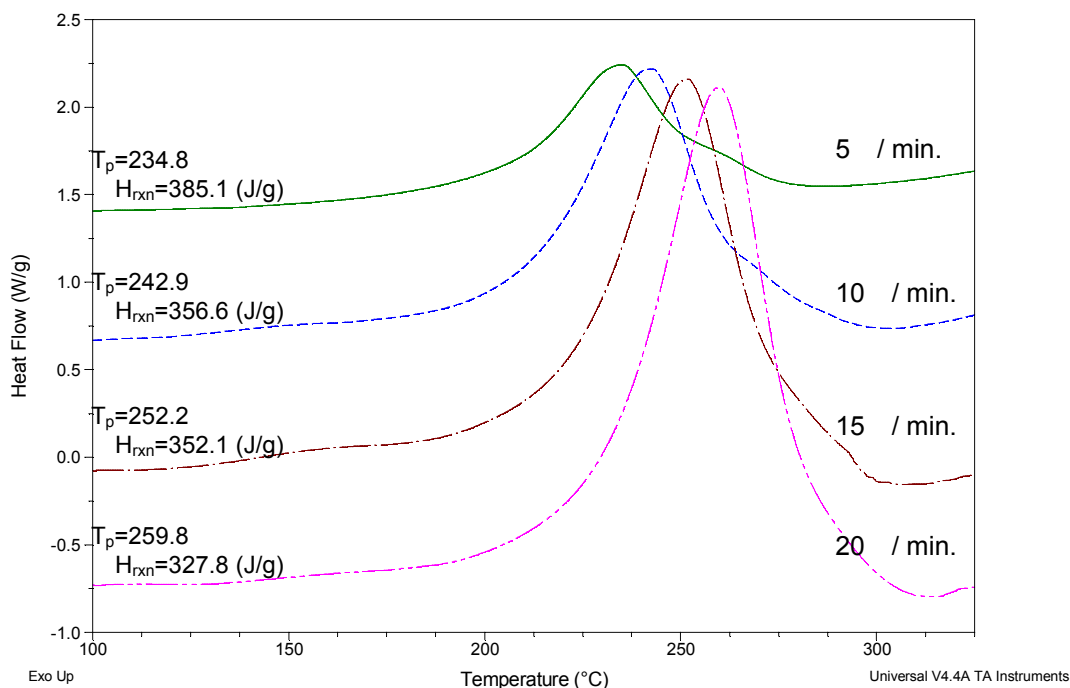


Figure 6-7. Dynamic DSC exothermic curves of Ba/ DGEBA resin at different scan rates: 5 / min., 10 / min., 15 / min. and 20 / min.

Table 6-1. The kinetic parameters evaluated for the curing of benzoxazine/ epoxy copolymers

Benzoxazine/ epoxy copolymer	Heating rate $\beta$ ( / min.)	Peak point $T_p$ (K)	Total heat $H_{rxn}$ (J/g)	$\ln (\beta/T_p^2)$	$1/T_p$	$E_a$ (KJ/ mol.)
Ba/ DGEBA	20	532.9	327.8	-9.561048	0.00188	113.5
	15	525.4	352.1	-9.820308	0.00190	
	10	516.0	356.6	-10.189745	0.00194	
	5	508.0	385.1	-10.851328	0.00197	
BZ-A6/ GT-1000	20	516.6	91.5	-9.495318	0.00194	59.4
	15	506.2	132.9	-9.715638	0.00201	
	10	493.2	146.0	-10.104914	0.00202	
	5	474.7	108.6	-10.726308	0.00210	

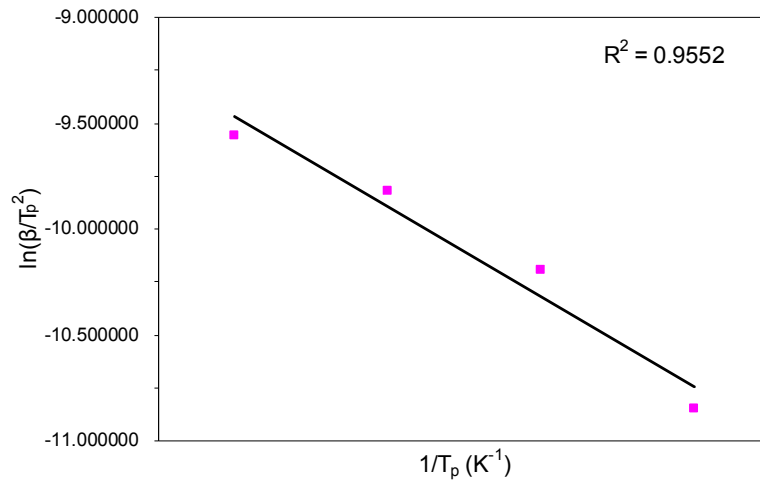


Figure 6-8. Plots for determination of the activation energy of Ba/ DGEBA copolymer by the Kissinger method.

Figure 6-9 shows the DSC exothermic peaks from these different dynamic heating rates of BZ-A6/ GT-1000 copolymer. From the same Kissinger method, we can calculate the activation energy,  $E_a$ , of BZ-A6/ GT-1000 copolymer from Figure 6-10 plot and the  $E_a$  is 59.4 KJ/ mol. which is summarized in Table 6-1.

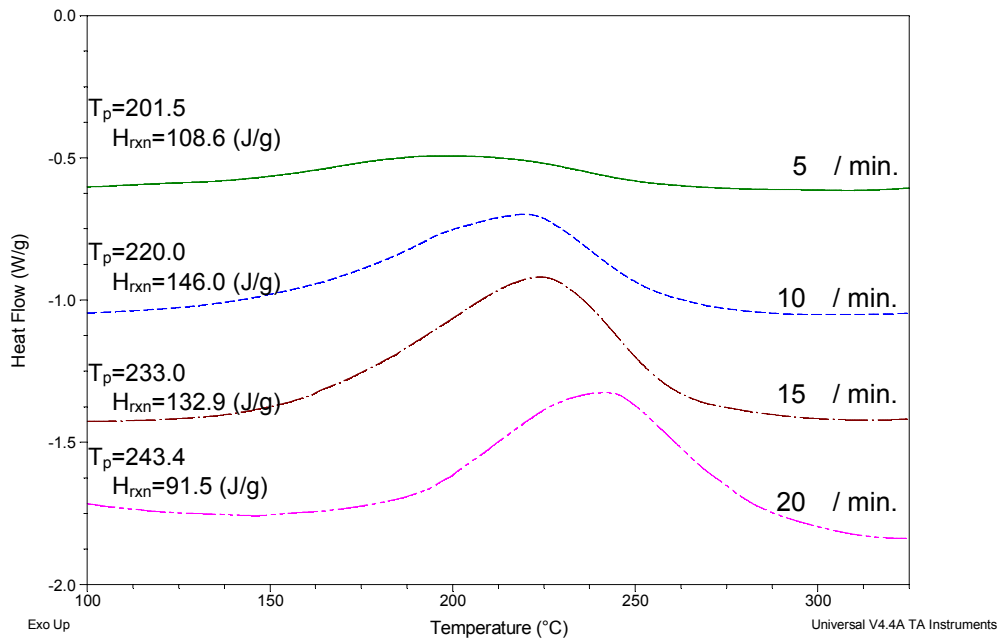


Figure 6-9. Dynamic DSC exothermic curves of BZ-A6/ GT-1000 resin at different scan rates: 5 / min., 10 / min., 15 / min. and 20 / min.

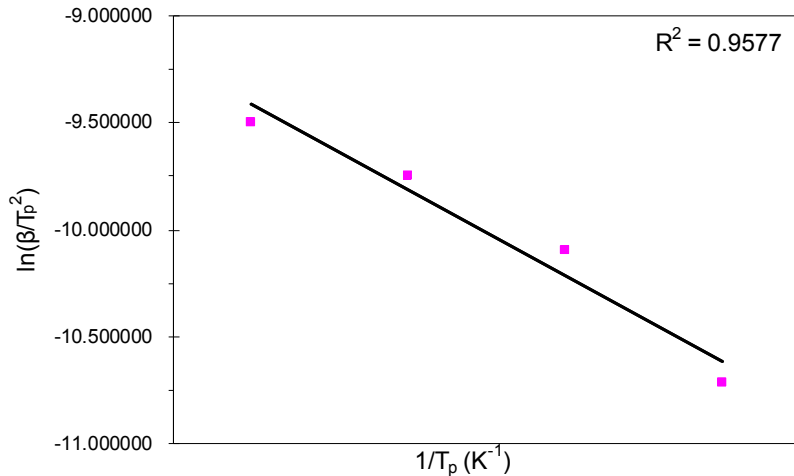


Figure 6-10. Plots for determination of the activation energy of BZ-A6/ GT-1000 copolymer by the Kissinger method.

The ring-opening of benzoxazine ring produces tertiary amine structure in the backbone of the phenolic resin. These tertiary amine groups can catalyze homopolymerization of epoxy groups. [22] Except tertiary amine groups in the backbone of the phenolic resin, there are tertiary amines including from imide group in BZ-A6 structure. There are more tertiary amines of BZ-A6/ GT-1000 than Ba/ DGEBA copolymer and the homopolymerization was more accelerated. It is obviously that  $E_a$  of siloxane containing copolymer, BZ-A6/ GT-1000, is lower than Ba/ DGEBA copolymer. Lower activation energy could be heat reacted easier than the copolymer of higher activation energy. From Figure 6-3, the onset temperature of cure of BZ-A6/ GT-1000 is 142.3 °C, which is much lower than the onset of Ba/ DGEBA, 227.9 °C. The reactive curing temperature was lower than 200 °C by selecting siloxane-imide containing benzoxazine/ epoxy copolymer system instead of the traditional bisphenol-A type benzoxazine/ epoxy copolymer. More tertiary amine groups in the siloxane-imide containing benzoxazine, BZ-A6, could accelerate the polymerization of the copolymer network of and lower the reactive temperature when copolymerization occurred.

### 6.3.4 Thermogravimetric analysis

Thermal stability of the benzoxazine/ epoxy copolymer was investigated by TGA. The decomposition reaction of the copolymer samples was observed to proceed in several stages. The TGA traces are shown in Figure 6-11 and the values of various decompositions and char yields are summarized in Table 6-2. Ba/ DGEBA copolymer showed sharp and low decomposition temperature, Figure 6-11 (a) and (c), compared with that of BZ-A6/ GT-1000 copolymer, Figure 6-11 (b) and (d), no matter under air or nitrogen atmosphere. In our previous study [17], the polybenzoxazine of BZ-A6 showed better thermal properties than Ba or BZ-A1, since the longer siloxane-imide segment is introduced into the benzoxazine. The char yield of copolymer of Ba/ DGEBA is almost zero under air atmosphere, but the copolymer of BZ-A6/ GT-1000 has the higher char yield to 24.5% at 850 °C. The copolymer of BZ-A6/ GT-1000 also shows better thermal stability than that of Ba/ DGEBA.

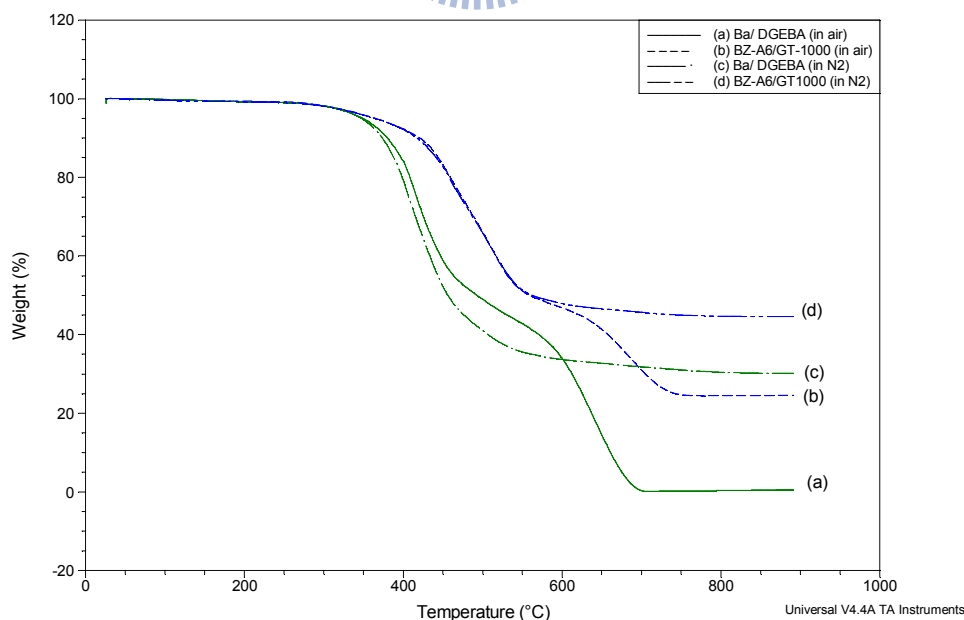


Figure 6-11. TGA thermograms of cured resin from (a) Ba/ DGEBA (in air) (b) BZ-A6/ GT-1000 (in air) (c) Ba/ DGEBA (in N<sub>2</sub>) (d) BZ-A6/ GT-1000 (in N<sub>2</sub>)



Table 6-2. Thermostability of cured resins from Ba/ DGEBA and BZ-A6/ GT-1000

Co-polymers	Curing Condition	T <sub>5% loss</sub> ( )/ N <sub>2</sub>	T <sub>10% loss</sub> ( )/ N <sub>2</sub>	Char Yield (wt%)/ N <sub>2</sub> at 850	T <sub>5% loss</sub> ( )/ air	T <sub>10% loss</sub> ( )/ air	Char Yield (wt%)/ air at 850
Ba/ DGEBA	200 /2h+	347.4	373.8	30.2	349.0	380.1	0.4
	230 /2h						
BZ-A6/ GT-1000	150 /2h+	364.9	417.2	44.6	364.7	420.9	24.5
	180 /2h						

T<sub>5% loss</sub>: The temperature for which the weight loss is 5%.

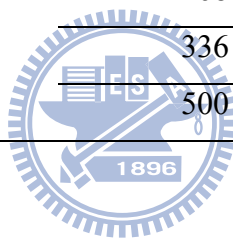
T<sub>10% loss</sub>: The temperature for which the weight loss is 10%.

### 6.3.5 UV stability properties

The hydrophobic and UV resistant properties of polybenzoxazine BZ-A6 have been discussed in our previous study. [17] Here, we examined the UV stability properties of benzoxazine/ epoxy copolymers. Table 6-3 presents the variation in water contact angles after exposure to UV-A radiation. When siloxane epoxy, GT-1000, was introduced to siloxane-imide containing benzoxazine, BZ-A6, the copolymer of BZ-A6/ GT-1000 also showed the hydrophobic property from the result of water contact angle to 110.5° after curing. The water contact angle of Ba/ DGEBA copolymer could achieved to 90.8° after crosslinked, but decreased to zero just after UV-A exposure for 24h. The cured Ba/ DGEBA copolymer has been decomposed and its surface property has became to hydrophilic from hydrophobic just after 24 h UV-A exposure. The water contact angle is measured as 106.0° after 96h exposure and as 101.6° after 500h exposure time. It could be observed the stable hydrophobic property of copolymer of BZ-A6/ GT-1000 since of its good UV stability property. The excellent UV resistant property as a result of the long siloxane segments in BZ-A6 and GT-1000.

Table 6-3. Contact angles of cured resins from Ba/ DGEBA and BZ-A6/ GT-1000 after UV exposure for various periods of time.

Copolymers	Curing conditions	UV exposure time (hrs)	Water contact angle (°)
Ba/ DGEBA	200 / 2h + 230 / 2h	0	90.8
		24	0
		96	0
		168	0
		336	-
		500	-
BZ-A6/ GT-1000	150 / 2h + 180 / 2h	0	110.5
		24	110.8
		96	106.0
		168	101.2
		336	102.5
		500	101.6



## 6.4 Conclusions

Siloxane-containing benzoxazine-epoxy copolymer which reacted without any external curing agent was prepared. It is observed that the copolymerization reaction occurs via the opening of benzoxazine ring then the phenolic hydroxyl functionalities from the polybenzoxazine precursor will react with epoxy. Curing of the benzoxazine-epoxy copolymer indicated a lower curing temperature since its lower activation energy. Siloxane-containing benzoxazine-epoxy copolymer exhibited good thermal stability as high T<sub>g</sub> and high decomposed temperature. The newly copolymer also shows higher thermal stability and UV stability than the conventional bisphenol A type benzoxazine-epoxy copolymer.



## References

- [1] Culbertson, B. M.; McGrath, J. E. *Advances in Polymer Synthesis*. **1985** New York: Plenum.
- [2] Takeichi, T. and Agag, T. *High Perform Polym* **2006**, *18*, 777.
- [3] Ghosh, N. N.; Kiskan, B. and Yagci, Y. *Prog Polym Sci* **2007**, *32*, 1344.
- [4] Ning, X. and Ishida, H. *J Polym Sci Part A: Polym Chem* **1994**, *32*, 1121.
- [5] Ishida, H. and Allen, D. J. *J Polym Sci Part B: Polym Phys* **1996**, *34*, 1019.
- [6] Shen, S. B. and Ishida, H. *J Appl Polym Sci* **1996**, *61*, 1595.
- [7] Takeichi, T.; Agag, T. and Yong, G. *Recent Res Dev Polym Sci* **2000**, *4*, 85.
- [8] Su, Y. C. and Chang, F. C. *Polymer* **2003**, *44*, 7989.
- [9] Wang, C. F.; Su, Y. C.; Kuo, S. W.; Huang, C. F.; Sheen, Y. C. and Chang, F. C. *Angew Chem Int Ed* **2006**, *45*, 2248.
- [10] Wang, C. F.; Wang, Y. T.; Tung, P. H.; Kuo, S. W.; Lin, C. H.; Sheen, Y. C. and Chang, F. C. *Langmuir* **2006**, *22*, 8289.
- [11] Liao, C. S.; Wu, J. S.; Wang, C. F. and Chang, F. C. *Macromol Rapid Commun* **2008**, *29*, 56.
- [12] Liao, C. S.; Wang, C. F.; Lin, H. C.; Chou, H. Y. and Chang, F. C. *J Phys Chem C* **2008**, *112*, 16189.
- [13] Wang, C. F.; Chiou, S. F.; Ko, F. H.; Chen, J. K.; Chou, C. T.; Huang, C. F.; Kuo, S. W. and Chang, F. C. *Langmuir* **2007**, *23*, 5868.
- [14] Macko, J. A. and Ishida, H. *Polymer* **2001**, *42*, 227.
- [15] Chen, K. C.; Li, H. T.; Chen, W. B. and Huang, S. C. 11<sup>th</sup> Pacific Polymer Conference **2009**.
- [16] Chen, K. C.; Li, H. T.; Chen, W. B.; Liao, C. H.; Sun, K. W. and Chang, F. C. *Polym Int* accepted

- [17] BZ-A6 paper Chen, K. C.; Li, H. T.; Huang, S. C.; Chen, W. B.; Sun, K. W. and Chang, F. C. *Polym Int* accepted
- [18] Park, S. J. and Heo, G. Y. *Macromol Chem Phys* **2005**, *206*, 1134.
- [19] Ishida, H. and Allen, D. J. *Polymer* **1996**, *37*, 4487.
- [20] Kimura, H.; Matsumoto, A.; Hasegawa, K.; Ohtsuka, K. and Fukuda, A. *J Appl Polm Sci* **1998**, *68*, 1903.
- [21] Kimura, H.; Murata, Y.; Matsumoto, A.; Hasegawa, K.; Ohtsuka, K. and Fukuda, A. *J Appl Polm Sci* **1999**, *74*, 2266.
- [22] Rao, B. S.; Reddy, K. R.; Pathak, S. K. and Pasala, A. R. *Polym Int* **2005**, *54*, 1371.
- [23] Ishida, H. and Rodriguez, Y. *Polymer* **1995**, *36*, 3151.
- [24] Su, Y. C.; Yei, D. R. and Chang, F. C. *J Appl Polym Sci* **2005**, *95*, 730.
- [25] Jubsilp, C.; Punson, K.; Takeichi, T. and Rimdusit, S. *Polym Degrad Stab* **2010**, *93*, 918.
- [26] Agag, T. and Takeichi, T. *Polymer* **2000**, *41*, 7083.
- [27] Takeichi, T.; Zeidam, R. and Agag, T. *Polymer* **2002**, *43*, 45.
- [28] Agag, T.; Tsuchiya, H. and Takeichi, T. *Polymer* **2004**, *45*, 7903.
- [29] Jamois, D.; Tessier, M. and Marechal, E. *J Polym Sci Chem* **1993**, *31*, 1951.
- [30] Ishida, H. and Rodriguez, Y. *Polymer* **1995**, *36*, 3151.
- [31] Barral, L.; Cano, J.; Lopez, I.; Bueno, L.; Nogueira, P.; Abad, M. and Ramirez, C. *J Polym Sci Polym Phys* **2000**, *38*, 351.
- [32] Kissinger, H. E. *Anal Chem* **1957**, *29*, 1702.
- [33] Ozawa, T. J. *Therm Anal* **1970**, *2*, 301.
- [34] Kamal, M. R. *Polym Eng Sci* **1974**, *27*, 782.

## Chapter 7

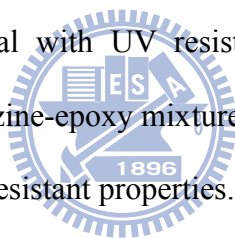
### Conclusions

We have synthesized a novel series siloxane-imide-containing benzoxazines (BZ-A1 and BZ-A6) which are with different siloxane-containing segments. The thermal property of the BZ-A1 polybenzoxazine is superior to those conventional polybenzoxazines lacking siloxane groups. The BZ-A1 polybenzoxazine possesses extremely low surface free energy ( $\gamma_s = 15.1 \text{ mJ/m}^2$ ) after curing at  $230 \text{ }^\circ\text{C}$  for 1 hr. Moreover, the surface free energy of the BZ-A1 polybenzoxazine is more stable than the conventional bisphenol A type polybenzoxazine. (PBa) during thermal curing and annealing process, indicating that the BZ-A1 polybenzoxazine is more suitable to apply as a low surface free energy material for high temperature and long time period requirements. The cured product from the BZ-A1, PBZ-A1, possesses extremely low surface free energy and improves thermal stabilities. This newly developed PBZ-A1 shows better stability on surface free energy under thermal curing and annealing while maintains its low surface free energy compare with the conventional bisphenol A type polybenzoxazine (PBa).

The cured product from the PBZ-A6 possesses extremely low surface free energy,  $12.4 \text{ mJ/m}^2$ , and improves thermal and UV stabilities. PBZ-A6 could be a free-standing film from introducing the flexible siloxane segment into benzoxazine. PBZ-A6 shows high  $T_g$  as  $186.4$  and perfect UV stability after 500 hrs exposure time. Through the incorporation of a longer siloxane-imide moiety BZ-A6 into the cured PBZ-A6, the toughness, flexibility, thermal properties, thermal and UV stability in terms of low surface free energy are all significantly improved over the conventional

Bis-A type PBZ. This PBZ-A6 has the potential applications in UV- or weather-resistant, self-cleaning coating materials.

Siloxane-imide-containing benzoxazine, BZ-A6, was copolymerized with siloxane-epoxy, GT-1000. The curing behavior of the copolymers was studied using DSC and FT-IR, which indicated a lower curing temperature of 150 °C. The activation energy ( $E_a$ ) of BZ-A6/ GT-1000 copolymer is 59.4 KJ/mol. from Kissinger method. The siloxane benzoxazine-epoxy mixture exhibited higher thermal stability, exhibited higher char yield as 44.6% and higher decomposed temperature at 364.9 °C. Moreover, the water contact angle of the BZ-A6/ GT-1000 copolymer is more stable than the conventional bisphenol A type benzoxazine-epoxy, Ba/ DGEBA, during the UV exposure process, indicating that the benzoxazine-epoxy mixture is more suitable to apply as a hydrophobic material with UV resistant requirement. There are wide applications of siloxane benzoxazine-epoxy mixture since its lower curing temperature and good temperature- and UV- resistant properties.



## List of Publications

### (A) Journal

1. **Kai-Chi Chen**, Hsun-Tien Li, Wen-Bin Chen, Chun-Hsiung Liao, Kien-Wen Sun, Feng-Chih Chang " **Synthesis and characterization of a novel siloxane-imide-containing polyenzoxazine** " *Polymer International* Accepted: 11 August 2010.
2. **Kai-Chi Chen**, Hsun-Tien Li, Shu-Chen Huang, Wen-Bin Chen, Kien-Wen Sun, Feng-Chih Chang<sup>1</sup> "**Synthesis and Performance Enhancement of a Novel Low Surface Free Energy Polybenzoxazines**" *Polymer International* Accepted: 07 November 2010.
3. **Kai-Chi Chen**, Hsun-Tien Li, Kien-Wen Sun, Feng-Chih Chang "**New Thermosetting Resin from Siloxane-Containing Benzoxazine and Epoxy Resin**" in submitted.



### (B) Conference

1. **Kai-Chi Chen**, Hsun-Tien Li, Wen-Bin Chen, Shu-Chen Huang "**Novel Low Surface Free Energy Material of Siloxane-Imide Containing Benzoxazine and Its High Performance Thermosets**" 11<sup>th</sup> Pacific Polymer Conference 2009 (PPC11, Cairns, Australia)
2. **Kai-Chi Chen**, Hsun-Tien Li, Wen-Bin Chen, Shu-Chen Huang "**Highly Temperature- and UV-Resistant Polybenzoxazines Prepared from Siloxane-Imide-Containing Benzoxazines**" 2010 *Material Research Society Fall Meeting* (Boston, USA)



## Introduction to the Author

English name: Kai-Chi Chen

Chinese name: 陳凱琪

Birthday: 1972. 04. 15

Address: 30264 新竹縣竹北市莊敬六街 13 號 3F-7



### Education:

1991.09 ~ 1995.06 **B. S.**, Department of Textile Engineering, Feng Chia University,  
Taichung, Taiwan

1996.09 ~ 1998.06 **M. S.**, Department of Materials Science and Engineering,  
National Taiwan University, Taipei, Taiwan

指導教授 林唯芳教授

2006.09 ~ 2011.01 **Ph. D.**, Institute of Applied Chemistry, National Chiao Tung  
University, Hsin Chu, Taiwan

指導教授 孫建文教授、張豐志 教授

### Working experience:

1998.10 ~ Researcher, Material and Chemical Research Laboratories, Industrial  
Technology Research Institute